Prepared for submission to JHEP

Flavor Physics at CEPC: a General Perspective

Wolfgang Altmannshofer[1], **Peter Athron**[2], **Lorenzo Calibbi**[3], **Lu Cao**[4,5], **Yuzhi Che**[6], **Long Chen**[7], **Mingshui Chen**[6], **Shanzhen Chen**[6], **Shan Cheng**[8], **Andreas Crivellin**[9], **Hanhua Cui**[6], **Olivier Deschamps**[10], **Sébastien Descotes-Genon**[11], **Xiaokang Du**[12], **Pablo Goldenzweig**[13], **Jiayin Gu**[14], **Feng-Kun Guo**[15,16,17], **Zhi-Hui Guo**[18], **Jibo He**[16], **Gino Isidori**[19], **Xu-Hui Jiang**[6,20], **Jernej F. Kamenik**[21], **Tsz Hong Kwok**[20], **Geng Li**[22], **Haibo Li**[6], **Honglei Li**[23], **Lingfeng Li**[20,24], **Qiang Li**[25], **Xin-Qiang Li**[26], **Yiming Li**[6], **Yubo Li**[27], **Yuji Li**[14], **Hao Liang**[6], **Zhijun Liang**[6], **Libo Liao**[28], **Zoltan Ligeti**[29], **Tao Liu**[20], **Peng-Cheng Lu**[7], **Alberto Lusiani**[30], **Hong-Hao Ma**[31], **Kai Ma**[32], **Juan-Juan Niu**[31], **Wenbin Qian**[16], **Qin Qin**[33], **Ariel Rock**[20], **Jonathan L. Rosner**[34], **Manqi Ruan**[6], **Dingyu Shao**[14], **Chengping Shen**[14], **Xiaoyan Shen**[6], **Liaoshan Shi**[6], **Zong-Guo Si**[7], **Cristian Sierra**[2], **Huayang Song**[15], **Wei Su**[28], **Fei Wang**[35], **Hengyu Wang**[6], **Jianchun Wang**[6], **Wei Wang**[36], **Xiaolong Wang**[14], **Yadi Wang**[37], **Yuexin Wang**[6,38], **Xing-Gang Wu**[39], **Yongcheng Wu**[2], **Yuehong Xie**[26], **Zijun Xu**[6], **Haijun Yang**[36], **Hongtao Yang**[40], **Fusheng Yu**[41], **Changzheng Yuan**[6], **Xing-Bo Yuan**[26], **Xuhao Yuan**[6], **Xi-Jie Zhan**[39], **Liming Zhang**[42], **Yang Zhang**[35], **Yanxi Zhang**[43], **Yu Zhang**[44], **Zhen-Hua Zhang**[45], **Zhong Zhang**[46], **MingRui Zhao**[47,48], **Qiang Zhao**[6], **Xu-Chang Zheng**[39], **Pengxuan Zhu**[15], **Yongfeng Zhu**[43], **Xunwu Zuo**[13], **Jure Zupan**[49]

[1] *University of California, Santa Cruz*
[2] *Nanjing Normal University*
[3] *Nankai University*
[4] *Deutsches Elektronen-Synchrotron*
[5] *University of Bonn*
[6] *Institute of High Energy Physics, Chinese Academy of Sciences*
[7] *Shandong University*
[8] *Hunan University*
[9] *Paul Scherrer Institut*
[10] *Université Clermont Auvergne, CNRS/IN2P3, LPC*
[11] *Université Paris-Saclay, CNRS/IN2P3, IJCLab*
[12] *Institute of Physics, Henan Academy of Sciences*
[13] *Karlsruhe Institute of Technology*
[14] *Fudan University*
[15] *Institute of Theoretical Physics, Chinese Academy of Sciences*
[16] *University of Chinese Academy of Sciences*
[17] *Beihang University*
[18] *Hebei Normal University*
[19] *Universität Zürich*

[20] *Hong Kong University of Science and Technology*
[21] *Jožef Stefan Institute*
[22] *Hangzhou Institute for Advanced Study, University of Chinese Academy of Sciences*
[23] *University of Jinan*
[24] *Brown University*
[25] *Northwestern Polytechnical University*
[26] *Central China Normal University*
[27] *Xi'an Jiaotong University*
[28] *Sun Yat-Sen University*
[29] *University of California, Berkeley*
[30] *Scuola Normale Superiore and INFN sezione di Pisa*
[31] *Guangxi Normal University*
[32] *Shaanxi University of Technology*
[33] *Huazhong University of Science and Technology*
[34] *University of Chicago*
[35] *Zhengzhou University*
[36] *Shanghai Jiao Tong University*
[37] *North China Electric Power University*
[38] *China Center of Advanced Science and Technology*
[39] *Chongqing University*
[40] *University of Science and Technology of China*
[41] *Lanzhou University*
[42] *Tsinghua University*
[43] *Peking University*
[44] *Hefei University of Technology*
[45] *University of South China*
[46] *University College London*
[47] *China Institute of Atomic Energy*
[48] *Niels Bohr Institute, University of Copenhagen*
[49] *University of Cincinnati*

Abstract: Among various options for future colliders, the electron-positron Higgs factory is regarded as the highest priority. It could not only probe new physics via Higgs measurements but also provide great opportunities for flavor physics explorations. Based on the Technical Design Report nominal luminosity of the Circular Electron Positron Collider (CEPC), we describe the flavor physics landscape at an electron-positron Higgs factory, focusing especially on the physics significance of operating such a machine at the Z pole energy. We summarize the prospects of multiple physics benchmarks and the relevant interpretation with phenomenology tools. Our study shows that an electron-positron Higgs factory capable of delivering more than $\mathcal{O}(10^{12})$ Z bosons could detect many unobserved rare and exotic physics processes, improve the precision of various measurements by orders of magnitudes, especially on B physics and τ precision measurements, and be sensitive to new physics up to the energy scales of 10 TeV or even higher. The flavor physics program at an electron-positron collider is not only an extension of the existing flavor physics facilities such as LHCb and Belle II, but is also complementary to the Higgs, electroweak, and QCD measurements to be conducted by the Higgs factory itself. The physics performance of flavor studies is significantly enhanced by combining operations at multiple center-of-mass energies. The flavor program plays a crucial role in the scientific reach and the discovery power of the electron-positron Higgs factory. We also specify the relevant requirements for detector performance and considerations for development.

Contents

1 Introduction

The Circular Electron Positron Collider (CEPC) [1, 2] was proposed in 2012 by the Chinese high-energy physics community to function primarily as a Higgs factory at a center-of-mass energy of 240 GeV. It is also set to operate as a Z factory at the Z pole, conduct precise WW threshold scans, and potentially be upgraded to operate at a center-of-mass energy of 360 GeV, *i.e.*, above the $t\bar{t}$ threshold. In the proposed nominal operation scenario [1, 3], the CEPC is anticipated to produce significant numbers of Higgs and Z bosons, W boson pairs and, potentially, top quarks. With respect to the accelerator design, the development of key technologies has led to a significant enhancement in the instantaneous luminosity per interaction point (IP) compared to those reported in the Conceptual Design Report (CDR), as shown in Figure 1. Based on this progress, the CEPC study group proposes a new nominal operation scenario, shown in Table 1, which would allow for precision measurements of Higgs boson couplings, electroweak (EW) observables, and QCD differential rates. It would also provide ample opportunities to search for rare decays and new physics (NP) signals. Moreover, the large quantities of bottom quarks, charm quarks, and tau leptons from the decays of Z bosons create opportunities for numerous critical flavor physics measurements. It should be noted that the results presented here are based on the updated running scenario using a 50 MW synchrotron radiation (SR) power beam [4].

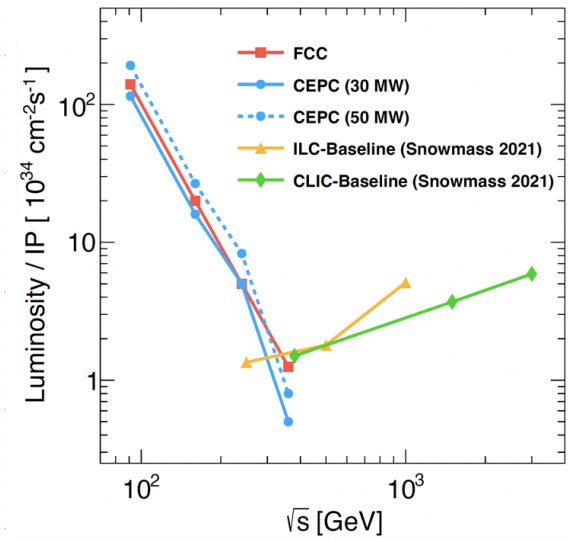

Figure 1: Designed luminosities of the CEPC at the Z pole, Higgs, WW and the $t\bar{t}$ thresholds operation modes with the baseline and upgrade shown in solid and dashed blue curves, respectively. Luminosities for several other proposals of e^+e^- colliders are also shown for comparison. See Ref. [1] for details.

Operation mode	Z factory	WW threshold	Higgs factory	$t\bar{t}$
$\sqrt{s}$ (GeV)	91.2	160	240	360
Run time (year)	2	1	10	5
Instantaneous luminosity ($10^{34}\text{cm}^{-2}\text{s}^{-1}$, per IP)	191.7	26.7	8.3	0.83
Integrated luminosity (ab^{-1}, 2 IPs)	100	6.9	21.6	1
Event yields	4.1×10^{12}	2.1×10^{8}	4.3×10^{6}	0.6×10^{6}

Table 1: Nominal CEPC operation scheme of four different modes. See [1, 3] for details.

Flavor physics, as a well-developed area within particle physics, has contributed substantially to the establishment of the Standard Model (SM) over recent decades. This was achieved through the examination of the properties of SM fermion flavors in a myriad of experiments, yielding significant findings and discoveries. The CEPC can serve as a flavor factory, and its flavor physics program enhances the CEPC's overarching physics objectives. The flavor sector provides substantial motivations for the CEPC operation, given the existing multitude of unknowns within the SM and beyond.

Understanding the flavor physics potential of the CEPC is not an isolated field of study, as it also influences other primary fields of explorations at the CEPC, including Higgs physics, EW precision observables (EWPOs), QCD, and Beyond the Standard Model (BSM) physics. For instance, within the SM the fermion mixing, specifically the Cabibbo-Kobayashi-Maskawa (CKM) matrix [5, 6] and its hierarchical structure, originates from the Yukawa couplings of the Higgs field to the fermion gauge eigenstates. While some of the diagonal Yukawa couplings will be pinned down by the direct Higgs measurements at CEPC [7], studying the origin of the off-diagonal flavor mixing terms and their CP-violating phases remains mainly within the realm of flavor physics. Conversely, while most heavy-flavored particles decay via EW transitions at the tree level, many rare processes are only induced by EW one-loop effects, *i.e.*, flavour changing neutral currents. Their measurements may also serve as alternative tests of the EW sector at an energy scale lower than Z-pole measurements. Meanwhile, many EWPOs necessitate precise flavor tagging and high-precision reconstruction, *e.g.*, the forward-backward asymmetry of charm and bottom quarks. Furthermore, most flavor physics studies involve QCD since all quarks are colored and τ leptons can decay to hadronic final states. In fact, most flavor physics studies rely on the theory of QCD, both perturbatively and non-perturbatively, to provide insights into the corresponding production, spectroscopy, and decays of hadronic states. In turn, the plethora of flavor measurements could provide crucial inputs to, and calibration of, QCD theory in multiple ways.

It is also noteworthy that flavor physics provides a set of probes sensitive to BSM physics. For instance, the decay of a heavy flavour fermion is suppressed by EW scale, such that it becomes relatively long lived. Such a narrow width makes it possible to reveal even small BSM effects, which are not easily observable otherwise. Finally, the ambitious goals of

Particle	BESIII	Belle II (50 ab^{-1} on $\Upsilon(4S)$)	LHCb (300 fb^{-1})	CEPC (4×Tera-Z)
B^0, $\bar{B}^0$	-	5.4×10^{10}	3×10^{13}	4.8×10^{11}
$B^\pm$	-	5.7×10^{10}	3×10^{13}	4.8×10^{11}
B_s^0, $\bar{B}_s^0$	-	6.0×10^8 (5 ab^{-1} on $\Upsilon(5S)$)	1×10^{13}	1.2×10^{11}
$B_c^\pm$	-	-	1×10^{11}	7.2×10^8
Λ_b^0, $\bar{\Lambda}_b^0$	-	-	2×10^{13}	1×10^{11}
D^0, $\bar{D}^0$	1.2×10^8	4.8×10^{10}	1.4×10^{15}	8.3×10^{11}
$D^\pm$	1.2×10^8	4.8×10^{10}	6×10^{14}	4.9×10^{11}
$D_s^\pm$	1×10^7	1.6×10^{10}	2×10^{14}	1.8×10^{11}
$\Lambda_c^\pm$	0.3×10^7	1.6×10^{10}	2×10^{14}	6.2×10^{10}
$\tau^+\tau^-$	3.6×10^8	4.5×10^{10}		1.2×10^{11}

Table 2: Expected yields of b-hadrons, c-hadrons, and τ leptons at BESIII, Belle II, LHCb Upgrade II, and CEPC (4×Tera-Z, namely 4×10^{12} Z bosons). For b- and c-hadrons, their yields include both charge conjugates, while the yield of τ leptons refers to the $\tau^+\tau^-$ events, namely the number of τ pairs. The production cross sections for $b\bar{b}$ and $c\bar{c}$ at center-of-mass energies corresponding to the $\Upsilon(4S)$ and $\Upsilon(5S)$ are taken from Ref. [8]. The b quark production cross section within LHCb detectors' acceptance is taken from Ref. [9]. To estimate the production fractions of B^0 and $B^\pm$ at LHCb, we utilize the B_s^0 and Λ_b^0 production fractions from Ref. [10] and assume $f_u + f_d + f_s + f_{\text{baryon}} = 1$, with $f_u = f_d$, and $f_{\Lambda_b^0} = f_{\text{baryon}}$. For Z decays, the production fractions of B^0, $B^\pm$, B_s^0, and Λ_b^0 are obtained from Ref. [11]. The B_c meson production fraction at LHCb is taken from Ref. [12], while its production fraction at the Z pole (including the contribution from B_c^* decays) is taken from Ref. [13]. For inclusive charm meson production at the Z pole including b-hadron decay products, see Refs. [14–18]. The yields of τ leptons at CEPC 4×Tera-Z scenario are rescaled from Ref. [2].

flavor physics studies motivate developments on the instrumentation frontier, demanding enhanced detector performance in vertexing, tracking, particle identification (PID), and calorimetry.

The successful realization of the flavor physics program at the CEPC relies on a number of key factors:

- An abundant luminosity of the Z pole dataset of the CEPC, which yields substantial heavy flavor statistics. With a high integrated luminosity and the large $\sigma(e^+e^- \to Z \to b\bar{b}, c\bar{c}, \tau^+\tau^-)$, the Tera-$Z$ will generate extensive statistics of heavy-flavored hadrons and τ leptons, rivaling other proposed flavor physics experiments [2]. This is demonstrated by the expected yields of b-hadrons in Belle II, LHCb and a representative future Z factory, as listed in Table 2. The Tera-Z yields approximately 4.8×10^{11} $B^0/\bar{B}^0$ or $B^\pm$ mesons, which is one order of magnitude larger than that expected at Belle II [8]. Even though this yield is roughly 2 orders of magnitude lower compared to that of LHCb, studies at the Tera-Z can benefit significantly from

the clean experimental environment and the precisely known center-of-mass energy.

- The clean environment of e^+e^- collisions constitutes another cornerstone, substantially diminishing the background level and systematic uncertainties associated with neutral particles. This environment is particularly beneficial to flavor physics studies involving heavy b-hadrons, especially given the significantly limited event reconstruction efficiency in the noisy data environment of the LHCb [19].

- The scale separation $m_Z \gg m_{b,c,\tau} \gtrsim \Lambda_{\rm QCD}$ underpins the success of the project, as it facilitates the production of a wide array of particle species. In addition, even decay products with low momentum at center-of-mass frame of heavy-flavored particles are expected to be boosted to higher energies and larger displacements, augmenting measurement precision.

- Lastly, state-of-the-art detector technologies and algorithms for data analysis under development today will be crucial when deployed in the CEPC era. These technologies will enhance the investigation of extremely rare decay modes that contain neutral or invisible particles, as the cleanliness of a lepton collider enables such studies. The evolving field of advanced algorithms, especially deep learning ones, could also benefit flavor physics at the CEPC in almost all aspects by fully utilizing the large amount of data recorded from the hardware.

While the flavor physics program at the CEPC benefits from the various advantages above, it confronts new challenges. The first of these challenges is related to the significant increase in event statistics at the CEPC, which is expected to be greater by a factor of $\gtrsim \mathcal{O}(10^5)$ than the LEP run at the Z pole. Given the improved detector systems and electronics, the volume of data to be processed will increase substantially. Meanwhile, the precision goals of flavor physics, driven by theoretical interests, will also reach an elevated level in the CEPC era. Therefore, it becomes essential to improve the understanding of backgrounds and to control systematic effects to prevent the dominance by systematic uncertainties, which could potentially undermine the benefits of the CEPC's high instantaneous luminosity.

A second challenge arises from the multitude of viable channels to be studied at the CEPC. Compared to the other proposed future flavor physics experiments (or the upgrades of the current ones), the improvement achievable at the CEPC varies significantly channel by channel. Initial studies indicate that while the CEPC could enhance the precision of measurements by orders of magnitude in many instances, the improvement could be marginal in others. Therefore, identifying the most valuable systems, or "golden channels" - those with the highest potential for significant progresses or even discovery potential - for investigation in the CEPC context could substantially reduce the allocation of future resources. As it stands, some of these golden modes at the CEPC may have been overlooked as they are not suited for the existing experiments.

Besides these aforementioned experimental challenges, control of theoretical uncertainties is critical for CEPC flavor physics measurements and their interpretation. Numerous

direct measurements need to be interpreted in appropriate theory frameworks before they are integrated into the knowledge of flavor physics. Theoretical inputs come in multiple forms, such as: the non-perturbative theory of hadronization; perturbative QCD and EW corrections to fermion production; lattice extrapolations of heavy flavor form factors; the relation between the CKM matrix elements and the observed CP asymmetries; and the proper modeling of the electron beam and detector system. To accurately scrutinize the SM and to search for NP, the precision of these theoretical tools must align with those of the experimental outputs.

The principal objective of this document is to summarize the discovery potential of flavor physics measurements at CEPC, relying, whenever possible, on Monte Carlo (MC) simulations and relevant phenomenological analyses. During the compilation of this white paper, simultaneous efforts were dedicated to promoting flavor physics programs for other proposed future lepton colliders, such as the Future Circular Collider (FCC-ee) [20, 21] and the International Linear Collider (ILC) [22], both of which also include a Z factory phase and higher energy operations. In particular, the FCC-ee Z pole run has a similar integrated luminosity (180 ab^{-1}) to the current CEPC proposal, and the higher-energy runs are likewise comparable. Since both proposals share similar detector performances [2, 23], and both adopt a particle flow oriented detector design [2] and IDEA detector design [24], the relevant FCC-ee studies were also incorporated into the current summaries, with only minimal rescaling applied as necessary.

This document is structured as follows. In Section 2, we provide an overview of the CEPC facility, delineating key features of the collider and the detector that are crucial for flavor physics. Additionally, the simulation methods utilized at the CEPC are explained. Section 3 delves into Flavor-Changing-Charged-Current (FCCC) semileptonic and leptonic b decays, discussing their theoretical framework, recent progress and future research directions. Rare b decays mediated by Flavor-Changing-Neutral-Current (FCNC) are explored in Section 4, featuring a preliminary theoretical interpretation and discussion of di-leptonic, neutrino and radiative modes. Section 5 is dedicated to the measurement of CP asymmetries. Sections 6 and 7 focus on charm/strange and τ physics respectively. Flavor physics measurements via leptonic or hadronic Z decays are discussed in Section 8. Section 9 extends the discussion to flavor physics at higher energies, including $|V_{cb}|$ measurements from on-shell W boson decays, Higgs exotic and FCNC, as well as touches upon other possibilities. Prospects of hadron spectroscopy and exotic states are covered in Section 10. The production of light BSM states from heavy flavor interactions forms the central theme of Section 11. The detector performance requirements for a successful flavor physics program at the CEPC are discussed in Section 12. Finally, a summary of the topics discussed in the document is presented in Section 13.

2 Description of CEPC Facility

2.1 Key Collider Features for Flavor Physics

As an e^+e^- collider operating around the EW scale, flavor physics studies at the CEPC are affected by three major features. Firstly, as $\sqrt{s} \gg m_{b,c,\tau}$, the CEPC produces highly

Operation mode	Z factory	WW threshold	Higgs factory	$t\bar{t}$
$\sqrt{s}$ (GeV)	91.2	160	240	360
Beam size σ_x (μm)	6	13	14	39
Beam size σ_y (μm)	0.035	0.042	0.036	0.113
Bunch length (total, mm)	8.7	4.9	4.1	2.9
Crossing angle at IP (mrad)		33		

Table 3: Beam size, bunch length, and crossing angle at different operation modes of the CEPC [1, 3].

relativistic heavy flavor quarks or leptons. Their boosted decay products allow for precise momentum and lifetime measurements. This is in contradistinction to the situations at low energy e^+e^- colliders such as Belle II [8], BaBar [25], BESIII [26], and other future proposals, such as the Super Tau-Charm Factory (STCF) [27]. Secondly, as an e^+e^- collider, the CEPC provides a clean environment for flavor physics studies with low QCD backgrounds, negligible pileup events, and an almost fixed E_{cm}. Compared to hadron collider experiments, such as the LHCb [28], the CEPC enables more effective identification and reconstruction of final states that include neutral or invisible particles. The above arguments show the uniqueness of CEPC flavor physics studies. Thanks to advanced accelerator design, the large instantaneous luminosity will allow to collect $\mathcal{O}(10^5)$ times more statistics than the LEP Z pole run [29]. As a consequence, the search and analysis strategies may differ significantly from those employed in the relevant studies at LEP. For instance, high signal statistics allows sharper cuts to reduce backgrounds. At the same time, one needs to carefully address other systematic uncertainty sources using the plethora of data. Hence, the large luminosity of the CEPC brings new challenges and existing projections based on LEP must be reconsidered. Such challenges are especially severe for precision measurements.

According to the CEPC CDR [2], the beam energy spread could typically be controlled to the level of 0.1%. This, together with a detector that can reconstruct precisely hadronic events – allowing for precise determination of missing energy/momentum – thus enables relevant physics measurements with high precision; for instance, tagging semileptonic heavy quark decay and searching for dark matter candidates in hadronic events, especially at the Z factory mode.

The CEPC uses a nano beam scenario and therefore the typical beam spot sizes are of order μm in the x direction, order nm in the y direction, and correspondingly of order a few hundred μm in the z direction. The beam sizes at different operation modes of the CEPC are summarized in Table 3. The accelerator will provide a collision area with a typical size of order μm in the transverse direction and of order $\sim \mathcal{O}(100)$ μm along the beam direction. The spatial uncertainty of the interaction point can therefore be limited, enabling high precision measurements with τ final states – for example, in dark matter searches with $Z \to \tau^+\tau^-$ events at Z factory.

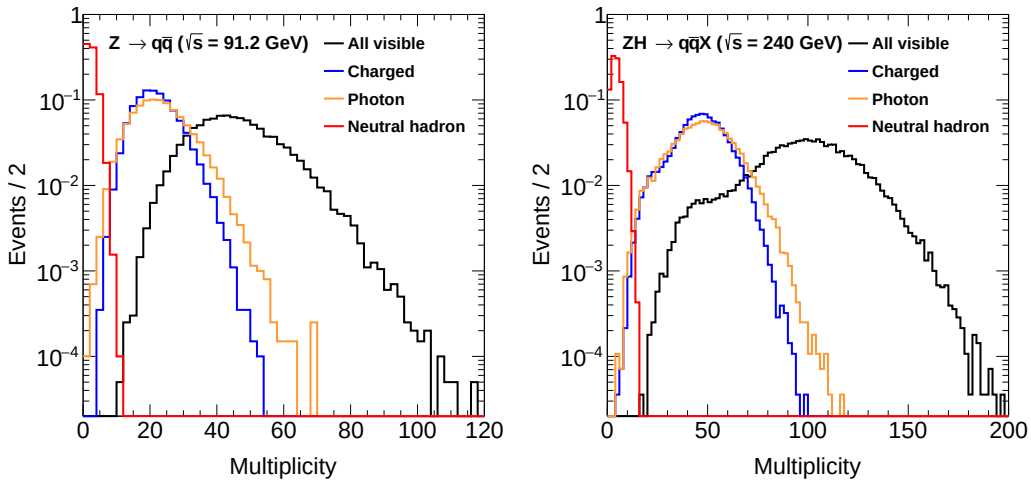

Figure 2: Multiplicities of different types of final state particles in $Z \to q\bar{q}$ (91.2 GeV) and $Z(\to q\bar{q})H(\to$ inclusive) (240 GeV) events.

2.2 Key Detector Features for Flavor Physics

Flavor physics program at Tera-Z is enormously rich and extremely demanding on detector performance. In general, a Tera-Z detector would have a large acceptance with a solid angle coverage of at least $|\cos\theta| < 0.99$. This detector would also have a low energy/momentum threshold at the 100 MeV level to record and recognize low energy objects that characterize certain hadron decays, *e.g.*, soft photons and pions generated from excited heavy hadrons, as well as some low energy hadrons that are essential for understanding relevant QCD processes [30].

To efficiently separate signal events from background, it is essential to identify the relevant physics objects and to precisely reconstruct their properties – especially their energy/momentum. For a Tera-Z detector, a typical benchmark is to reconstruct the intermediate particles, such as $\pi^0 \to \gamma\gamma$, $K^0_S \to \pi^+\pi^-$, $\phi \to K^+K^-$, $\Lambda \to p\pi^-$, etc., inside hadronic Z events. A more challenging case would be to identify the decay products of a target heavy flavor hadron which may decay into $\mathcal{O}(10)$ particles with a complicated and rich decay cascading order inside a jet. These decay products include not only charged final state particles (leptons and charged hadrons), but also photons, neutral hadrons, and the missing energy/momentum induced by neutrinos. A hadronic Z event could have up to 100 final state particles, as shown in Figure 2. To successfully separate and reconstruct the decay products of the target particle is a key challenge for measurements performed in hadronic Z events, for which it is necessary to employ the particle flow method [31, 32]. Such a method emphasizes the separation of final state particles and has been proven capable of providing better reconstruction of both the hadronic system and of the missing energy/momentum.

In addition, good intrinsic resolution of subdetectors, (*i.e.*, momentum reconstruction by the tracker and energy measurement by the calorimeter), is always critical for flavor physics measurements. It not only leads to the precise reconstruction of physics proper-

ties such as particle masses, but also significantly reduces the combinatorial background especially present in physics measurements with narrow resonances. In particular, determining how to achieve an excellent electromagnetic (EM) energy resolution with a particle flow oriented high-granularity calorimeter is indeed challenging but necessary for the flavor physics program, since photons and neutral pions are common decay products in many fundamental flavor physics measurements. A benchmark analysis [33] of the measurement of the standard CKM unitarity triangle angle α via $B^0 \to \pi^0\pi^0$ suggests an EM resolution of order $\mathcal{O}(3\%/\sqrt{E/\mathrm{GeV}})$ to fulfill the requirement of $3\,\sigma$ separation between B^0 and B^0_s with a 30 MeV B-meson mass resolution.

Most of the flavor physics measurements at the CEPC will involve hadronic events, especially di-jet events at the Z pole. It is essential to identify the origin of a jet, *i.e.*, to determine whether it originates from a quark, an anti-quark, or even a gluon. The jet origin identification [34], to a certain extent, shall be regarded as a natural extension of jet flavor tagging, quark-gluon jet separation, and jet charge measurements, which is indispensable in flavor physics measurements such as CKM and CP violation measurements.

A successful flavor physics program also needs high efficiency/purity PID. An efficient PID not only suppresses the combinatorial background, induced by misidentified particles, but also separates decays with similar topologies in the final states, such as $B^0_{(s)} \to \pi^+\pi^-$, $B^0_{(s)} \to K^+K^-$, and $B^0_{(s)} \to K^\pm\pi^\pm$ [35]. A decent PID is also critical for the jet origin identification [34, 36] and relevant physics measurements such as the Higgs rare/exotic decay measurement [34]. The benchmark analysis of $B^0_s \to \phi\nu\bar{\nu}$ [37] shows that a relative uncertainty of $\mathrm{BR}(B^0_s \to \phi\nu\bar{\nu})$ less than 2% at a Tera-Z collider requires a $3\,\sigma$ $K^\pm/\pi^\pm$ separation for the identification of charged hadrons, see the left panel of Figure 3. This requirement can be addressed by multiple PID technologies. For instance, the CEPC baseline detector can separate different species of hadrons using dE/dx information measured by TPC and TOF information provided by either a dedicated TOF device, or by combining TOF and ECAL together. Detector optimization studies [38] suggests that dE/dx needs to reach 3% in combination with a TOF resolution of 50 ps to statisfy this PID requirement. In addition, the dN/dx cluster-counting method proposed by the IDEA drift chamber [39] is promising to further improve the PID performance.

A high-precision and low-material vertex system is vital for the CEPC flavor physics program. Precise vertex measurements provide pivotal information to distinguish the species of the initial quark that fragments into a jet, namely the jet origin identification. Precise vertex information is also critical for determining the decay time or lifetime of heavy flavor hadrons with high precision. To match the characteristic timescales such as those of $B^0_s - \bar{B}^0_s$ mixing (~ 56 fs), of D_s decay (~ 500 fs), and of τ decay (~ 290 fs), the decay time resolution is required to reach order $\mathcal{O}(10)$ fs. These accurate lifetime measurements will also benefit flavor tagging and time-dependent CP violation measurements. In addition, a high-performance vertex system can provide a precise reconstruction of the secondary vertices that characterize some of the heavy flavor hadron decays, such as the example shown in Figure 4. Such a system can also help to suppress the backgrounds, especially from the IP. One concrete application can be the measurements of FCCC $\mathrm{BR}(H_b \to H_c\tau\nu_\tau)$, where the reconstruction of the b hadron H_b can significantly rely on the determination of the de-

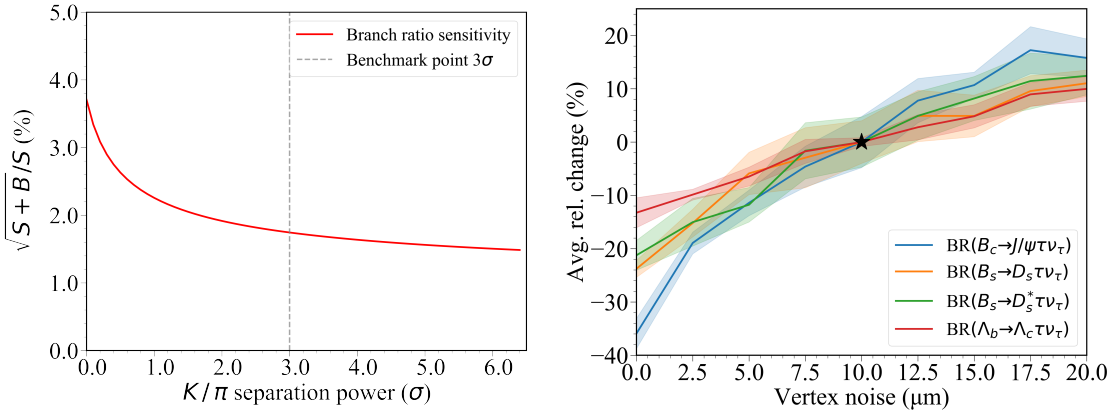

Figure 3: **LEFT:** Uncertainty of measuring BR($B_s^0 \to \phi\nu\bar{\nu}$) as a function of PID performance, parameterized by the K/π separation power [37]. **RIGHT:** Precision variance of measuring BR($H_b \to H_c\tau\nu_\tau$) as a function of detector vertex noise [40], with starred reference point set by a vertex uncertainty of 10 μm.

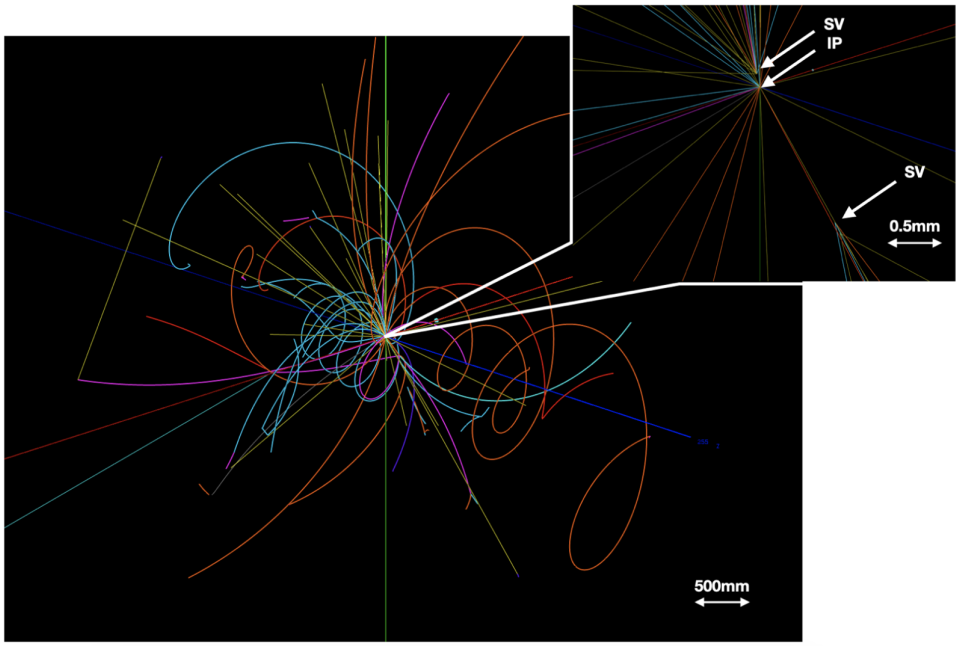

Figure 4: Display of a $Z \to b\bar{b}$ event with typical secondary vertices (SV).

cay vertex of the charmed hadron H_c and on the measurement of the muon track originating from the τ decay [40]. As shown in the right panel of Figure 3, the improved resolution of vertex system can uniformly benefit these measurements, yielding an improvement in precision of $\mathcal{O}(10\%)$ level.

The above-mentioned requirements are also highly beneficial for the physics programs at higher center-of-mass energies, *i.e.*, the 160 GeV W^+W^- threshold scan, the 240 GeV

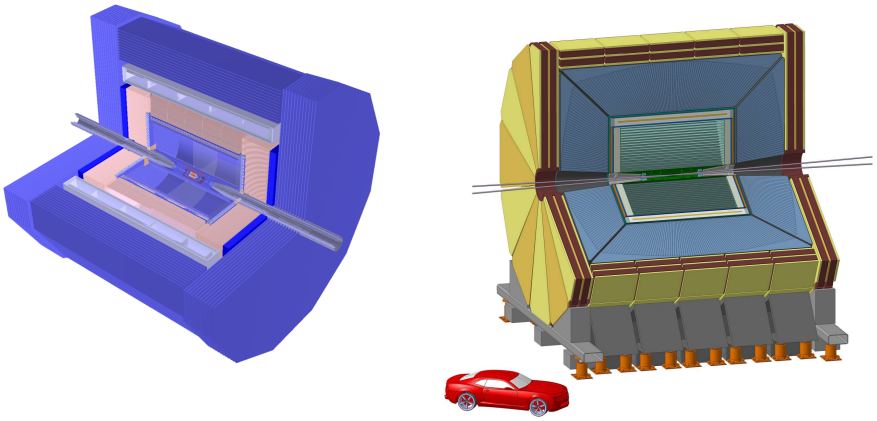

Figure 5: Schematic layouts of the CEPC baseline detector [2] (left) and the IDEA detector [41] (right).

Higgs run, and the 360 GeV top-pair operation. On top of their core physics programs, such as W mass and precise Higgs/top properties measurements, the data samples and key detector features also support an intensive flavor physics program, see Section 9.

To address these physics requirements, intensive efforts on detector conceptual design, on physics performance study, and on key technology R&D have been performed. We refer to two benchmark detector concepts in this white paper. These concepts are used in the simulations in this manuscript, providing reference performance for relevant physics potential studies.

The starting point of our discussion is the CEPC baseline detector as delineated in its CDR study [2]. Guided by the particle flow principle, the CEPC baseline design features a high-precision tracking system, a high-granularity calorimeter system, and a high magnetic field. As shown in detail in Figure 5, the CEPC baseline detector consists, from inside to outside, of a silicon pixel vertex detector, a silicon tracker, a time projection chamber (TPC), a silicon-tungsten sampling EM calorimeter (Si-W ECAL), a steel-glass resistive plate chambers sampling hadronic calorimeter (SDHCAL), a superconducting solenoid providing a magnetic field of 3 Tesla, and a flux return yoke embedded with a muon detector. Additionally, the Si-W ECAL could also be instrumented with a few timing layers to enable time-of-flight (TOF) measurements with a precision of 50 ps or even better [2, 42].

Alongside the CEPC baseline detector, an alternative detector concept known as IDEA (Innovative Detector for Electron-positron Accelerator) [41] is also utilized in various studies covered in this white paper. In comparison to the CEPC baseline detector, the IDEA detector incorporates a dual readout calorimeter system to attain superior energy resolution for both EM and hadronic showers. Moreover, the IDEA detector operates with a reduced magnetic field of 2 Tesla while compensating for this reduction by offering a larger tracking volume. The overall structure of the IDEA detector can be seen in Figure 5.

By virtue of the particle flow oriented design, the CEPC baseline detector performs well in efficient tracking, lepton identification, and precise reconstruction of hadronic systems.

Item	Baseline [2]	Objective	Comments
Basic Performance			
Acceptance	$\lvert\cos\theta\rvert < 0.99$ [2]		
Threshold	200 MeV [43, 44]	100 MeV	For tracks & photons
Beam energy spread	$\mathcal{O}(0.1\%)$ [2]		
Tracker momentum resolution	$\mathcal{O}(0.1\%)$ [2]		
ECAL energy resolution	$17\%/\sqrt{E} \oplus 1\%$ [2]	$3\%/\sqrt{E}$ [33]	
HCAL energy resolution	$60\%/\sqrt{E} \oplus 1\%$ [2]		
Vertex resolution	10–200 μm [2]		
Jet energy resolution	3–5% [2, 45]		For 20–100 GeV
$\ell - \pi$ mis-ID	$< 1\%$ [46]		In jet, $\lvert\vec{p}\rvert > 2$ GeV
$\pi - K$ separation	$> 2\sigma$ [2]	$> 3\sigma$ [37]	In jet, $\lvert\vec{p}\rvert > 1$ GeV, TOF+dE/dx
Flavor Physics Benchmarks (Depending on the Above)			
$\sigma(m_{H,W,Z})$	3.7% [2]		Hadronic decays
b-jet efficiency×purity	$\sim 86\%$ [34]		In Z hadronic decays
c-jet efficiency×purity	$\sim 64\%$ [34]		In Z hadronic decays
b-jet charge tagging $\epsilon_{\text{eff}} = \epsilon(1-2\omega)^2$	$\sim 37\%$ [34]		For B_s^0
c-jet charge tagging $\epsilon_{\text{eff}} = \epsilon(1-2\omega)^2$	$\sim 60\%$ [34]		
π^0 efficiency×purity	$\gtrsim 70\%$ [44]	$\gtrsim 80\%$ [33]	In Z hadronic decays, $\lvert\vec{p}_{\pi^0}\rvert > 5$ GeV
K_S^0, Λ efficiency	60%-85% [47]		In Z hadronic decays, all tracks
τ efficiency×purity	70% [48]		In $WW \to \tau\nu q\bar{q}'$, inclusive
τ mis-ID	$\mathcal{O}(1\%)$ [48]		In $WW \to \tau\nu q\bar{q}'$, inclusive

Table 4: Summary of detector performance of the CEPC baseline detector and some objectives for flavor physics benchmarks.

These excellent features of the CEPC baseline detector provide a solid basis for flavor physics studies. The expected performance of the CEPC baseline detector is summarized in Table 4. Notably, the baseline tracking system demonstrates an efficiency close to 100% and a relative momentum resolution approaching $\mathcal{O}(10^{-3})$ for individual tracks with momenta exceeding 1 GeV within the barrel region, as illustrated in Figure 6. As depicted in left panel of Figure 7, the baseline photon energy resolution is $17\%/\sqrt{E} \oplus 1\%$, achieved by the sampling Si-W ECAL, which features the high granularity critical for particle flow reconstruction. In terms of PID performance, the CEPC baseline design achieves a K/π separation better than $2\,\sigma$ in the momentum range up to 20 GeV by effectively combining TOF and dE/dx information, as shown in Figure 8. The inclusive $Z \to q\bar{q}$ sample exhibits an overall $K^{\pm}$ identification efficiency and purity exceeding 95% [38]. Regarding hadronic systems, the CEPC baseline detector attains a boson mass resolution (BMR) better than 4% for hadronically decaying W, Z, and Higgs bosons, as illustrated in right panel of Figure 7. This not only enables a separation exceeding $2\,\sigma$ between W and Z bosons in their hadronic decays, but also enhances the precision of missing energy/momentum measurements, which are vital for flavor physics investigations.

Following the completion of the CEPC CDR, there are still ongoing research efforts focused on the detector design to further optimize the baseline performance parameters and to cater to the requirements for the CEPC flavor physics program. These optimization

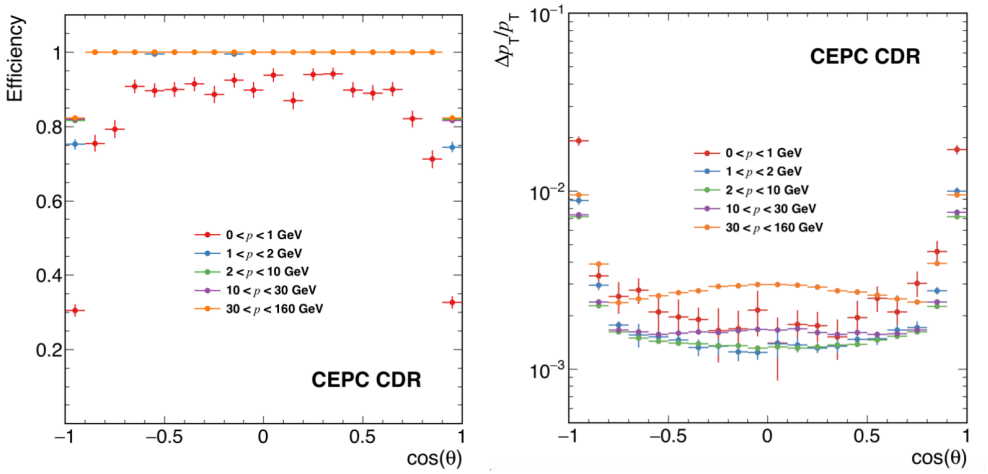

Figure 6: Single track reconstruction efficiency (left) and momentum resolution (right) of the CEPC baseline detector [2].

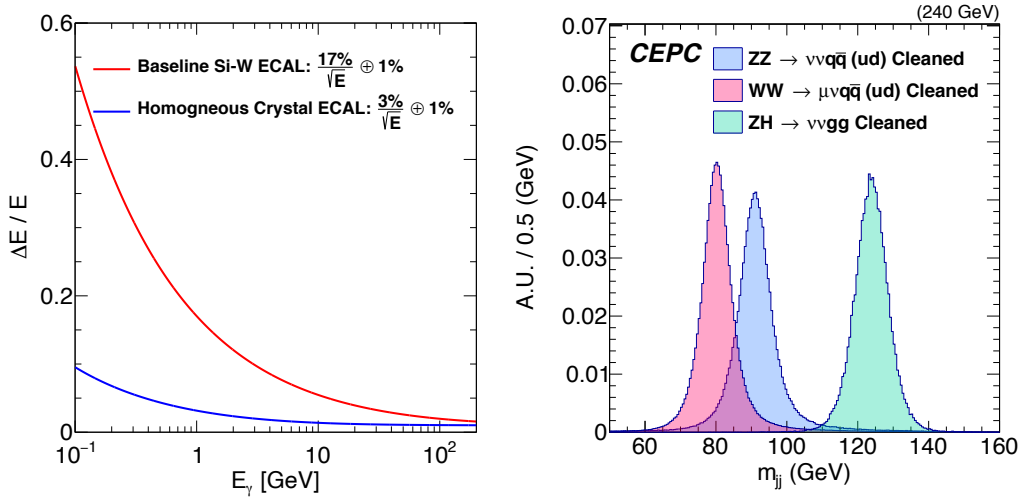

Figure 7: **LEFT:** Comparison of the CEPC baseline photon energy resolution achieved by the sampling Si-W ECAL [2] and expected photon energy resolution of homogeneous crystal ECAL. **RIGHT** Reconstructed boson masses of cleaned $\nu\bar{\nu}q\bar{q}$, $l\nu q\bar{q}$, and $\nu\bar{\nu}H$, $H \to gg$ events [45].

efforts primarily concentrate on three key aspects: EM energy resolution, PID performance, and jet charge measurements. To address the demand for improved separation of B^0 and B_s^0 with EM final states, a significantly enhanced EM energy resolution of $3\%/\sqrt{E}$ [33] is pursued, as compared to the baseline resolution of $17\%/\sqrt{E} \oplus 1\%$ shown in left panel of Figure 7. Accompanying this resolution enhancement, a corresponding photon energy threshold of 100 MeV is envisioned. To attain this level of EM resolution while maintaining compatibility with Particle Flow Algorithm (PFA) performance, novel concepts for high-resolution and high-granularity crystal ECAL designs have been proposed [49–51], and

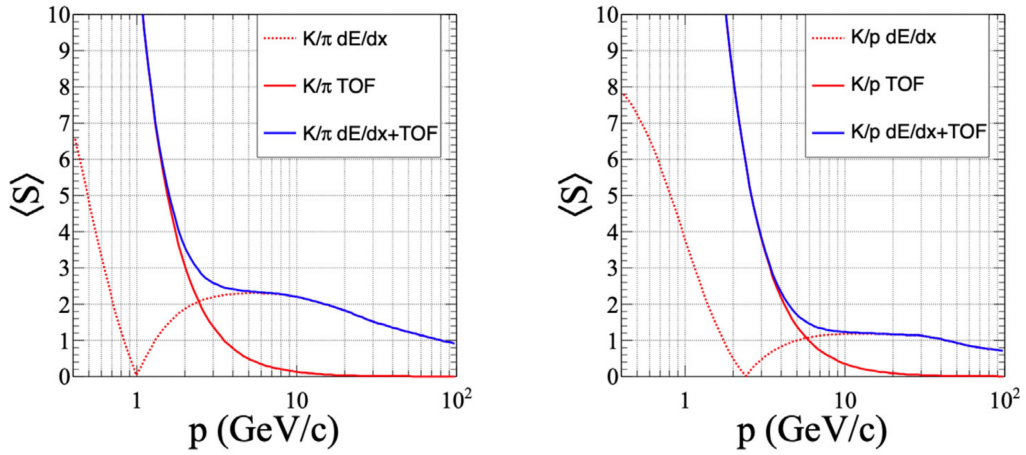

Figure 8: Separation power of K/π (left) and K/p (right) using different techniques [38].

relevant R&D studies [52] are progressing. For PID performance, a K/π separation better than $3\,\sigma$ is desired. This improved PID capability can be achieved by combining various techniques, including TOF [53, 54], dE/dx [38, 55], and dN/dx [39] measurements. The performance of jet charge measurement is typically characterized by the effective tagging efficiency (power) $\epsilon_{\text{eff}} \equiv \epsilon_{\text{tag}}(1-2\omega)^2$, where ϵ_{tag} is the flavor tagging efficiency and ω is the wrong tag fraction. The study [36] develops a Leading Particle Jet Charge method (LPJC) and combines it with a Weighted Jet Charge (WJC) method to form a Heavy Flavor Jet Charge method (HFJC). This study evaluates the effective tagging power for c/b jets at the CEPC Z pole operation and finds it to be 39%/20%. Additionally, by implementing benchmark impact parameter cuts of 0.02/0.04 mm to distinguish the origin of the leading charged particle (whether from the decay of the leading heavy hadron or QCD fragmentation), the effective tagging power for c/b jets was found to be 39.0%/26.8%. Furthermore, a dedicated b-jet charge tagging algorithm developed specifically for the study of $B_s^0 \to J/\psi\phi$ at the CEPC [56] achieved an effective tagging power of 20%.

Recently, the idea of jet origin identification has been proposed. This idea aims at identifying simultaneously the jets originated from eleven different colored particle species of the SM, namely 5 quarks (u, d, s, c, b), the corresponding anti-quarks, and gluons. The jet origin identification combines the concepts of jet flavor tagging, jet charge measurement, strange jet and gluon jet identification together. The idea of jet origin identification is then realized at the full simulated data of CEPC CDR baseline detector and using state-of-the-art reconstruction tools, including the Arbor Particle flow reconstruction and the ParticleNet algorithm [57], which simultaneously reaches jet flavor tagging efficiencies of 92%, 79%, 67%, 37%, and 41% and jet charge flip rates of 18%, 7%, 15%, 15%, and 19% for b, c, s, u, and d quarks, respectively, and meanwhile it could deliver a gluon jet identification efficiency of 66% [34], see Figure 9. These performances infer an effective tagging power of 37%/54% for b/c-jet, respectively, see Table 4. Consequently, a range of $\epsilon_{\text{eff}} \in [15, 37]\%$ and $[39, 54]\%$ are determined for the future b-jet and c-jet charge tagging power at the CEPC, see Table 4.

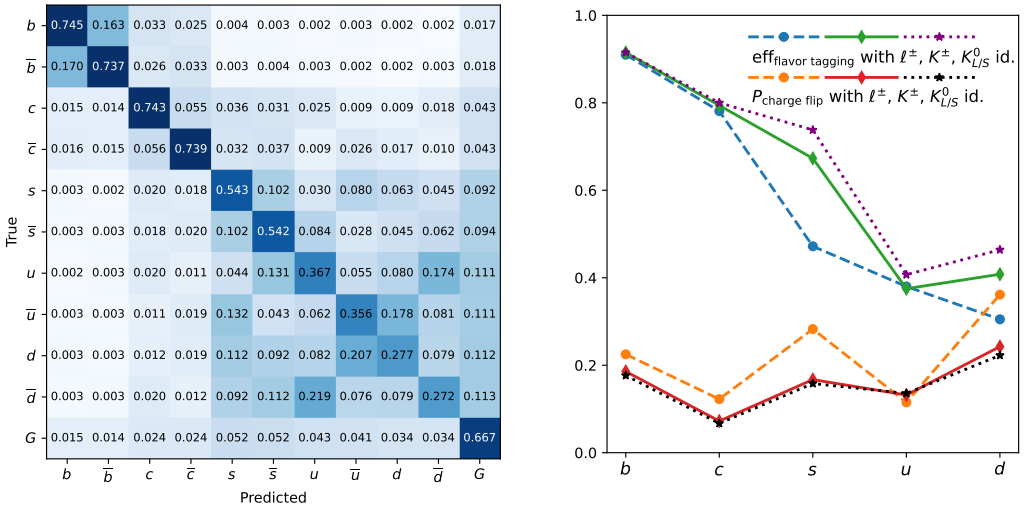

Figure 9: Jet origin identification performance [34] of full simulated Higgs/Z to di-jet processes with CEPC conceptual detector. **LEFT:** The confusion matrix M_{11} with perfect identification of leptons and charged hadrons. **RIGHT:** Jet flavor tagging efficiency and charge flip rates for quark jets with different scenarios of particle identification: with only lepton identification, plus identification of charged hadrons, plus identification of neutral kaons.

The jet origin identification has significant impact on many physics measurements at the future electron positron Higgs factories. For instance, the rare and exotic hadronic Higgs boson decays (see Section 9.2), the determination of CKM matrix elements directly from W boson decay (see Section 9.1), the time-dependent CP measurements, the measurements of weak mixing angle, the differential measurements with multi-jet final states, etc.

2.3 Simulation Method

To explore the flavor physics potential of the CEPC, various benchmark analyses that have been evaluated at the simulation level are covered in this manuscript. Many of them are performed in the CEPC official software framework, illustrated in Figure 10, with full simulation and reconstruction of the baseline detector. Limited by the available computing resource, a dataset of $\mathcal{O}(10^9)$ generator level inclusive $Z \to q\bar{q}$ events is generated for the physics potential studies at Tera-Z. Since the full simulation of the whole dataset is computationally expensive and time-consuming, pre-selections are generally applied to refine the dataset into core subsets. The analysis of $B_c \to \tau\nu_\tau$ in Section 3, the study of $B_s^0 \to \phi\nu\bar{\nu}$ in Section 4, and the ϕ_s measurement via $B_s^0 \to J/\psi\phi$ in Section 5 are three typical examples.

For some studies, especially those that are oriented towards phenomenology and detector requirements, fast simulation is usually adopted. Based on the understanding of detector responses and validated by the full simulation results, key detector performance is parameterized and modelled, and its effect on final physics observables is evaluated ac-

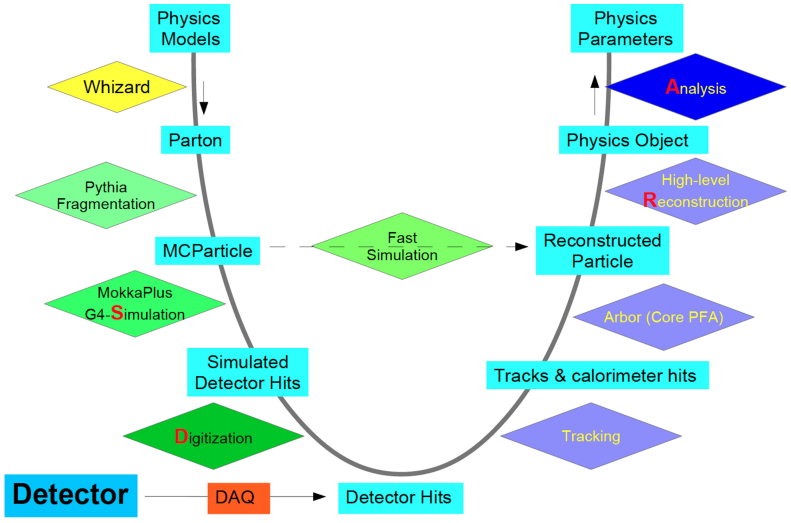

Figure 10: The CEPC official software chain and analysis flow [58]. More detailed information can be found in the CEPC CDR [2].

cordingly. This evaluation is used in studies such as the measurement of the α angle via $B^0_{(s)} \to \pi\pi$ channels discussed in Section 5. In this way, we can investigate the whole parameter space as much as possible with fast convergence.

To make the physics picture complete, we also list many benchmarks that have not been fully explored and recommend them for future studies of the CEPC flavor physics program. Conjectures are made for some benchmarks, such as τ relevant studies in Section 7 and exclusive hadronic Z decays in Section 8.2.

3 FCCC Semileptonic and Leptonic *b*-Hadron Decays

Historically, β decays, probably the best-known FCCC processes, have resulted in the discovery of weak interactions. While the sensitivities to heavy-flavor semileptonic and leptonic FCCC decays in ongoing experiments are limited, they will be a significant topic for flavor physics in the CEPC era. Firstly, measuring the signal rates of these channels can be used to determine the values of the CKM matrix elements such as V_{cb} and V_{ub} [59]. Moreover, by performing these measurements, one can test lepton flavor universality (LFU), one of the most important predictions of the SM, see Ref. [60–62] for reviews. In this way, FCCC measurements can serve as an efficient way to probe NP that couples with different strengths to different lepton families. For instance, given a relative deviation $\delta_{\rm SL}$ in the signal rate from the SM prediction, the energy scale probed can reach

$$\Lambda^{\rm SL}_{\rm NP} \sim (G_F |V_{cb}| \delta_{\rm SL})^{-\frac{1}{2}} \sim (1.5\ {\rm TeV}) \times \delta_{\rm SL}^{-\frac{1}{2}} \tag{3.1}$$

for $b \to c\ell\nu$ transitions and

$$\Lambda^{\rm SL}_{\rm NP} \sim (G_F |V_{ub}| \delta_{\rm SL})^{-\frac{1}{2}} \sim (5\ {\rm TeV}) \times \delta_{\rm SL}^{-\frac{1}{2}} \tag{3.2}$$

Figure 11: Illustrative Feynman diagrams for the decay $B_c^+ \to \tau^+\nu_\tau$. **LEFT**: SM example. **RIGHT**: BSM example.

for $b \to u\ell\nu$ transitions. Notice that here the NP effective interactions have been assumed to be agnostic about the SM flavor structure and have strengths of $\mathcal{O}(1)$.

The operation of the CEPC at the Z pole enables the detector to access a full spectrum of b hadrons with high statistics, including multiple heavy-flavored mesons like B_c and baryons like Λ_b, which are b-hadrons not accessible at the past and planned runs of the B-factories. Measuring their (semi)leptonic decays would cross-validate our current understanding of FCCCs and further reveal hitherto unexplored physics. Particularly interesting among the list of expected measurements are the ones involving τ decays. These measurements are crucial for, *inter alia*, achieving a full test of LFU. However the multibody decays of τ leptons complicate the event topology and kinematics. Even worse, the signature of neutrinos as missing momentum is hardly accessible at hadron colliders. The event reconstruction thus becomes a challenging task. In contrast, the reconstruction of these events including the τ leptons and other particles may greatly benefit from the excellent collider environment of the CEPC and the high-performance of its detector. These measurements thus define one of the "golden" channels for flavor physics at the CEPC.

The above discussion can also be applied to the measurement of FCNC processes. Since such processes are forbidden at tree level and suppressed at loop level in the SM, these channels are capable of probing NP (see detailed discussions in Section 4). The results obtained from both classes of measurements can be interpreted in various NP models. In a simplified NP model, these processes can arise from either colorless or colored mediators. The simplest colorless example might be a family non-universal Z' boson with off-diagonal couplings to both quarks and leptons, thus yielding FCNC processes, see, *e.g.*, [63, 64]. This setup can be extended to a framework with an extra $SU(2)$ gauge triplet, where the additional W' gauge bosons will contribute to the FCCC processes [65]. Another example is provided by leptoquarks, namely scalar or vector bosons that couple to quarks and leptons simultaneously and therefore carry color. Leptoquarks are predicted by a wide range of ultraviolet (UV) theories such as grand unified theories, supersymmetry, composite Higgs models, etc. – for a review see [66]. Such interpretations are model-dependent, hence often limited in their applicability.

Alternatively, one can interpret the results in an Effective Field Theory (EFT) framework. The EFT is usually defined to parameterize the NP effects by integrating out the short distance physics. As a manifestation of physics at a low energy scale, the EFT is insensitive to the concrete format of UV physics. Here, let us consider the low-energy EFT (LEFT) [67] with a natural cutoff at the EW-breaking scale. For $b \to c\ell\nu$ transitions, we

have the dimension-6 LEFT Hamiltonian

$$\mathcal{H}^{\text{eff}}_{b\to c\ell\nu} = \frac{4G_F}{\sqrt{2}} V_{cb} \sum_i C_i O_i + \text{h.c.}\,, \tag{3.3}$$

where O_i denote the left(right)-handed scalar, vector, an tensor operators, namely

$$\begin{aligned} O_{S_{L(R)}} &= (\bar{c} P_{L(R)} b)(\bar{\ell} P_L \nu)\,, \\ O_{V_{L(R)}} &= (\bar{c}\gamma^\mu P_{L(R)} b)(\bar{\ell}\gamma_\mu P_L \nu)\,, \\ O_T &= (\bar{c}\sigma^{\mu\nu} b)(\bar{\ell}\sigma_{\mu\nu} P_L \nu)\,, \end{aligned} \tag{3.4}$$

and C_i represent the corresponding Wilson coefficients. The SM can only contribute to C_{V_L} via the exchange of a W boson. Any deviation from this prediction will indicate the presence of NP, and the specific pattern of such deviation will carry crucial information on the nature of the underlying NP sector. For example, the $B_q \to \tau\nu$ ($q = u, c$) process, shown in Figure 11, is sensitive to the axial vector ($C_{V_L} - C_{V_R}$) and pseudoscalar ($C_{S_L} - C_{S_R}$) Wilson coefficients:

$$\begin{aligned} \text{BR}(B_q^+ \to \tau^+\nu_\tau) = \tau_{B_q^+} \frac{G_F^2 |V_{qb}|^2 f_{B_q^+}^2 m_{B_q^+} m_\tau^2}{8\pi} \left(1 - \frac{m_\tau^2}{m_{B_q^+}^2}\right)^2 \\ \times \left| 1 + (C_{V_L} - C_{V_R}) - \frac{m_{B_q^+}^2}{m_\tau\,(m_b + m_q)} (C_{S_L} - C_{S_R}) \right|^2 , \end{aligned} \tag{3.5}$$

where G_F is the Fermi constant, m_τ is the mass of the τ lepton, and $m_{B_q^+}$, $\tau_{B_q^+}$ and $f_{B_q^+}$ denote the B_q^+ mass, lifetime and decay constant, respectively.

The SM prediction for the BR of the decay $B_c \to \tau\nu$ is rather large, $\sim 2.3 \times 10^{-2}$ [69], but the current constraint is comparatively weak, $\text{BR}(B_c \to \tau\nu) \lesssim 30\%$. Detailed studies indicate that a Tera-Z factory can measure this BR with a precision of $\mathcal{O}(10^{-4})$ [68–70]. In particular, the CEPC study in Ref. [68] employs a full simulation and incorporates leptonic τ decays $\tau^\pm \to \ell^\pm \nu\bar{\nu}$. The main features to distinguish B_u^+ from B_c^+ arise from the difference in their lifetime and the hadrons associated with their hadronization processes. As illustrated by Figure 12, a measurement of the SM rate of $B_c \to \tau\nu$ with relative precision as high as $\mathcal{O}(1\%)$ can be achieved at the Tera-Z run of the CEPC. The study in Ref. [69] instead focuses on the 3-prong τ decay, $\tau^\pm \to \pi^\pm\pi^\pm\pi^\mp\nu$. Within the considered analysis scenarios, the expected precision of the measurements of the SM rates ranges from 1.6% to 2.3% for $B_c^+ \to \tau^+\nu_\tau$ and from 1.8% to 3.6% for $B^+ \to \tau^+\nu_\tau$.

Under the assumption that NP effects such as LFU violating interactions are absent, Eq. (3.5) can be used to extract $|V_{qb}|$ from $B_q \to \tau\nu$ decay rates, as demonstrated in [69]. Such a determination of $|V_{qb}|$ is of particular interest at future e^+e^- flavor machines, because it provides a clean and independent measurement compared to the current results [11, 71–73] and may cast new light on the long-standing discrepancy between the inclusive and exclusive determinations [11]. The $|V_{qb}|$ determination from the $B_q \to \tau\nu$ depends on precise inputs of the decay constants $f_{B_q^+}$ as well as the production fractions

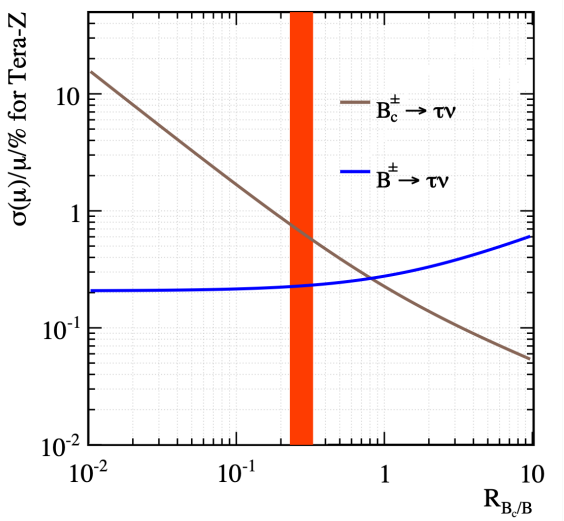

Figure 12: Relative precision of measuring the $B^{\pm}_{(c)} \to \tau\nu$ rate at the CEPC Tera-Z, as a function of $R_{B_c/B} \equiv N(B^{\pm}_c \to \tau\nu)/N(B^{\pm} \to \tau\nu)$ [68]. Here the red band denotes the SM prediction for $R_{B_c/B}$.

of the B^+_q mesons. For instance, the current relative precision is $\sim 0.7\%$ for $f_{B^+_u}$ [74] and $\sim 4.6\%$ for $f_{B^+_c}$ [75], which will be improved in the coming decade. The B^+ production fraction is currently known with a $\sim 2\%$ precision [76] and will be significantly improved in the CEPC era with the abundant $Z \to b\bar{b}$ data. As for the B^+_c production fraction, however, no existing measurement or future projection is currently available. For this reason, we focus the following discussion on the determination of $|V_{ub}|$.

With the high precision measurement of $\mathrm{BR}(B^+ \to \tau^+\nu_\tau)$ expected at Tera-Z factories [68, 69] and the theoretical uncertainties described above, we expect the determination of $|V_{ub}|$ to reach a relative precision of 1% or better. In comparison, the Belle II experiment is expected to perform a similar determination with a relative precision of 2-3% employing the full integrated luminosity [8]. This can also be compared to the current best measurements [11], which are $(4.19 \pm 0.12^{+0.11}_{-0.12}) \times 10^{-3}$ from the inclusive determination, and $(3.51 \pm 0.12) \times 10^{-3}$ from the exclusive determination, which denote a relative discrepancy of more than 15%.

In summery, the $|V_{ub}|$ measurement from $B_u \to \tau\nu$ at CEPC can provide crucial information to resolve the tension between inclusive and exclusive determination. In principle, the same statement also applies to the $B_c \to \tau\nu$ decay and the determination of $|V_{cb}|$, although the exact precision that one can reach relies on the values of $f_{B^+_c}$ and the B_c yield at the Z pole, which call for further studies.

As mentioned above, one can test LFU by employing the $b \to c\ell\nu$ measurements. LFU follows from the fact that, in the SM, the three lepton families have the same gauge charges. Hence, in the SM, any difference between the decays into different leptons can only arise from the Yukawa sector. To perform the test of LFU, one typically introduces ratios of

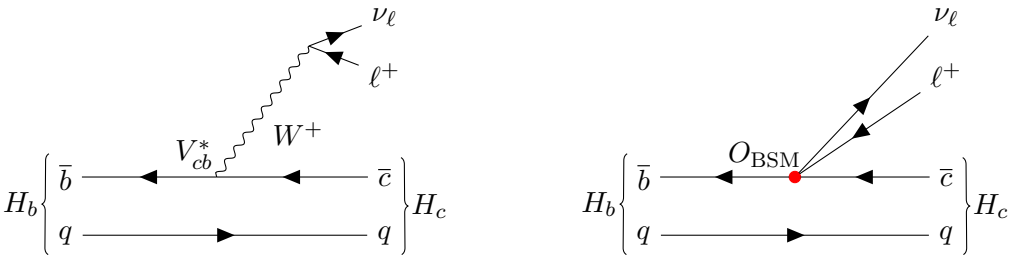

Figure 13: Illustrative Feynman diagrams for the transition $H_b \to H_c \ell^+ \nu_\ell$. **LEFT**: SM example. **RIGHT**: BSM example.

R_{H_c}	SM Value	Tera-Z	4×Tera-Z	10×Tera-Z
$R_{J/\psi}$	0.289	4.3×10^{-2}	2.1×10^{-2}	1.4×10^{-2}
R_{D_s}	0.393	4.1×10^{-3}	2.1×10^{-3}	1.3×10^{-3}
$R_{D_s^*}$	0.303	3.3×10^{-3}	1.6×10^{-3}	1.0×10^{-3}
R_{Λ_c}	0.334	9.8×10^{-4}	4.9×10^{-4}	3.1×10^{-4}

Table 5: SM predictions for the R_{H_c} observables and relative precision for their measurements at Tera-Z, 4×Tera-Z, and 10×Tera-Z, considering statistical uncertainties only [40].

branching ratios such as

$$R_{H_c} = \frac{\mathrm{BR}(H_b \to H_c \tau \nu_\tau)}{\mathrm{BR}(H_b \to H_c \ell' \nu_{\ell'})}, \tag{3.6}$$

where $H_{b(c)}$ represents a $b(c)$-hadron, and $\ell' = e, \mu$ unless stated otherwise. For these observables, the systematics, such as the uncertainties from the CKM matrix elements and form factors, largely cancel. As an illustration, we show the Feynman diagrams for the SM and BSM contributions to the $H_b \to H_c \ell^+ \nu_\ell$ transitions in Figure 13.

For the test of LFU at the Z pole, a variety of R_{H_c} observables (R_{D_s}, $R_{D_s^*}$, $R_{J/\psi}$, and R_{Λ_c}) have been recently investigated employing the fast simulation template of the CEPC [40]. The relative precisions that can be achieved, considering statistical errors only, are summarized in Table 5. Systematic uncertainty in the R_{H_c} measurements are expected to cancel largely since R_{H_c} denotes a ratio of two parallel measurements. This study indicates that at Tera-Z, a relative precision of $\lesssim 5\%$ for $R_{J/\psi}$, as well as $\lesssim 0.4\%$ and $\sim 0.1\%$ for $R_{D_s^{(*)}}$ and R_{Λ_c}, respectively, could be reached. Due to the complex topology and dynamics, these outcomes rely heavily on a vertex-based strategy for event reconstruction. Thus, they would benefit from a higher detector performance in general. Concretely, the $R_{J/\psi}$ measurement benefits the most from the improvement of tracker resolution, (see right panel of Figure 3 also), in reconstructing the $B_c^\pm$ vertex as well as in identifying the J/ψ one, while the $R_{D_s^{(*)}}$ measurements gain more from the increase of soft photon identification efficiency in distinguishing the D_s^* and D_s modes via the decay $D_s^* \to D_s \gamma$.

Note that these measurements cover a variety of $b \to c\tau\nu$ transitions: such as the ones from pseudoscalar ($B_{s,c}$) to vector (D_s^*, J/ψ) or pseudoscalar (D_s); those from baryon (Λ_b) to another baryon (Λ_c); and the decays of a pseudoscalar (B_c) to a pair of fermions. Consequently, they can be employed to constrain different LEFT operators that can induce

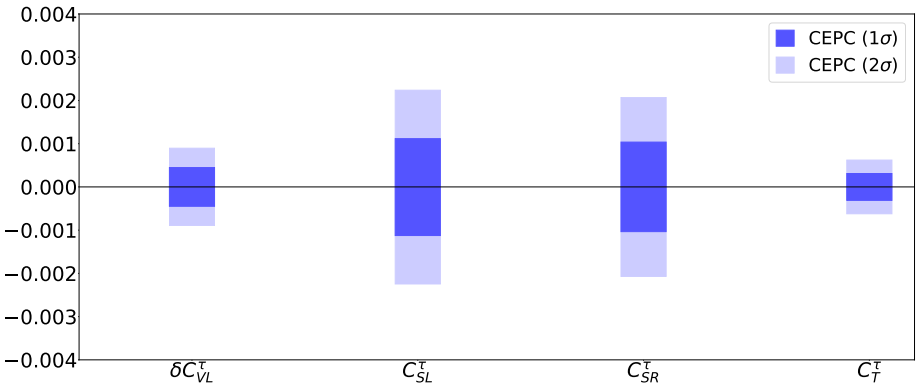

Figure 14: Marginalized constraints on the Wilson coefficients of $b \to c\tau\nu$ LEFT at the CEPC, with $\delta C^{\tau}_{V_L} = C^{\tau}_{V_L} - \delta C^{\tau}_{V_L,\mathrm{SM}}$. This plot is taken from Ref. [40].

Process	Observable
$b \to c l\nu$	$R_{H_c}(R_{J/\psi}, R_{D_s^{(*)}}, R_{\Lambda_c})$
$B_c \to \tau\nu$	$\lvert V_{cb}\rvert$
$B \to \tau\nu$	$\lvert V_{ub}\rvert$

Table 6: List of benchmark FCCC semileptonic and leptonic b-decay channels that can be investigated at CEPC.

$b \to c\tau\nu$ transitions. Following the approach in Ref. [40], we present in Figure 14 the marginalized constraints on the Wilson coefficients of $b \to c\tau\nu$ LEFT at the CEPC, based on the results of [40, 68]. In this context, these Wilson coefficients can be universally constrained to a level of $\mathcal{O}(10^{-3})$.[1]

Additionally, several unexplored topics of FCCC physics deserve attention. Firstly, in view of the scientific significance of testing LFU, it is necessary to establish the CEPC sensitivity for a full list of R_{H_c} measurements including the traditional R_D and R_{D^*}, higher-resonant $R_{D^{**}}$ [77], remaining baryonic modes such as R_{Ξ_c}, etc., and their corresponding differential measurements. Also, to provide an LFU test for all three generations, it is natural to extend the studies to the measurements of $\mathrm{BR}(b \to c\mu\nu)/\mathrm{BR}(b \to ce\nu)$, where it is crucial to reduce the systematics to a level comparable to the statistical errors. The relevant benchmark channels that can be investigated at CEPC are listed in Table 6. Secondly, the superior precision of measuring the B meson flight distance at the CEPC creates a new opportunity for the measurement of time-dependent CP-violation in semileptonic $b \to c\ell\nu$ decays. With this approach, the CP-violating markers in $B^0_{(s)} - \bar{B}^0_{(s)}$ mixing, which are encoded as $\mathcal{A}^d_{\mathrm{SL}}$ and $\mathcal{A}^s_{\mathrm{SL}}$ [78, 79] respectively, can be extracted by measuring the B^0 and B^0_s decays. As these measurements can contribute significantly to the global constraints on the parameters β and β_s [80, 81], where the current experimental precision remains far from the SM predictions, it is of high value to perform a more dedicated sensitivity analysis

[1] In this analysis, the operator O_{V_R} has been turned off, as it cannot be generated by UV physics respecting the $SU(2)_L$ gauge symmetry at a dimension-six level.

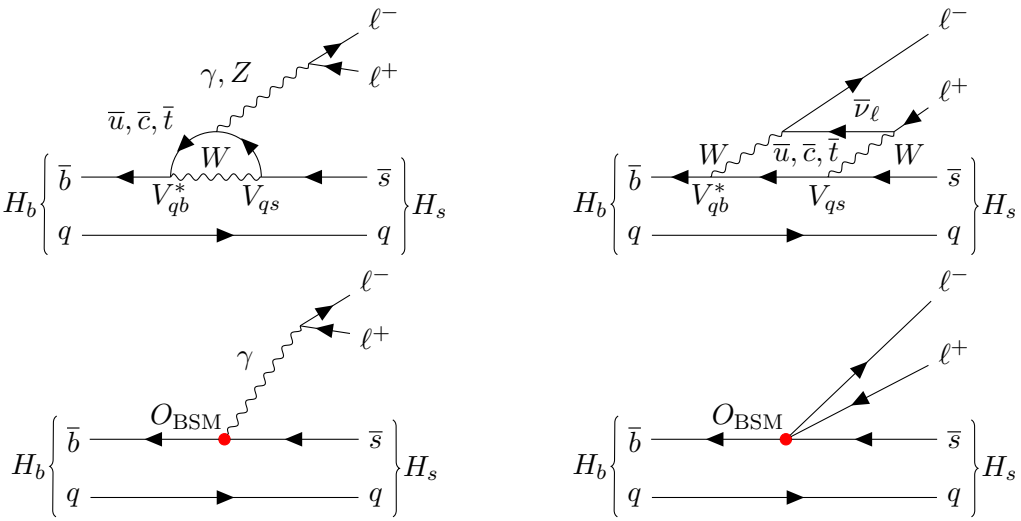

Figure 15: Illustrative Feynman diagrams for the transition $H_b \to H_s \ell^+ \ell^-$. **UPPER**: SM examples. **BOTTOM**: BSM examples.

with either fast or full simulations.

4 Rare *b*-Hadron Decays

FCNC transitions are prohibited at tree level in the SM. While being enabled by EW penguin or box diagrams (see Figure 15), these transitions are subject to a joint suppression by off-diagonal CKM matrix elements and loop factors, and thus are rare. Because of this feature, the FCNC processes emerge uniquely sensitive to weak NP effects that may otherwise evade detection. Given a relative deviation of $\delta_{\rm rare}$ in signal rate from the SM prediction, the energy scale probed can reach [82]

$$\Lambda_{\rm NP}^{\rm rare} \sim \left(\frac{\alpha}{4\pi}\frac{m_t^2}{m_W^2} G_F |V_{tb}V_{ts}^*| \delta_{\rm rare}\right)^{-\frac{1}{2}} \sim (30\ {\rm TeV}) \times \delta_{\rm rare}^{-\frac{1}{2}} \tag{4.1}$$

and

$$\Lambda_{\rm NP}^{\rm rare} \sim \left(\frac{\alpha}{4\pi}\frac{m_t^2}{m_W^2} G_F |V_{tb}V_{td}^*| \delta_{\rm rare}\right)^{-\frac{1}{2}} \sim (67\ {\rm TeV}) \times \delta_{\rm rare}^{-\frac{1}{2}} \tag{4.2}$$

for the $b \to s$ and $b \to d$ transitions, respectively. Notably, while the FCNC processes are rarer than the FCCC ones in the SM, $\Lambda_{\rm NP}^{\rm rare}$ can be comparable to, or even higher than, $\Lambda_{\rm NP}^{\rm SL}$ as long as $\delta_{\rm rare} \lesssim 100\delta_{\rm SL}$ is achieved.

Similar to the $b \to c\ell\nu$ transitions investigated in Section 3, we have the dimension-6 LEFT Hamiltonian for the $b \to s$ transitions:

$$\mathcal{H}_{b\to s}^{\rm eff} = -\frac{4G_F}{\sqrt{2}} V_{tb}V_{ts}^* \frac{\alpha}{4\pi} \sum_j (C_j O_j + C_j' O_j') + (C_L O_L + C_R O_R) + {\rm h.c.}, \tag{4.3}$$

where the operators of interest include

$$\begin{aligned} O_S^{(\prime)} &= m_b(\bar{s}P_{R(L)}b)(\bar{\ell}\ell), & O_P^{(\prime)} &= m_b(\bar{s}P_{R(L)}b)(\bar{\ell}\gamma^5\ell), \\ O_9^{(\prime)} &= (\bar{s}\gamma^\mu P_{L(R)}b)(\bar{\ell}\gamma_\mu\ell), & O_{10}^{(\prime)} &= (\bar{s}\gamma^\mu P_{L(R)}b)(\bar{\ell}\gamma_\mu\gamma^5\ell), \\ O_{T(T5)} &= (\bar{s}\sigma_{\mu\nu}b)(\bar{\ell}\sigma^{\mu\nu}(\gamma^5)\ell), & O_7^{(\prime)} &= \frac{1}{e}m_b(\bar{s}\sigma^{\mu\nu}P_{R(L)}b)F_{\mu\nu}, \\ O_{L(R)} &= (\bar{s}\gamma^\mu P_{L(R)}b)(\bar{\nu}\gamma_\mu P_L\nu). \end{aligned} \tag{4.4}$$

Among these operators, the first five encode the scalar-, vector-, and tensor-mediated $b \to s$ transitions with a pair of charged leptons and may violate LFU. The presence and absence of a "prime" denote the $b \to s$ currents which are subject to the left- and right-handed chiral projections respectively, while the opposite convention applies to the dipole operators $O_7^{(\prime)}$. $O_{L(R)}$ encodes the vector-mediated $b \to s$ transitions with a pair of neutrinos. $O_7^{(\prime)}$ is an EM dipole operator which can either yield decays with an on-shell photon or mediate $b \to s\ell\ell$ transitions (see the bottom left panel in Figure 15). Note that, when the strange-quark and lepton masses are neglected, the SM contributes to O_9, O_{10}, O_L and O_7 only.

In this section, we will mostly focus on the measurements of $b \to s\tau\tau$, $b \to s\nu\bar{\nu}$ and $b \to s\gamma$ transitions. The CEPC offers a great platform for these studies, particularly during its Z pole run. The extraordinarily high luminosity delivered by the CEPC ensures considerable signal statistics for even the most elusive decay modes with BRs typically $\lesssim 10^{-5}$. Moreover, as compared to the LHCb detector, the planned detectors of the CEPC are better suited for the reconstruction of τ leptons and thus the measurement of $b \to s\tau\tau$, for the measurement of missing energy and hence of $b \to s\nu\bar{\nu}$, and for photon identification as needed for the measurement of $b \to s\gamma$. A combination of these advantages yields an enhanced sensitivity for both testing the SM and probing NP effects. The CEPC thus represents an ideal facility for investigating these rare FCNC decays and the underlying physics. It is worth noting that both $b \to s\nu\bar{\nu}$ and, especially, $b \to s\tau\tau$ transitions, for which we have very poor experimental information so far, are extremely sensitive probes of a wide class of motivated NP models with new dynamics coupled mainly to the third generation [83, 84]. For the convenience of the discussion below, we summarize the projected sensitivities to $b \to s\tau\tau$ and $b \to s\nu\bar{\nu}$ transitions, together with the $b \to c\tau\nu$ processes discussed in Section 3, in Figure 16. At the end of this section, we will extend the discussions to the possibilities of testing the SM global symmetries with forbidden b-hadron decays.

4.1 Di-lepton Modes

In general, the reconstruction of $b \to s\tau\tau$ is more involved compared to the reconstruction of $b \to see, s\mu\mu$. As the τ decays result in neutrino production, the $b \to s\tau\tau$ events are not fully visible to a detector. This difficulty, however, can be well-addressed at a machine like the CEPC. In a recent study [85] (for discussions on $B^0 \to K^{*0}\tau^+\tau^-$, also see [88]), the sensitivity for measuring a set of benchmark $b \to s\tau\tau$ transitions, including $B^0 \to K^{*0}\tau^+\tau^-$, $B_s^0 \to \phi\tau^+\tau^-$, $B^+ \to K^+\tau^+\tau^-$ and $B_s^0 \to \tau^+\tau^-$, at the Z pole has been systematically analyzed. To utilize the machine's capability, a tracker-based scheme to

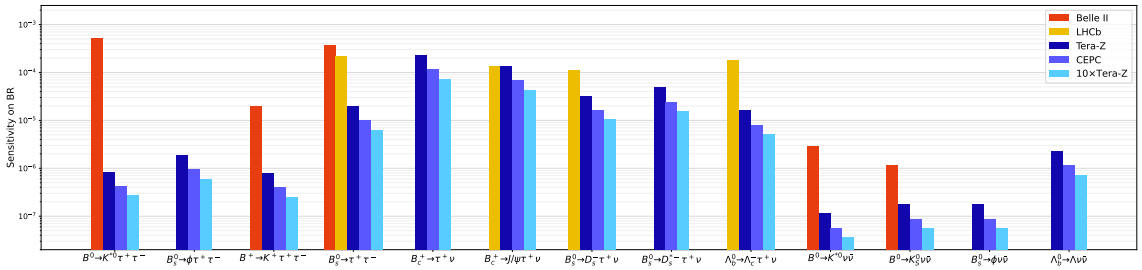

Figure 16: Projected sensitivities of measuring the $b \to s\tau\tau$ [85], $b \to s\nu\bar{\nu}$ [37, 86] and $b \to c\tau\nu$ [40, 68] transitions at the Z pole. The sensitivities at Belle II @ 50 ab^{-1} [8, 87] and LHCb Upgrade II [19, 61] have also been provided as a reference. Note that LHCb sensitivities are generated by combining the analyses of $\tau^+ \to \pi^+\pi^-\pi^-(\pi^0)\nu$ and $\tau \to \mu\nu\bar{\nu}$. This plot is taken from Ref. [40], with additional $b \to s\nu\bar{\nu}$ modes included.

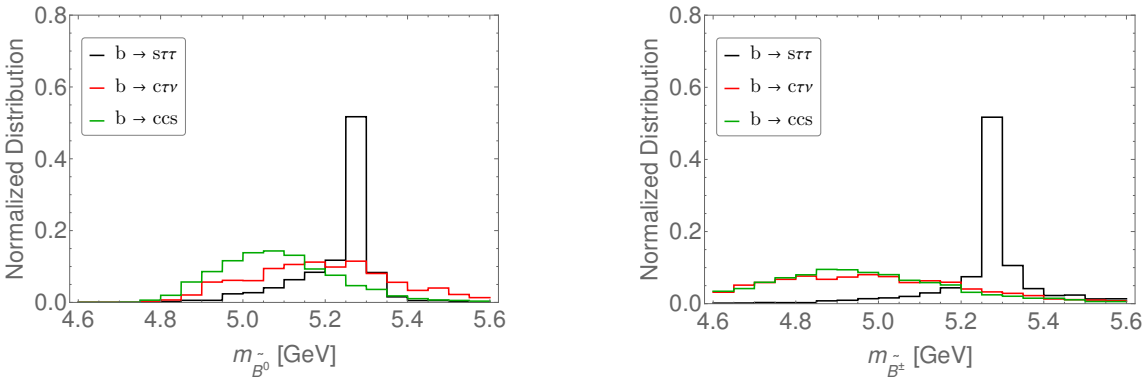

Figure 17: Mass reconstruction for the signal b-mesons in the measurements of $b \to s\tau\tau$ at the Z pole, with $\tau^\pm \to \pi^\pm\pi^\pm\pi^\mp\nu$ [85]. **LEFT:** $B^0 \to K^{*0}\tau^+\tau^-$. **RIGHT:** $B^+ \to K^+\tau^+\tau^-$. The major backgrounds arise from the $b \to c\tau\nu$ and $b \to ccs$ transitions and are both reconstructed.

reconstruct the signal B mesons that works for these $b \to s\tau\tau$ channels has been developed, achieved by using the decay modes of $\tau^\pm \to \pi^\pm\pi^\pm\pi^\mp\nu$. Such a tracker-based scheme also benefits from the particle kinematics at the Z pole. Due to their boost, the signal b hadrons tend to travel further (compared to, *e.g.*, Belle II) before their decay, which benefits the relevant tracker measurements. The predominant backgrounds for these measurements are the Cabibbo-favored $b \to c+X$ processes. Recall that both $D^\pm$ and $D_s^\pm$ mesons have masses and lifetimes comparable to those of τ leptons and thus may decay to a vertex of $\pi^\pm\pi^\pm\pi^\mp$ with extra particles. Therefore, they can fake the τ leptons in the signal. In Figure 17 we demonstrate the mass reconstruction for the signal b-mesons in the measurements of $B^0 \to K^{*0}\tau\tau$ and $B^+ \to K^+\tau^+\tau^-$ at the Z pole. These two channels involve the decay of b-mesons into vector and pseudoscalar mesons respectively. They are sensitive to the LEFT in approximately orthogonal ways and thus are complementary in probing NP [85].

As illustrated in Figure 16, the Tera-Z and 10×Tera-Z machines would be able to measure the BRs of $B^0 \to K^{*0}\tau^+\tau^-$, $B_s^0 \to \phi\tau^+\tau^-$ and $B^+ \to K^+\tau^+\tau^-$ with an absolute

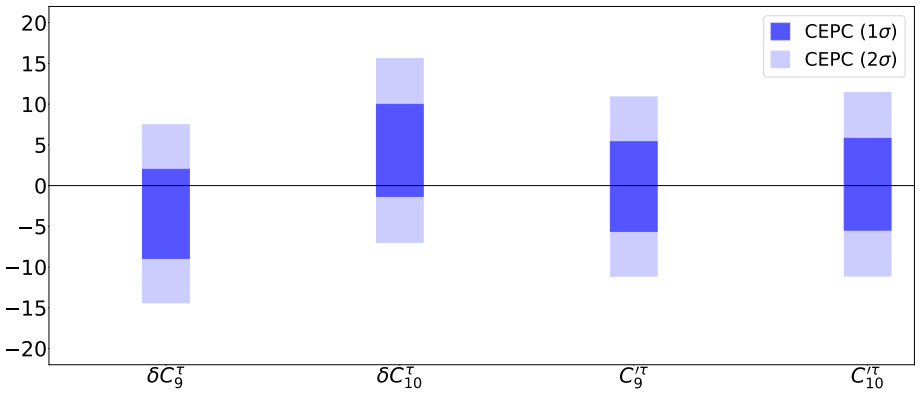

Figure 18: Marginalized constraints on the Wilson coefficients of $b \to s\tau\tau$ LEFT (vector current only) at the CEPC, with $\delta C_9^\tau = C_9^\tau - C_{9,\mathrm{SM}}^\tau$ and $\delta C_{10}^\tau = C_{10}^\tau - C_{10,\mathrm{SM}}^\tau$. This plot is adapted from Ref. [85].

precision of $\mathcal{O}(10^{-7} - 10^{-6})$, as well as $\mathrm{BR}(B_s^0 \to \tau^+\tau^-)$ with an absolute precision of $\mathcal{O}(10^{-6} - 10^{-5})$. In comparison, Belle II and LHCb either have no sensitivity to these measurements or can only yield a sensitivity that is one to two orders of magnitude weaker. With the baseline luminosity, this indicates that the CEPC will be able to identify $\sim \mathcal{O}(1)$ deviations from the SM predictions. These measurements can be further applied to probe the $b \to s\tau\tau$ LEFT operators. Figure 18 shows the marginalized constraints on the corresponding Wilson coefficients in the presence of the vector-mediated operators only.

In spite of this progress, the study of FCNC b rare decays at CEPC should be extended in multiple directions. Firstly, the CEPC constraints on the LEFT operators in Eq. (4.3) should be improved. Currently, the sensitivity to $\mathrm{BR}(B_s \to \tau^+\tau^-)$ is too weak to probe unconstrained parameter space. $\mathrm{BR}(B^0 \to K^{*0}\tau^+\tau^-)$ and $\mathrm{BR}(B_s^0 \to \phi\tau^+\tau^-)$ are both pseudoscalar to vector transitions and have a similar dependence on the NP parameters. This leaves a few directions poorly constrained in the LEFT parameter space. To improve the constraints on the relevant LEFT coefficients, one can consider: (i) introducing differential observables, such as forward-backward asymmetry and τ polarimetry [88]; and (ii) incorporating $b \to s\tau\tau$ transitions of different nature, such as the baryonic decay $\Lambda_b \to \Lambda\tau^+\tau^-$. Interestingly, within the context of an $SU(2)_L$-invariant EFT, sizable NP contributions to the $b \to s\tau\tau$ transitions are usually accompanied with large effects on the left-handed vector current NP operators that contribute to the LFU observables $R_{D^{(*)}}$, which currently exhibit some tension with the SM predictions [89, 90].

A second area of improvement would be to advance the study on LFU tests at the CEPC. The CEPC analysis in Ref. [85] focuses on the di-τ mode of $b \to s$ transitions. To paint a full picture in this context, it is of high value to extend the analysis to $b \to s\ell\ell$. The measurements of, *e.g.*, $R_{K^{(*)}}$, R_{pK} [91], R_ϕ [92], $R_{f_2'}$ [92] and even R_Λ could provide important insights regarding LFU. For some of these measurements, the systematic uncertainties induced by PID could be dominant. The superior electron- and muon-ID capabilities of future detectors are anticipated to offer an edge over LHCb. Notably, the luminosity advantage of the CEPC in measuring the $b \to s\tau\tau$ transitions could be extended

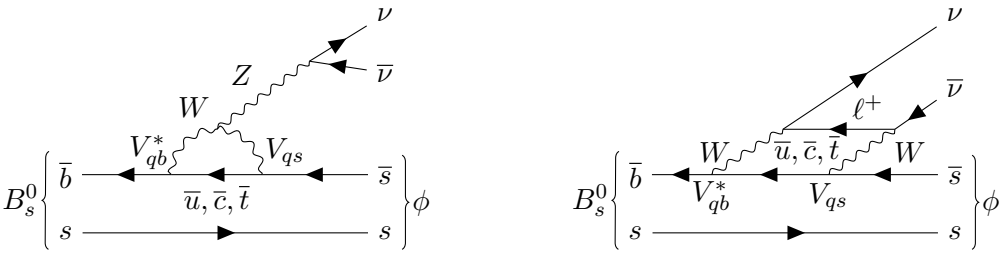

Figure 19: Illustrative Feynman diagrams for the transition $B_s^0 \to \phi\nu\overline{\nu}$ in the SM. **LEFT**: EW penguin diagram. **RIGHT**: EW box diagram.

to ultra-rare channels such as $B_s^0 \to \mu^+\mu^-$. The measurement of BR($B_s^0 \to \mu^+\mu^-$) in the SM is known to be statistically limited, due to its tiny value of around $\sim 3.0 \times 10^{-9}$ [93]. With a yield of $\sim 1.2 \times 10^{11}$ for B_s^0 mesons at the CEPC, about 360 $B_s^0 \to \mu^+\mu^-$ events are expected to be produced, which provides a good opportunity to improve the precision of its measurements.

Finally, the sensitivity studies should be extended to the $b \to d\ell^+\ell^-$ transitions at the CEPC. The $b \to d\ell^+\ell^-$ transitions represent another independent category of FCNC rare b-decays, and hence play a role complementary to the $b \to s\ell^+\ell^-$ transitions in exploring flavor physics. The measurements of these channels including both signal rate and CP violation [94, 95] may share difficulties similar to those of $b \to s\ell^+\ell^-$ decays, and hence would impose similar requirements for the detector performance at the CEPC. All of these issues deserve further detailed examinations.

4.2 Neutrino Modes

The $b \to s\nu\bar{\nu}$ decay is immune to non-factorizable corrections and photonic contributions. Therefore, the theoretical calculation for its SM rate is cleaner than that for the $b \to s\ell\ell$ transitions, which yields $\text{BR}(B_s^0 \to \phi\nu\bar{\nu})_{\text{SM}} = (9.93 \pm 0.72) \times 10^{-6}$ [37]. The $b \to s\nu\bar{\nu}$ decay can be used to probe light dark sectors, such as dark photons, sterile neutrinos, axions/axion-like-particles (ALPs), or neutral scalars, which may significantly alter the kinematics of visible particles [96, 97], (for discussions on the light dark sectors at CEPC, also see Section 11). Also, due to the constraints of $SU(2)_L$ for the BSM well above the EW scale, the impacts of NP on the $b \to s\nu\bar{\nu}$ and $b \to s\ell^+\ell^-$ decays could be interconnected. Thus, the measurement of $b \to s\nu\bar{\nu}$ offers a complementary probe to look into the underlying physics [83, 98].

A dedicated study of the $B_s^0 \to \phi\nu\bar{\nu}$ decay (see Figure 19) at the Z pole has been conducted, using full simulation samples aligned with the CEPC detector profile [37]. This study, facilitated by the large B_s^0 statistics at the CEPC (see Table 2), suggests that a precise measurement of such a rare decay is possible. Explicitly, the accurate ϕ and B_s^0 reconstructions in this analysis reduce the $Z \to q\bar{q}$ events by a factor $\sim \mathcal{O}(10^{-8})$, with a signal efficiency $\sim 3\%$, leaving primarily the $Z \to b\bar{b}$ events as the backgrounds. As a result, a relative precision $\lesssim 2\%$ can be achieved for measuring the SM $B_s^0 \to \phi\nu\bar{\nu}$ signal, as shown in the left panel of Figure 20. Particularly, with a high signal-to-background ratio

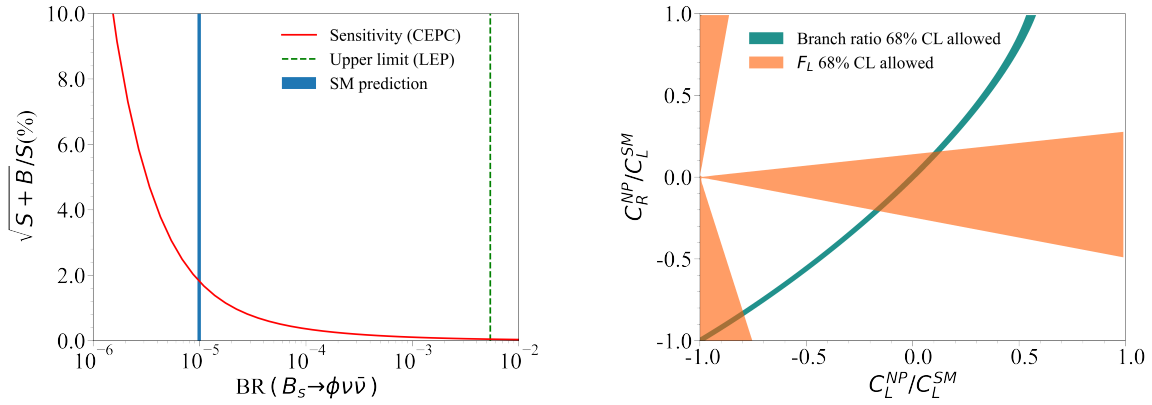

Figure 20: **LEFT**: Relative precision for measuring the signal strength of $B_s^0 \to \phi\nu\bar{\nu}$ at Tera-Z, as a function of its BR. **RIGHT**: Constraints on the LEFT coefficients $C_L^{\rm NP} \equiv C_L - C_L^{\rm SM}$ and C_R with the measurements of the overall $B_s^0 \to \phi\nu\bar{\nu}$ decay rate (green band) and the ϕ polarization F_L (orange regions). These plots are taken from Ref. [37].

of $\simeq 77\%$, the robustness of this measurement against potential systematic uncertainties is largely assured. This study has also shown that the constraints obtained from this measurement can contribute pivotally to the global determination of NP effects, *e.g.*, the ones encoded in the LEFT, (see the right panel of Figure 20).

In addition to the $B_s^0 \to \phi\nu\bar{\nu}$ decay, there exist a set of other physical processes that can be applied to study the $b \to s\nu\bar{\nu}$ transitions at the CEPC, for example $B^+ \to K^+\nu\bar{\nu}$, $B^+ \to K^{+*}\nu\bar{\nu}$, and $B^0 \to K^{0*}\nu\bar{\nu}$. Interestingly, the Belle II collaboration has recently performed a search for the rare $B^+ \to K^+\nu\bar{\nu}$ decay using an inclusive tagging approach, and obtained a branching fraction of $(2.7 \pm 0.7) \times 10^{-5}$ [99], with a significance of 3.5 standard deviation with respect to the background-only hypothesis. This measurement also shows a 2.9 standard deviation departure from the SM expectation [100, 101]. The expected sensitivity of the branching ratios for $B \to K^{(*)}\nu\bar{\nu}$ with 50 ab^{-1} by combining the charged and neutral B decay modes are of the order of 10% [87]. Yet, by leveraging its advantages in reconstructing the missing energy and producing the b-hadrons, the CEPC may push this precision to a much higher level. Such expectations have been confirmed by a recent study at FCC-*ee* [86].

Furthermore, probes of other decay modes involving long-lived s-hadrons, such as $B^0 \to K_S^0\nu\bar{\nu}$, $\Lambda_b \to \Lambda\nu\bar{\nu}$ and $\Xi_b^\pm \to \Xi^\pm\nu\bar{\nu}$ could also help pin down the $b \to s\nu\bar{\nu}$ transition. The decays of the intermediate neutral particles in general give rise to vertices with a displacement of $\mathcal{O}(10)$ cm. Therefore the precision of these channels highly depends on the reconstruction and resolution of these significantly displaced vertices. From a preliminary estimate [102], it is possible to achieve an 80% reconstruction efficiency for the K_S^0 and Λ vertices at a CEPC environment, opening up the opportunity to perform a combined constraint of $bs\nu\bar{\nu}$ effective interactions with all the aforementioned decay modes. In particular, the baryonic processes such as $\Lambda_b \to \Lambda\nu\bar{\nu}$ and $\Xi_b^\pm \to \Xi^\pm\nu\bar{\nu}$ are unique opportunities at the CEPC as they are above the production threshold of the Belle II experiment. Since the

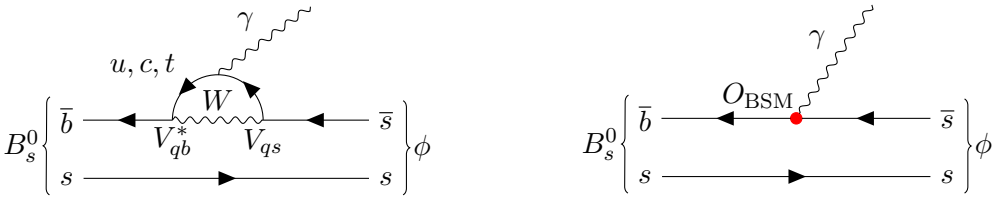

Figure 21: Illustrative Feynman diagrams for the decay $B_s^0 \to \phi\gamma$. **LEFT**: SM example. **RIGHT**: BSM example.

form factors of these baryonic modes are different from those of the mesonic modes, studies of these channels will bring independent crucial information to understand the symmetry structure of the $b \to s\nu\bar{\nu}$ transition in a global fit.

4.3 Radiative Modes

The third category of FCNC rare B decays consistes of the radiative ones, such as $b \to s\gamma, d\gamma$. These modes are sensitive to the EM dipole operators O_7 and O_7'. A wealth of data, including the inclusive $B \to X_{s,d}\gamma$ decays, as well as the direct CP violation A_{CP} and time-dependent CP violation S_{CP} in various $b \to s\gamma$ decays, has yielded complementary insights into the corresponding Wilson coefficients C_7 and C_7'. At the CEPC, however, the reach for FCNC radiative modes is yet to be fully explored, despite their scientific significance [103]. One such example is the $B_s^0 \to \phi\,(\to K^+K^-)\,\gamma$ decay, illustrated in Figure 21. Achieving a high accuracy in reconstructing the signal B_s^0 meson necessitates superior photon angular and energy resolution. For the LHCb Upgrade II, it was found that $\mathrm{BR}(B_s^0 \to \phi\gamma)$ could be measured with a statistical uncertainty $\sim 0.1\%$, and the CP parameters can also be well measured [19, 104]. These sensitivities are expected to be further improved at the CEPC due to the potentially high performance of its ECAL. This study can be extended to baryonic radiative decays of the $b \to s\gamma$ type, such as $\Lambda_b \to \Lambda\gamma$ and $\Xi_b \to \Xi\gamma$, again with an expected sensitivity better than the LHCb [105]. The study can also be extended to $b \to d\gamma$ decays, which can broaden our understanding of the FCNC transition amplitudes and potentially refine the CKM matrix determinations. Finally, if the ECAL of the CEPC allows an efficient reconstruction of $\pi^0, \eta \to \gamma\gamma$ [33], the double-radiative decays of $B_{s,d} \to \gamma\gamma$ could be measured [106]. Theoretical studies show that the $\Lambda_{\rm QCD}/m_b$ power corrections in these channels are well under control, making them new benchmark probes of non-standard dynamics [107, 108]. The SM predictions for their BRs are given by [107, 108]

$$\mathrm{BR}(B_s^0 \to \gamma\gamma) = (3.8^{+1.9}_{-2.1}) \times 10^{-7}\ ,\ \mathrm{BR}(B^0 \to \gamma\gamma) = (1.9^{+1.1}_{-1.0}) \times 10^{-8}\ . \tag{4.5}$$

Belle II has assessed its sensitivities to be respectively $\sim 23\%$ and $\sim 10\%$ [8] relative to the theoretical estimates in Ref. [109] that, we notice, are a factor of few larger than those provided above. Recently, an analysis combining the Belle and available Belle II data set a 90% credibility level upper limit of $\mathrm{BR}(B^0 \to \gamma\gamma) < 6.4 \times 10^{-8}$ [110].

4.4 Tests of SM Global Symmetries with Forbidden Modes

An important class of observables include b-hadron decays that are forbidden because of the global symmetries of the SM. Aside from gauge symmetries, the SM respects or approximately respects a series of global symmetries, yielding, at different levels, the conservation of lepton family numbers, total lepton number and baryon number. The only-known breaking effects for these symmetries are highly suppressed in collider environments: lepton family numbers in the charged lepton sector are only violated through neutrino mixing and thus suppressed by the small neutrino mass differences; lepton and baryon numbers are only violated by the non-perturbative $SU(2)_L$ sphaleron which breaks lepton number and baryon number but conserves their difference exactly. The observation of Lepton Flavor Violation (LFV) in the charged lepton sector, as well as Lepton Number Violation (LNV), Baryon Number Violation (BNV) in any perturbative processes thus would be an indisputable evidence for BSM physics. Interestingly, LFV and LFU violation (LFUV) receive contributions respectively from the flavor off-diagonal and the flavor diagonal counterparts of the same classes of EFT operators and thus they are often correlated in UV complete NP models. The modes that are forbidden in the SM often yield striking signals that are dramatically distinct from the background events. Just like the case of LFU tests, the CEPC with its large statistics and clean environment can play a significant role in exploring these global symmetries, by performing null tests or searching for forbidden b-hadron decays.

Some of the FCNC studies presented in the previous subsections can be extended to the null tests of SM global symmetries, in a straightforward way. For example, one can investigate the LFV effects in the b-hadron decays [111], such as $H_b \to H_{d/s}\tau\ell$, where ℓ denotes an electron or a muon. These decays are significant for testing the current anomalies in semi-leptonic b-hadron decays [89] and, more in general, heavy NP coupling preferably to the third generation [83, 84]. In the past, experimental efforts have primarily focused on the modes $B^+ \to K^+\tau\ell$, yielding $\mathcal{O}(10^{-5})$ upper limits on their branching ratios [112, 113]. Topological reconstruction techniques, employing a fast parametric simulation with momentum reconstruction resolutions and high-resolution vertex detector performance, have been implemented to simulate LFV signal events for $B^0 \to K^{*0}\mu\tau$ as well. Initial explorations have demonstrated the potential detector requirements, offering guidance for future design and performance goals for the vertex detector of future CEPC experiments. As for LFV two-body decays, preliminary studies have shown that – while the CEPC constraints on the decays such as $B^0_{(s)} \to \mu^\pm e^\mp$ and $B^0_{(s)} \to \tau^\pm \mu^\mp$ can at most match the LHCb sensitivity [19] – an improvement in the sensitivity to $B^0_{(s)} \to \tau^\pm e^\mp$ could be achieved at the CEPC due to the expected excellent electron identification.

The CEPC also provides a platform for testing LNV and BNV in b-hadron decays. For instance, LNV can be tested by measuring the same-sign di-lepton decay $B^+ \to \pi^-(K^-)\ell^+\ell^+$, where the sensitivities are primarily influenced by statistics and lepton charge identification. Unlike the LHCb analysis which has focused on the di-muon mode [114, 115], the CEPC may have a good sensitivity for the same-sign di-electron mode also, given its low misidentification rates for electrons. The BNV measurements may feature the signals such

as forbidden baryon-antibaryon oscillations [116] and explicit BNV decays. One example in the latter case is $\Lambda_b^0 \to h^-(h^0)\ell^+$, which arise from the dimension-6 BNV operators $qq'q''\ell$ where $B-L$ is conserved.

Interestingly, BNV is one of the three Sakharov conditions required for dynamically generating the baryon asymmetry of the Universe (BAU). Hence, the measurement of BNV modes may provide valuable clues for resolving this long-standing cosmological puzzle. For example, introducing a dark matter candidate carrying baryon number, the B-mesogenesis model [117] predicts the violation of baryon number separately in the visible sector and dark matter sector, simultaneously achieving baryogenesis and the correct dark matter relic abundance. This model can be tested by measuring invisible decays of neutral bottom baryons such as Λ_b^0 – for further discussions on its collider phenomenology, see [118–120]. In a recent study [121], it has been shown that the important constraints on the model parameters can be obtained at the Z pole run of the CEPC .

5 CP Violation in b-Hadron Decays

In the SM, the flavor properties of quarks can be encoded in the CKM matrix, including what concerns the phenomena involving CP violation. [Andrea Crivellin: what about hadronic B decays testing U-spin and e.g. via polarization observables?] The independent entries include three Euler angles entangling the three generations and one CKM phase as the only source of CP violation in the SM [6]. Yet, addressing the puzzle of BAU dynamically requires additional sources for CP violation, as one of the Sakharov conditions. This consideration has motivated extensive explorations on the CP violation in last decades. b-hadron decays provide a handle particularly suitable for this study. Theoretically, it has been demonstrated in Ref. [122] that the CP violation in B meson systems can drive the BAU generation via EW baryogenesis. Experimentally, the measurements of heavy-flavor physics represent one of the most important tasks for revealing the fundamental rules on quarks. At the CEPC, such measurements are expected to greatly benefit from its high statistics, low backgrounds, efficient hadron ID, and extreme displacement resolution. As customary, the observables, handled by proper analysis of amplitudes, can be fed into the global fit of the CKM matrix. Any deviation from the CKM unitarity would be a smoking-gun signature for NP including new possible CP violation.

Generally, there are three classes of observables for the CP violation measurements: direct CP violation in decay, CP violation in mixing and CP violation through the interference between mixing and decay [2]. For a given decaying process, if the initial particle does not mix with its CP conjugate and the final state is not a CP eigenstate, the CP violation can be directly measured based on a time-integrated asymmetry in statistics between this process and its CP-conjugate. The effective statistics in this case is not only

[2] In a recent study [123], it was proposed that there exists the double-mixing CP violation in cascade decays involving two neutral mesons in the decay chain, induced by the interference of different meson oscillating paths. The double-mixing CP violation in channels like $B_s^0 \to \rho^0 K \to \rho^0(\pi^-\ell^+\nu)$ and $B^0 \to D^0 K \to D^0(\pi^+\ell^-\bar{\nu})$ is supposed to be very significant. The asymmetry depends on two time variables, the oscillating time of $B_{(s)}^0$ and the oscillating time of K, so a two-dimensional time-dependent analysis can be performed through its measurements.

directly proportional to the overall signal rate but also to the efficiency in tagging the initiating heavy-flavor particle. As introduced in Section 2.2, the effective tagging efficiency ϵ_{eff} can be expressed as $\epsilon_{\text{tag}}(1-2\omega)^2$ for the specific processes, where ϵ_{tag} and ω are the raw tagging efficiency and mistagging rate, respectively [124]. Currently, the time-integrated CP violation measurements play a significant role in many aspects of flavor physics. One example is the the determination of the CKM angle γ, where important contributions come from time-integrated CP violation measurements in $B^+ \to D^{(*)0}K^{(*)+}$ decays [11].

The observables of CP violation in mixing involve decaying processes of neutral particles where these particles can oscillate into their CP conjugate before the decay, due to a mixing induced at loop level. If the final state is CP-even or CP-odd, an interference can occur between the decaying amplitudes with and without a mixing, yielding a CP violating term. B^0 and B_s^0 as neutral heavy-flavor mesons are particularly relevant here. As their oscillations are apparent, both classes of observables can be measured by examining the time-dependent asymmetry between a given decaying process and its CP-conjugate. General pattern holds for this time-dependence despite the diversity of these decaying processes. The asymmetry is proportional to both oscillatory factors with the period determined by the mass difference (Δm) between the mass eigenstates of initial particles and non-oscillatory factors caused by the decay-width difference ($\Delta\Gamma$) of these mass eigenstates. Because of $\Delta m \gg \Delta\Gamma$ for the B^0 and B_s^0 mesons, the oscillatory factors are relatively more relevant for their CP violation measurements [11]. The mistagging probability ω becomes significant in this case, as the algorithm must determine the initial b quarks' charge after the $b-\bar{b}$ oscillation happens. Another factor affecting the overall precision is the decay time determination, which is mainly limited by the vertex resolution of the tracking system.

The charge determination of initial b quark is crucial for measuring the CP violation in b-hadron decays. This is, however, challenging particularly for the last two classes of CP violation observables, as the decays of initial $B_{(s)}^0$ mesons could be affected by oscillations and thus lose the relevant information. One way to address this difficulty is to utilize the information of the companion b-hadron. If the companion b quark hadronizes into non-oscillatory species, such as $B^{\pm}$, and is subsequently identified, then the charge of the original signal b quark can be identified. Alternatively, one can employ the products of QCD shower and hadronization, as they manifest the original b-quark charge before the oscillation occurs to the b-hadron. For example, the B_s^0 meson is often accompanied by a K^+ meson flying in the same direction, since the strange quarks are produced in pair from QCD. A recent study [56] suggests that ϵ_{eff} can be $\gtrsim 20\%$ at the CEPC, much higher than a typical value of 5% at LHCb [125]. This result is also consistent with the outcome from another CEPC study where leading charged particle in a jet and momentum-weighted jet charge are combined [36], yielding an $\epsilon_{\text{tag}} \sim 39\%$ and 20% for inclusive c or b jets respectively. Notably, utilizing the method of jet origin identification and the ParticleNet algorithm developed in Ref. [34], the jet charge flip rates could be controlled to 19% and 7% for inclusive b and c jets, corresponding to an effective tagging power of 37% and 54%, respectively. More details can be found in Section 2.

The decay-time measurement at the CEPC benefits from its clean collision environ-

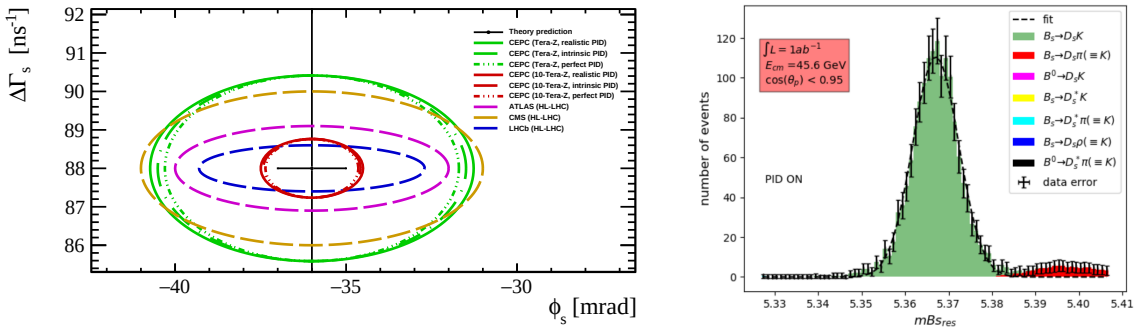

Figure 22: **LEFT:** Projected sensitivities (68% confidence level (C.L.)) of measuring the parameters $\Delta\Gamma_s$ and $\phi_s = -2\beta_s$ at the CEPC [56], through the time-dependent CP violation in the decay $B_s^0 \to J/\psi(\to \mu^+\mu^-)\phi(\to K^+K^-)$. **RIGHT:** B_s^0 mass reconstruction in the decays $B_s^0 \to D_s^{\pm}(\to \phi\pi^{\pm} \to K^+K^-\pi^{\pm})K^{\mp}$ at the Z pole of FCC-ee [126].

ment and well-designed tracking system. The full simulation in Ref. [56] reports a CEPC resolution of $\lesssim 5$ fs for measuring the 4-prong decay $B_s^0 \to J/\psi\phi \to \mu^+\mu^-K^+K^-$, which is much better than the typical LHCb level of $\gtrsim 20-30$ fs. This will bring great benefits to the time-dependent CP violation measurements and also, for the role of Δm and $\Delta\Gamma$ as basic inputs, the global CKM fit. Additionally, a study in the FCC-ee context [126] suggests a relative uncertainty $\lesssim 3\times10^{-5}$ for the B_s^0 Δm measurement, which is about one order of magnitude better than the current one. We hope that dedicated studies in the future could help validate such results and reveal the full potential of the CEPC for measuring these basic flavor physics inputs.

One important application of time-dependent CP violation measurements is to test the "bs" unitarity triangle. For this purpose, the decay $B_s^0 \to J/\psi\phi \to \mu^+\mu^-K^+K^-$ has been widely used [127, 128]. Figure 22 displays in its left panel the projected CEPC sensitivities based on this channel [56]. The performed full simulation indicates that the CEPC could reduce the uncertainty of measuring the angle parameter β_s=-$\phi_s/2$ to 4.6 mrad [56], improving the existing precision by several times. FCC-ee also reported the time-dependent measurement of the CP violation in the decays $B_s^0 \to D_s^{\pm}K^{\mp}$ and $B_s^0 \to J/\psi\phi \to \mu\mu KK$ Ref. [126], which are simulated with fast simulation. The right panel of Figure 22 shows the mass reconstruction of B_s^0 mesons achieved in this study. Most combinatoric and misidentification-induced backgrounds can be removed with the developed PID algorithm, yielding a sharp peak of signal events. In this context, the triangle parameter α_s and β_s can be measured with uncertainties of 0.4° and 0.035°, respectively [126]. Taken into account the recent progress from CEPC on jet origin ID that could significantly enhance the effective tagging power, as well as differences in luminosity assumption, these two results agrees.

Yet, the oscillating effects of neutral B mesons are not always trackable. One example is the decays $B_{(s)}^0 \to \pi^0\pi^0 \to 4\gamma$, where the tracker loses its power and reconstructing $B_{(s)}^0$ decay time becomes extremely challenging. One can thus perform time-integrated measurements only for these decays. A sensitivity study on this case has been taken with

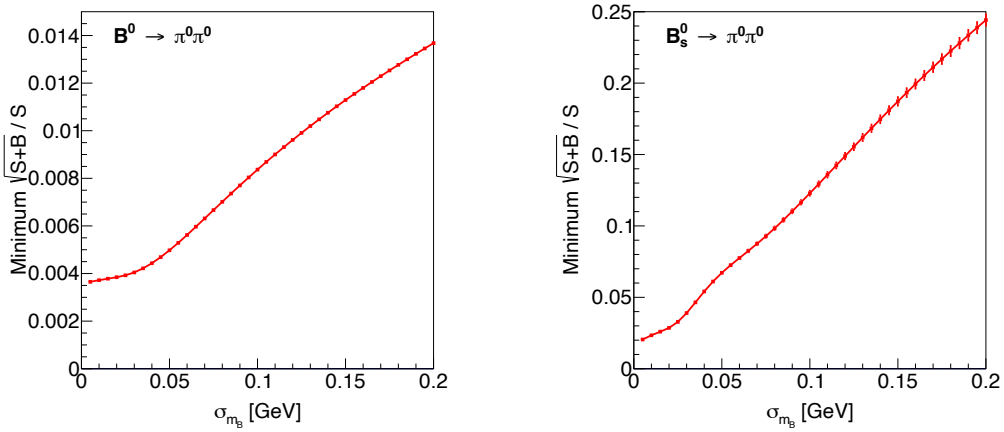

Figure 23: Relative uncertainties (statistical only) of measuring BR($B^0 \to \pi^0\pi^0 \to 4\gamma$) (left) and BR($B_s^0 \to \pi^0\pi^0 \to 4\gamma$) (right) at the CEPC as a function of the B-meson mass resolution σ_{m_B}. The plots are taken from Ref. [33].

the CEPC fast simulation in Ref. [33]. Figure 23 displays the obtained relative uncertainties (statistical only) as a function of the B-meson mass resolution (σ_{m_B}). For measuring BR($B^0 \to \pi^0\pi^0 \to 4\gamma$) and BR($B_s^0 \to \pi^0\pi^0 \to 4\gamma$), the Tera-$Z$ precisions are expected to be $\lesssim \mathcal{O}(1\%)$ and $\lesssim \mathcal{O}(10\%)$, respectively. Here the magnitude of σ_{m_B} is highly dependent on the ECAL performance, where the shown benchmark corresponds to an ECAL resolution $\sim 3\%/\sqrt{E/\text{GeV}}$ which could be achieved with full crystal ECAL [129]. $B^0 \to \pi^0\pi^0$ mode would play a key role in constraining the CKM angle α [130]. The two B mesons produced at Z pole are not entangled, unlike the entangled B production by $\Upsilon(4S) \to 2B$ decays in B-factories. Consequently, the time-integrated CP violation observables at CEPC are slightly different from B-factory counterparts, making them complementary. Combining future CEPC and Belle II $B \to \pi\pi$ results, a projected sensitivity on α can be as small as of 0.4° if all theoretical errors are resolved. The result is illustrated in Figure 24, where we show that the two curves from CEPC $B \to \pi\pi$ measurements can constrain α much better than the current data (dot-dashed blue curves). Due to the time-integrated CP violation difference mentioned above, the fit combining the current B-factory measurements improves slightly compared to the one without [33].

The possibility of performing time-dependent CP violation measurements in the $B^0 \to \pi^0\pi^0$ decay using the $\pi^0 \to e^+e^-\gamma$ Dalitz decay has been explored by the Belle II collaboration [8]. The sensitivity relies on the quality of reconstructing the $\pi^0 \to e^+e^-\gamma$ decay vertex, which is yet to be studied at the CEPC. Note, for the decays of charged B mesons, where there is no characteristic oscillation pattern for the CP violation, the time-integrated CP violation measurements are applied usually. One study based on the decays $B^\pm \to D^0(\bar{D}^0)K^\pm$ can be found in Ref. [102]. This work exploits high acceptance and excellent reconstruction of K_S^0 from $D^0 \to K_S^0\pi^0$, assuming that a crystal ECAL is available. As a result, the γ_s parameter for the bs unitarity triangle could be determined up to a precision $\sim \mathcal{O}(1°)$.

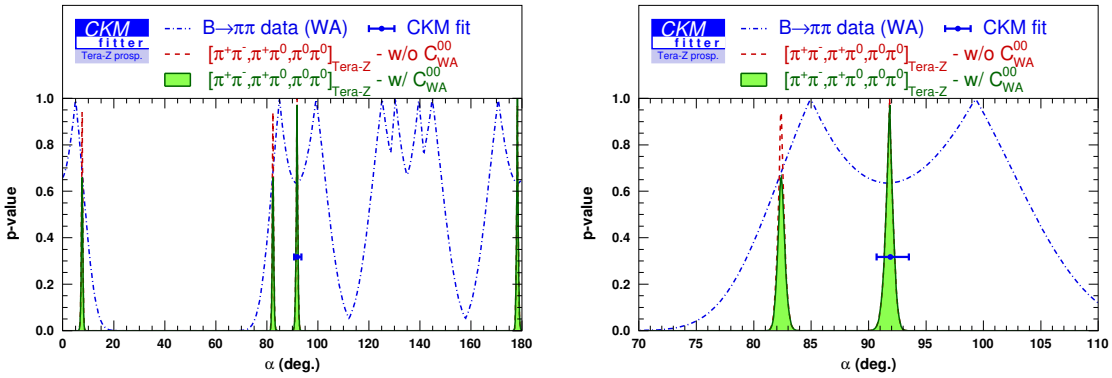

Figure 24: The p-value for α from current $B^0 \to \pi\pi$ measurements (dotted-dashed blue curve) and the current global CKM fit result (blue error bars). We also show two different scenarios of CEPC measurements as a Tera-Z factory. The first case comes from using the CEPC data alone (dashed red). The other combines CEPC results with the current world average of B-factory measurements (filled green). Both the scans over the whole range of α (left) and around the value favored by the global CKM fit (right) are shown. See [33] for more details.

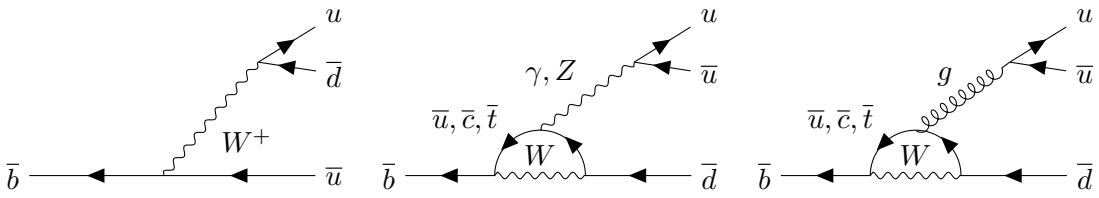

Figure 25: Illustrative Feynman diagrams for the transition $\bar{b} \to \bar{u}u\bar{d}$. **LEFT**: tree level. **MIDDLE**: EW penguin diagram. **RIGHT**: QCD penguin diagram.

Despite the analyses discussed above, several directions regarding the CP violation at the Z pole have yet to be explored. Firstly, digging out the potential of a Z factory for the CKM global fit demands a systematic sensitivity study on the measurements of input parameters. Such a task is yet to be addressed. For example, the β angle is known to be primarily determined by the measurements of the $b \to c\bar{c}s$ transitions such as $B^0 \to J/\psi K^0$ and their time-dependent CP violation [11]. A dedicated simulation may validate the projected Z-factory sensitivities in Ref. [20] or push them even further. Also, the $b \to u\bar{u}d$ transitions (see Figure 25), *e.g.*, multiple CP violation observables in $B \to \rho\rho$ and $B \to \rho\pi$ final states can be relevant for the determination of the α angle. More opportunities for studying CP violation beyond the currently well-established observables at CEPC are also expected due to its unique detector and kinematic conditions. However, additional theoretical input is needed to make specific recommendations for phenomenological studies.

6 Charm and Strange Physics

The high BR($Z \to c\bar{c}$) $\simeq$ 12% comparable to BR($Z \to b\bar{b}$) $\simeq$ 15% makes the CEPC a c-factory as well. Charm physics studies will enjoy the high luminosity, low background level, and good detector system at the CEPC. Unfortunately, few solid statements about charm physics are available at the current stage. On the other hand, the recent observation of CP violation in charm decays [131–133] raises the necessity of further charm physics studies and constraints on possible NP contributions.

Possible worthwhile avenues of investigation for charm physics at the CEPC, akin to the discussion in Section 3 and 4, include semileptonic c-hadron decays. Theoretical discussions were conducted for rare $c \to u\nu\bar{\nu}$ decays [134], yet the phenomenology at the Z pole remains unexplored. In addition, hadronic c decay modes play key roles in both charm and b physics, given that the $b \to c+X$ EW transition is the dominant b decay mode. Decays involving neutral particles can enhance the c-hadron tagging efficiency, *e.g.*, $D^0 \to K^-\pi^+\pi^0$ with its BR=14.2% and its reconstructable decay vertex. Other similar modes include $D^0 \to K^0_S\pi^+\pi^-\pi^0$ (BR=5.1%) or $D^0 \to K^-2\pi^+\pi^-\pi^0$ (BR=4.2%). For D_s, reconstructions like $D_s^+ \to K^+K^-\pi^+\pi^0$ (BR=6.3%), $D_s^+ \to \eta\rho^+$ (BR=8.9%), or $\eta'\rho^+$ (BR=5.8%) were considered. c-hadron decays to CP eigenstates, such as $D^0 \to K^0_S\pi^0, K^0_S\omega, K^0_S\phi$, were valuable for extracting CP violation parameters from $B \to DK$ type decays and are hence important for determining the CKM angle γ [11], as stated in Section 5. Regarding direct CP violation effects in charm decays, a precise reconstruction of the final states is a crucial ingredient of the measurement of the parameter $\Delta\mathcal{A}_{\rm CP} \equiv \mathcal{A}_{\rm CP}(K^+K^-) - \mathcal{A}_{\rm CP}(\pi^+\pi^-)$: for the sake of comparison, the LHCb Upgrade II prospect is $\sim 3 \times 10^{-4}$ [19]. Other decays useful for probing CP violation include $D^+ \to \pi^+\pi^0$, $D^0 \to K^0_SK^0_S$, and $D^+_{(s)} \to K^+K^0_S\pi^+\pi^-$, among others.

To have a successful strange physics program at CEPC, the high-quality identification and reconstruction of strange hadrons is necessary. A full-simulation study has showcased the promising reconstruction quality for K^0_S and Λ decaying into a pair of charged tracks at the CEPC, featuring efficiencies $\gtrsim 80\%$ and purity $\sim 95\%$ [47]. These strange hadrons, with lifetimes of $\mathcal{O}(100)$ ps, are suitable for the CEPC's tracking system. In contrast, higher-intensity experiments like the kaon factories prioritize longer-lived $K^\pm$ and K^0_L states, even in planned upgrades [135–137]. Hence, the exploration of the K^0_S and Λ physics potential at CEPC is essential. With its PID-friendly environment, CEPC facilitates the investigation of rare K^0_S or Λ decays with reduced background systematics compared to LHCb [138]. A case in point is the rare decay $K^0_S \to \mu\mu$, with its current BR limit being $\mathcal{O}(100)$ times greater than its SM prediction $\sim 5 \times 10^{-12}$ [139]. With more than 10^{12} K^0_S produced in hadronic Z decays, CEPC shall be sensitive to large BR($K^0_S \to \mu\mu$) deviations from its SM value. Generically, when searching for $K \to \mu\mu$ displaced vertexes at CEPC, the contribution from $K^0_L \to \mu\mu$ is always dominant due to its larger BR $\sim 7 \times 10^{-9}$. However, when the vertex's decay lifetime is comparable to that of K^0_S, the contribution from $K^0_L \to \mu\mu$ decay becomes important [139]. If $K^0(\bar{K}^0)$ are generated by QCD symmetrically without being tagged, the interference between K^0_S and K^0_L decays is not observable. [Soeren Prell: Has there been any studies of this?] On the other hand, for events like $Z \to s\bar{s}$, the initial strange

quark sign tagging prior to $K^0 - \bar{K}^0$ mixing is achievable, analogous to b or c tagging. Observing CP violation from interference between K^0_S and K^0_L decays in this tagged case is possible, allowing the extrapolation of $|V_{td}V_{ts}|\sin(\beta+\beta_s)$ [139, 140]. Due to the small decay rate, systematic effects must be evaluated carefully in simulation, which will be left to future studies. There also lies the CEPC potential for other rare decays involving neutral final states, like $K^0_S \to \mu\mu\gamma$ or $K^0_S \to \mu\mu\pi^0$, which require future investigations.

Rare charm decays are mediated by the up-type FCNC, where the internal quarks in the loops are b, s, d, whose masses are not too different from each other, while rare b decays by down-type FCNC, where the quarks in the loops are dominated by top. Therefore, the GIM suppression is more effective in rare charm than in rare b decays, and the sensitivity of rare charm decays to NP is also expected to be high [141–143]. Nevertheless, due to the large resonance contributions, it is much more challenging to control the hadronic effects in charm decays. Furthermore, the usually adopted heavy quark expansion methods in rare b decays become much less reliable when applied to the rare charm decays. Therefore, the short-distance physics in rare charm decays cannot be probed through simple observables like the BRs. Instead, we can consider the so-called "null tests", *i.e.*, the observables that are strongly suppressed within the SM due to exact or approximate symmetries and largely free of hadronic uncertainties. Typical examples include potential deviations from the LFU in semileptonic $c \to u\ell^+\ell^-$ decays [144], the lepton flavor violating decays like $D \to \pi e\mu$ and $D_s \to Ke\mu$ [145], the angular observables in semileptonic $c \to u\ell^+\ell^-$ decays [146, 147], as well as the di-neutrino decay modes like $D \to \pi\nu\bar{\nu}$ and $D_s \to K\nu\bar{\nu}$ [134, 148]. Any observation of a non-standard effect in these null tests would be a robust evidence for NP.

7 τ Physics

With BR($Z \to \tau^+\tau^-$) $\simeq 3\%$ [149], the CEPC is anticipated to yield $\simeq 1.2 \times 10^{11}$ $\tau^+\tau^-$ pairs [2] – see Table 2. The machine could thus produce five orders of magnitude more τ leptons than the LEP [150]. The absence of accompanying particles showers and large boosts ($\gamma_\tau \simeq 26$) in τ production at the Z pole renders these events particularly favorable for precise measurements and searches for rare or forbidden processes. The amount of τ events at the CEPC is nearly triple that expected at Belle II ($\simeq 4.5 \times 10^{10}$ τ pairs) [8, 151], while the reconstruction efficiency of the τ leptons and the identification of some particular decay modes could be significantly better due to the larger boost and the particle flow oriented detector design at CEPC. Similarly, the τ event yield at the CEPC is anticipated to be several times those at the proposed STCF project ($\simeq 3.5 \times 10^{10}$ τ pairs in 10 years) [27, 152]. These attributes make the CEPC an excellent environment for τ physics which could significantly contribute to the future of the field. The preliminary study in Ref. [48] investigated the tagging efficiency of inclusive τ hadronic modes using CEPC full simulations, obtaining an efficiency times purity value of approximately 70%, ascertained from W^+W^- events. Concurrently, research is being undertaken to scrutinize the exclusive tagging of prominent τ decay modes with the dual-readout calorimeter at the Z pole [153]. Preliminary results suggest that the average τ-tagging accuracy of seven common decay modes is around 90%. Detector performances of τ-tagging at the Z pole with the aid of

Measurement	Current	Belle II	FCC	CEPC prelim.
Lifetime [sec]	$(2903 \pm 5) \times 10^{-16}$		$\pm 6 \times 10^{-18}$	
BR($\tau \to e\nu\bar{\nu}$)	$(17.82 \pm 0.04)\%$		$\pm 0.003\%$	
BR($\tau \to \mu\nu\bar{\nu}$)	$(17.39 \pm 0.04)\%$		$\pm 0.003\%$	
m_τ [MeV]	1776.93 ± 0.09		$\pm$ 0.0023 (stat.) $\pm$ 0.025 (syst.)	
BR($\tau \to \mu\mu\mu$)	$< 2.1 \times 10^{-8}$	3.6×10^{-10}	1.4×10^{-11}	10^{-10}
BR($\tau \to \mu\gamma$)	$< 4.4 \times 10^{-8}$	6.9×10^{-9}	1.2×10^{-9}	10^{-10}

Table 7: Current limits [149] and projected sensitivities at Belle II [8, 151, 158], the FCC-*ee* [155–157] and CEPC [159] Z factories, for some τ physics measurements. For other LFV modes of the type $\tau \to \ell^{(\prime)}\ell\bar{\ell}$, for which dedicated studies are still missing, we expect that CEPC can achieve a sensitivity similar to that estimated for $\tau \to \mu\mu\mu$. Similarly, a sensitivity for $\tau \to e\gamma$ of the same order of magnitude as that for $\tau \to \mu\gamma$ can be plausibly reached.

machine learning algorithms were also investigated in Ref. [154], where it was showed that deep learning models applied to the IDEA detector design can classify different τ decay modes with an average accuracy of 91% and discriminate τ jets from QCD jets with an accuracy larger than 95%.

Recent τ physics projections and potential measurements at the Z pole of an e^+e^- collider have been comprehensively summarized in Refs. [155–157]. These analyses, predominantly founded on rapid simulations within the FCC-*ee* context, provide valuable benchmarks. These comprehensive studies focus on precision decay time and mass measurements, LFU tests in leptonic τ decays, and LFV searches in τ decays.

7.1 LFV in τ Decays

LFV τ decays are complementary to LFV observables at higher energy scales (see Section 8.1), which highlights the theoretical importance of these modes in discriminating among different NP models [160–162]. Table 7 displays current limits and FCC-*ee* projections from Refs. [155–157] and CEPC preliminary estimates from Ref. [159] for the purely leptonic LFV τ decay mode $\tau \to \mu\mu\mu$ and the radiative one $\tau \to \mu\gamma$. At the CEPC, the former search is expected to be background free due to the excellent muon identification and momentum reconstruction. On the other hand, radiative LFV τ decays are subject to background from $Z \to \tau\tau\gamma$ followed by ordinary leptonic τ decays, which can be alleviated by precise measurements of photon momenta. The CEPC prospects should be also compared with the future reach of Belle II. Based on projections from the existing Belle results, the prospects for over 50 distinct LFV τ decay modes have been presented in Ref. [8] and recently revised in Ref. [151, 158]. With 50 ab^{-1} of collected data, Belle II is expected to set limits in the $10^{-10} - 10^{-9}$ range for most decay modes with a notable exception of the radiative decays, $\tau \to \ell\gamma$. The BRs for these decays can not be constrained much below

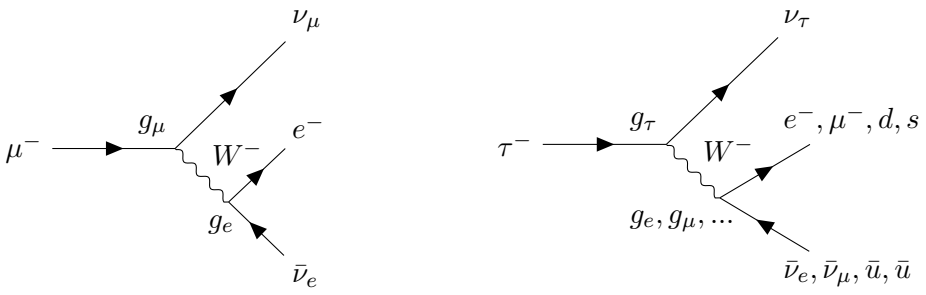

Figure 26: Illustrative Feynman diagrams for the muon and tau decays. In the SM, $g_e = g_\mu = g_\tau$ is predicted.

the 10^{-8} level, as a consequence of the difficult background from initial-state-radiation photons affecting e^+e^- colliders running at energies around the Υ(nS) resonances. As we can see, a Tera-Z factory can play a crucial role in discovering or constraining τ LFV by searching for the radiative modes — and, more in general, it will be complementary to Belle II measurements, reaching a comparable sensitivity for the purely leptonic modes as shown in Table 7.

The CEPC sensitivity to LFV τ decays can be interpreted in terms of constraints on EFT operators. For instance, the limit $\mathrm{BR}(\tau \to \mu\gamma) < 10^{-10}$ would imply the lower bound $\Lambda > 2800$ TeV on the energy scale of the LFV dipole operators $\frac{1}{\Lambda^2}(\bar{\mu}\sigma^{\mu\nu}P_{L,R}\tau)\Phi F_{\mu\nu}$, where Φ is the Higgs field and $F_{\mu\nu}$ is the EM field tensor. Similarly, $\mathrm{BR}(\tau \to \mu\mu\mu) < 10^{-10}$ would translate into the constraint $\Lambda > 44$ TeV on the scale of four-lepton LFV operators of the kind $\frac{1}{\Lambda^2}(\bar{\mu}\gamma^\mu P_{L,R}\tau)(\bar{\mu}\gamma_\mu P_{L,R}\mu)$.

To achieve the sensitivities displayed in Table 7, the ECAL/PFA performance will be crucial, especially when the LFV final states have one or more neutral components. Besides the radiative decays, other examples of such a situation include $\tau \to \ell h^0$ with $h^0 = \pi^0(\to \gamma\gamma)$, $\eta(\gamma\gamma)$, $\eta'(\pi^+\pi^-\eta)$, etc. Additionally, since LFV τ decays do not feature neutrinos, the m_τ invariant mass reconstruction plays a crucial rule in suppressing large backgrounds from ordinary τ decays. For explicit discussions of the $\tau \to \ell\gamma$ phenomenology at Tera-Z factories, see [155, 159], while studies of the prospects for hadronic LFV τ decays, such as $\tau \to \ell\pi$ or $\tau \to \ell\rho$, are still lacking and will require future dedicated efforts. Finally, we notice that, in presence of a light NP boson a with LFV couplings to SM leptons, decays such as $\tau \to \ell a$ can also occur. We will discuss such exotic LFV τ decay modes in Section 11.

7.2 LFU of τ Decays

In Table 7, we report current accuracy and Tera-Z prospects of measurements of the τ mass, lifetime, and the BRs of standard leptonic τ decays. These are the crucial quantities to perform tests of the LFU in τ and μ decays. The SM predicts LFU of weak charged currents, that is, that the three lepton families couple with the same strength to $W^\pm$ bosons, *i.e.*, $g_e = g_\mu = g_\tau = g$, where $g = e/\sin\theta_W$ is the $SU(2)_L$ gauge coupling, cf. Figure 26. Inspecting the processes in this figure, one can see that the LFU prediction can be tested

by measuring the following quantities:

$$\left(\frac{g_\mu}{g_e}\right)^2 = \frac{\mathrm{BR}(\tau \to \mu\nu\bar{\nu})}{\mathrm{BR}(\tau \to e\nu\bar{\nu})} \frac{f(m_e^2/m_\tau^2)}{f(m_\mu^2/m_\tau^2)} \frac{R_W^{\tau e}}{R_W^{\tau\mu}}\,, \tag{7.1}$$

$$\left(\frac{g_\tau}{g_{e/\mu}}\right)^2 = \frac{\tau_\mu}{\tau_\tau}\left(\frac{m_\mu}{m_\tau}\right)^5 \frac{\mathrm{BR}(\tau \to \mu/e\,\nu\bar{\nu})}{\mathrm{BR}(\mu \to e\nu\bar{\nu})} \frac{f(m_e^2/m_\mu^2)}{f(m_{\mu/e}^2/m_\tau^2)} \frac{R_W^{\mu e} R_\gamma^\mu}{R_W^{\tau\mu/e} R_\gamma^\tau}\,, \tag{7.2}$$

where $\tau_{\tau/\mu}$ is the decaying lepton lifetime, $f(x) = 1 - 8x + 8x^3 - x^4 - 12x^2 \log x$ is a phase-space factor, $R_W^{\ell'\ell} = 1 + \frac{3}{5}\frac{m_{\ell'}^2}{m_W^2} + \frac{9}{5}\frac{m_\ell^2}{m_W^2}$ and $R_\gamma^\ell = 1 + \frac{\alpha(m_\ell)}{2\pi}\left(\frac{25}{4} - \pi^2\right)$ are EW and QED radiative corrections respectively [11, 163].[3] Using the purely leptonic processes in Figure 26, the current experimental determination of the coupling ratios results to be compatible with LFU at the per mil level [11, 164]:

$$\frac{g_\mu}{g_e} = 1.0002 \pm 0.0011\,, \quad \frac{g_\tau}{g_e} = 1.0018 \pm 0.0014\,, \quad \frac{g_\tau}{g_\mu} = 1.0016 \pm 0.0014\,. \tag{7.3}$$

As muon physics quantities are known with high precision, the above uncertainties mainly stem from the measurements of τ leptonic BRs, lifetime and mass. The present relative uncertainties on $\mathrm{BR}(\tau \to e\nu\bar{\nu})$ and $\mathrm{BR}(\tau \to \mu\nu\bar{\nu})$ are respectively 2.2‰ and 2.3‰ [149], which yield an impact of 1.1‰ on the measurement of coupling ratios. As we can see, they constitute the source of largest uncertainty at the moment. The impact of τ_τ on the uncertainty of g_τ/g_ℓ is at a comparable level, namely 0.9‰, given its current 1.7‰ relative precision [149]. The current world average for m_τ is substantially more precise, with a relative error of 5×10^{-5} [149], which contributes to the uncertainty of g_τ/g_ℓ only at the 0.2‰ level.

As shown in Table 7, an improvement by a factor of few for the precision of the m_τ measurement is possible at Tera-Z factories, such that m_τ would be known precisely enough to allow to perform the LFU test in Eq. (7.2) with an uncertainty at the 0.1‰ level or below. Moreover, substantial improvements on the determination of m_τ are also to be expected at BESIII [165], Belle II [8] – which recently released the single most precise measurement, $m_\tau = 1777.09 \pm 0.08(\mathrm{stat}) \pm 0.11(\mathrm{syst})$ MeV [166] – and at STCF [27]. Therefore, m_τ is not expected to be a limiting factor for an improved LFU test. As suggested by Table 7, Tera-Z factories can play a major role for what concerns the measurements of the BRs and lifetime. Actually, the current world average for $\mathrm{BR}(\tau \to \ell\nu\bar{\nu})$ is dominated by the measurements at the LEP that are statistically limited, although the systematic errors are typically just a factor of two smaller than the statistical ones [149].[4] Differently, the measurements of τ_τ at the LEP have comparable statistical and systematic uncertainties, which are respectively twice and three times larger than those of the most precise measurement of τ_τ from the Belle experiment [168]. The τ_τ measurements however are simpler at a Tera-Z factory than those at Belle, given the large boost stemming from $m_Z \gg m_\tau$, while the statistics is

[3] Numerically one obtains $R_\gamma^\mu/R_\gamma^\tau - 1 \simeq 8.0 \times 10^{-5}$ [11], $R_W^{\tau e}/R_W^{\tau\mu} - 1 \simeq -\frac{9}{5}\frac{m_\mu^2}{m_W^2} \simeq -3.1 \times 10^{-6}$ and $R_W^{\mu e}/R_W^{\tau\ell} - 1 \simeq -\frac{3}{5}\frac{m_\tau^2}{m_W^2} \simeq -2.9 \times 10^{-4}$.

[4] A precise measurement of the ratio $\mathrm{BR}(\tau \to \mu\nu\bar{\nu})/\mathrm{BR}(\tau \to e\nu\bar{\nu})$ has been recently published by Belle II [167], which lead to the improved g_μ/g_e measurement displayed in Eq. (7.3).

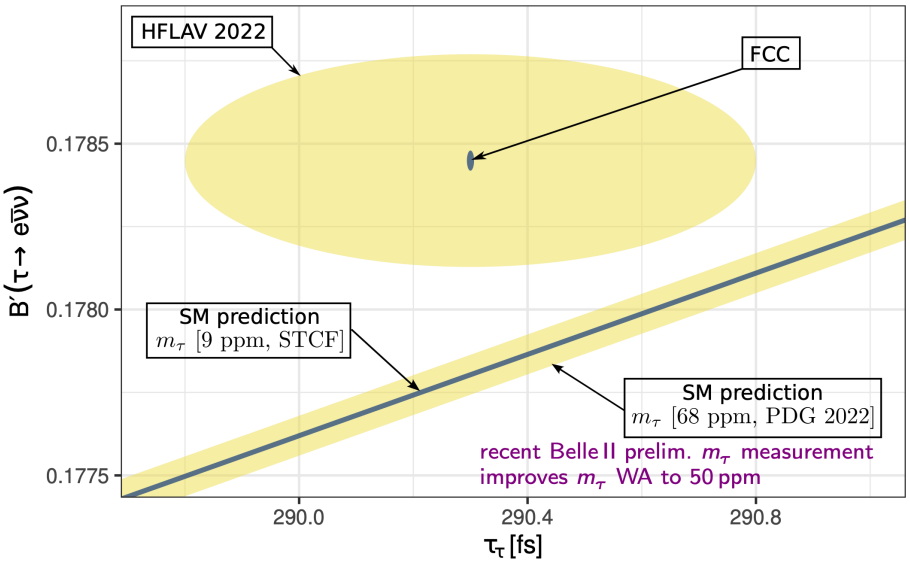

Figure 27: Expected precision of measuring the SM properties of τ lepton in the CEPC/FCC-*ee* era. The yellow (blue) areas correspond to the present (future) $\Delta\chi^2 = 1$ regions. This plot is taken from Ref. [156] – see also [155, 157]. [LC: Lusiani promised to send us a new plot with recent updates and the "Tera Z" label]

not going to be a concern at the CEPC also. So the main challenge will be to control the systematics on τ_τ and BR($\tau \to \ell\nu\bar{\nu}$) at a level better than the LEP ones.

To achieve such a goal is possible. As the systematics at the LEP are mainly caused by its sample size, with much higher luminosities, the CEPC may reduce the systematics by one order of magnitude for the BR($\tau \to \ell\nu\bar{\nu}$) measurements and to a level comparable to the statistical ones for the τ_τ analyses [155–157]. Testing the LFU in Eq. (7.3) thus may reach a precision level of $\pm 10^{-4}$. Figure 27 summarizes the expected precision of measuring the SM properties of τ lepton in the CEPC/FCC-*ee* era. This precision would make the CEPC very sensitive to the LFUV NP, such as those discussed in the literatures on the $R_{D^{(*)}}$ anomaly [11] and, more generally, with new dynamics coupled mainly to the third generation [84]. As shown, *e.g.*, in Refs. [169, 170], the tests of LFU in the τ sector are already providing important constraints on such models.

As another example of the discovery potential of these measurements, we can consider the operator $\frac{1}{\Lambda^2} i(\Phi^\dagger \tau^I \overleftrightarrow{D}_\mu \Phi)(\bar{L}_3 \tau^I \gamma^\mu L_3)$ (with $L_3 \equiv (\nu_\tau,\ \tau_L)^T$), which only involves (left-handed) τ leptons and is flavor-conserving. The presence of such an operator would induce a shift $g_\tau = g\left(1 + \frac{v^2}{\Lambda^2}\right)$ [67], where $v \simeq 246$ GeV is the vacuum expectation value of the Higgs field. A precision of 0.1‰ level in the determination of g_τ/g_ℓ would then test a NP sector generating such an operator (but not the corresponding ones involving muons or electrons) up to $\Lambda \approx 20$ TeV.

7.3 Opportunities with Hadronic τ Decays

Hadronic τ decays represent an important branch of τ physics. Currently, many leading constraints on the branching fractions of the various exclusive hadrnoic τ decay channels are set up by the LEP [171, 172], including $\tau^- \to \pi^- K_L^0 K_S^0 \nu_\tau$ [173], $\tau^- \to K^- 3\pi^0 \nu_\tau$ [174], $\tau^- \to \pi^- \pi^0 \nu_\tau$ [175] and so forth. The CEPC's performance in these measurements, especially for the processes with relatively high hadron multiplicity (*e.g.*, 3 and 5 hadrons) and in a large hadron invariant mass region, is expected to exceed the LEP. It is promising that CEPC has a good opportunity to provide more precise measurements for a significant portion of inclusive and exclusive hadronic τ decay channels [149], which highlights the advantage of high-energy e^+e^- colliders over other flavor factories in this field.

Hadronic τ decays bring in new physical opportunities while many of them are yet to be explored, especially at the CEPC. For example, inclusive hadronic decays are crucial for extracting the strong coupling constant $\alpha_s(m_\tau)$ [163, 176], which is currently limited by uncertainties in the large-recoil region. Precise measurements on the invariant-mass distributions of the hadronic systems in exclusive τ decays can tightly constrain the properties of different types of hadron resonances, which will in turn provide valuable inputs to study the CP violation in hadronic τ decay processes. Another example is the measurement of $\tau \to K(+X)$ decays, which is useful for the determination of $|V_{us}|$. Then such measurements can offer an alternative important way to address the Cabbibo anomaly [11], i.e., the unitarity violation of the first row of the CKM matrix. Additionally, polarization measurements of the τ leptons produced via Z decays can provide additional tests of the LFU and relevant inputs for the EWPT global fit [177–179]. These measurements are often performed in the hadronic decays $\tau \to \rho\nu$ and $\tau \to \pi\nu$. For more theoretical insights and details on hadronic τ decays, see [163, 176].

Finally, hadronic τ decays could be employed to improve the measurements of the currently weakly-constrained τ electric dipole moment (d_τ) and τ anomalous magnetic moment (a_τ), along the lines taken for Belle II in *e.g.*, Ref. [180, 181]. Very recently CMS has reported the present best limit on the τ magnetic moment with $a_\tau = 0.0009^{+0.0032}_{-0.0031}$ [182]. Interestingly, before the latter measurement, the tightest constraint with $-0.052 < a_\tau < 0.013$ at 95% C.L., was given by the DELPHI experiment that used τ lepton pairs from the photon-photon collisions off the Z pole [183]. These experimental limits are still a factor of few larger than the SM prediction, *i.e.*, $a_\tau^{\rm SM} = 0.00117721(5)$ [184], while it has been shown that a_τ could be tested at the level of $\sim 10^{-6}$ in the Belle II experiment [180, 181], the potential role of future e^+e^- facility in this endeavor still needs to be further studied.

In addition, hadronic τ decays can be also employed to study CP violation [185–189]. One benchmark mode is the decay $\tau \to K_S^0 \pi \nu_\tau$. It has been shown [190, 191] that the well-established CP violation in $K^0 - \bar{K}^0$ mixing can induce an $\mathcal{O}(10^{-3})$ asymmetry between the rates of τ^+ and τ^- decays. Furthermore, NP may provide contribution interfering with the SM amplitudes. Assuming that the hadronic τ decays indeed receive additional contributions from NP degrees of freedom, which carry different weak and strong phases from that of the SM contribution, one can then construct CP-violating observables in terms of the interference between the SM and NP amplitudes. Due to the linear dependence on the

NP amplitude, these observables may have a sensitivity to NP comparable to processes that are forbidden or strongly suppressed within the SM, such as $\tau \to \mu\gamma$ and the electric dipole moment of leptons, which are usually quadratic in the NP amplitude [188]. Searches for CP violation in the decay $\tau \to K^0_S \pi \nu_\tau$ have been performed in several experiments. After initial null results from CLEO [192, 193] and Belle [194], the BaBar collaboration reported in Ref. [195] the observation of anomalous CP violation based on the difference between τ^+ and τ^- decay rates. This measurement is in tension with the SM prediction [190, 191, 196] with a significance of $2.8\,\sigma$. The result prompted a number of NP explanations involving, *e.g.*, the introduction of non-standard tensor interactions [196–198].

CP violation in $\tau \to K^0_S \pi \nu_\tau$ can be also measured through angular distributions of its decay products, for both unpolarized and polarized τ leptons, even if their rest frame can not be exactly reconstructed [186]. The observable is defined as [8]

$$A_i^{CP} = \frac{\int_{s_{1,i}}^{s_{2,i}} \int_{-1}^{1} \cos\alpha \left[\frac{d^2\Gamma(\tau^- \to K^0_S \pi^- \nu_\tau)}{ds\, d\cos\alpha} - \frac{d^2\Gamma(\tau^+ \to K^0_S \pi^+ \bar{\nu}_\tau)}{ds\, d\cos\alpha} \right] ds\, d\cos\alpha}{\frac{1}{2} \int_{s_{1,i}}^{s_{2,i}} \int_{-1}^{1} \left[\frac{d^2\Gamma(\tau^- \to K^0_S \pi^- \nu_\tau)}{ds\, d\cos\alpha} + \frac{d^2\Gamma(\tau^+ \to K^0_S \pi^+ \bar{\nu}_\tau)}{ds\, d\cos\alpha} \right] ds\, d\cos\alpha} \,, \tag{7.4}$$

which is the difference between the angular differential decay widths of τ^- and τ^+ weighted by $\cos\alpha$, where α is the angle between the directions of the K and τ momenta in the $K\pi$ rest frame. This observable can be analyzed in individual bins of the $K\pi$ invariant mass squared (s), with the i-th bin defined by an interval $[s_{1,i}, s_{2,i}]$ [194]. As discussed above, CP violation in $K^0 - \bar{K}^0$ mixing induces a non-vanishing effect for this observable [199, 200]. Direct CP violation then arises from, *e.g.*, the interference between an S-wave from exotic scalar-exchange diagrams and a P-wave from SM W-exchange diagrams, provided that the couplings of the exotic scalars with fermions are complex. This possibility has been studied for both polarized and unpolarized beams [185, 186]. While still plagued by large experimental uncertainties, the current constraints could be significantly improved with more precise measurements expected to be performed at Belle II [8], as well as at future Tera-Z [176] and STCF [201] facilities.

8 Flavor Physics in Z Boson Decays

The LFV and LFU can be tested in multiple ways at the CEPC, which vary from heavy flavor to Z and Higgs boson decays. Among them the Z boson decays are of particular interest for the Tera-Z events expected to be accumulated in the CEPC Z-pole run. In addition to these effects, the Z boson decays can be also applied for examining QCD factorization theorem and investigating hadron inner structure. We will explore these topics in Section 8.1 and Section 8.2, respectively.

8.1 LFV and LFU

Let us consider first searches for LFV in Z boson decays. In Table 8, we summarize the current limits on $Z \to \ell\ell'$ and the projected sensitivities at the high-luminosity run of the LHC (HL-LHC) and at the FCC-ee and CEPC Z factories. While the current limits can be improved at HL-LHC, such improvement is expected to be within one order of magnitude

as a consequence of the large background from $Z \to \tau\tau$. This background is difficult to deal with at hadron colliders, however it can be well addressed at a machine like CEPC due to its excellent identification of τ leptons. Moreover, a major advantage of a e^+e^- collider is the precise knowledge of the initial state kinematics, such that the constraint on the di-lepton invariant mass, $m^2_{\ell\ell'} = m^2_Z$, is only limited by the beam energy spread, in contrast to hadronic machines where this constraint is instead limited by the large width of the Z boson. Hence, a high accuracy in measuring the momenta of the tracks and a good control of the beam energy are crucial ingredients for this kind of searches. Additionally, the sensitivity to BR($Z \to \mu e$) is limited by the background from $Z \to \mu\mu$ with one of the muons being misidentified as an electron in the ECAL [155]. Precise PID is then another important requirement.

As demonstrated in Refs. [202, 203], although the allowed rate of $Z \to \mu e$ generally lies well below the expected sensitivity,[5] a Tera-Z factory, with its $\mathcal{O}(10^{12})$ Z decays, holds promise for $Z \to \tau\ell$ decays, whose rate can be as large as BR($Z \to \tau\ell$) $\approx 10^{-7}$ without violating the indirect limits set by the LFV measurement in τ decays [202].

In Ref. [202], the present and future limits on LFV Z decays have been interpreted as constraints on the NP energy scale within the dimension-6 SM EFT (SMEFT) $\mathcal{H}_{\text{SMEFT}} \supset \frac{1}{\Lambda^2}\sum_a C_a Q_a$ [204, 205], where

$$Q^{(1)}_{\varphi\ell} \equiv i(\Phi^\dagger \overleftrightarrow{D}_\mu \Phi)(\bar{L}\gamma^\mu L)\,,\ Q^{(3)}_{\varphi\ell} \equiv i(\Phi^\dagger \tau^I \overleftrightarrow{D}_\mu \Phi)(\bar{L}\tau^I\gamma^\mu L)\,,\ Q_{\varphi e} \equiv i(\Phi^\dagger \overleftrightarrow{D}_\mu \Phi)(\bar{E}\gamma^\mu E) \tag{8.1}$$

are Higgs current operators and

$$Q_{eZ} \equiv (\sin\theta_w Q_{eB} + \cos\theta_w Q_{eW}) \tag{8.2}$$

with $Q_{eB} \equiv (\bar{L}\sigma^{\mu\nu}E)\Phi B_{\mu\nu}$ and $Q_{eW} \equiv (\bar{L}\sigma^{\mu\nu}E)\tau^I\Phi W^I_{\mu\nu}$ is a linear combination of dipole operators. Here L and E are, respectively, the SM doublet and singlet lepton fields (with flavor indices omitted), Φ is the Higgs doublet, $B_{\mu\nu}$ and $W^I_{\mu\nu}$ ($I = 1, 2, 3$) are, respectively, the $U(1)_Y$ and $SU(2)_L$ field strengths, τ^I are the Pauli matrices, and $\Phi^\dagger \overleftrightarrow{D}_\mu \Phi$ is defined as $\Phi^\dagger(D_\mu\Phi) - (D_\mu\Phi)^\dagger\Phi$. In Figure 28, we illustrate the NP scale associated to these LFV operators that the CEPC can reach searching for $Z \to \tau\mu$ if a sensitivity such as in Table 8 is achieved. As one can see, NP scales up to $20-30$ TeV can be probed at the CEPC. Such a performance is comparable with that of Belle II through searches for LFV τ decays – assuming an integrated luminosity of 50 ab^{-1}. Searches for $Z \to \tau e$ are expected to deliver similar sensitivities [202].

The study in Ref. [203] considers an alternative probe at future electron-positron colliders: the non-resonant production of $\tau\mu$, and examines the CEPC's expected sensitivity to $e^+e^- \to \tau\mu$ signals. This signal exhibits a characteristic dependence on the center-of-mass energy, depending on the nature of the dominant LFV operator. The contributions of operators containing the Z boson, Eq. (8.1) and Eq. (8.2), are resonantly enhanced on the Z pole. At higher energies, dipole interactions as in Eq. (8.2) yield a cross section that

[5] Barring unlikely accidental cancellations among different contributions, searches for LFV in muon decays set the indirect constraint BR($Z \to \mu e$) $\lesssim 10^{-12}$ [202].

Measurement	Current	HL-LHC	FCC	CEPC prelim.
$\mathrm{BR}(Z \to \tau\mu)$	$< 6.5 \times 10^{-6}$	1.4×10^{-6}	10^{-9}	10^{-9}
$\mathrm{BR}(Z \to \tau e)$	$< 5.0 \times 10^{-6}$	1.1×10^{-6}	10^{-9}	
$\mathrm{BR}(Z \to \mu e)$	$< 2.62 \times 10^{-7}$	5.7×10^{-8}	$10^{-8} - 10^{-10}$	10^{-9}

Table 8: Current 95% CL limits on LFV in Z decays [206, 207] and projected sensitivities at HL-LHC and the FCC-ee [155] and CEPC [159] Z factories (see also [203]). For HL-LHC, we naively scaled the current limits, which were obtained by ATLAS employing 139 fb^{-1} of data [206, 207], according to the target luminosity 3000 fb^{-1}.

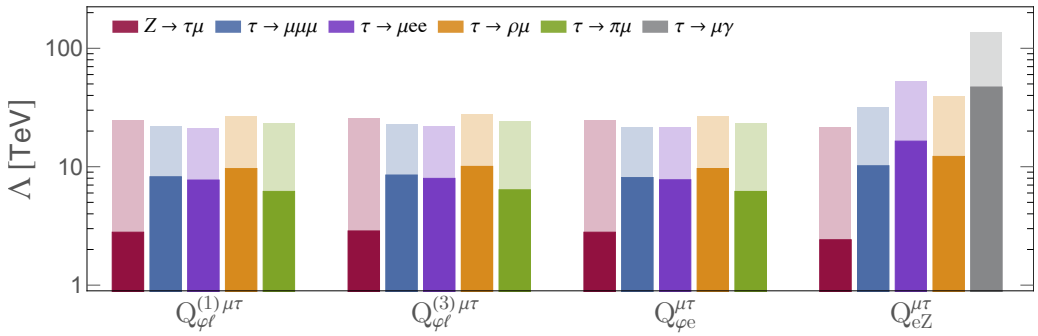

Figure 28: Sensitivity reach for probing the NP scale of the LFV operators in Eq. (8.1) and Eq. (8.2). Here the current bounds (dark-colored bars) are set by ATLAS [206] ($Z \to \tau\mu$) and B factories [149] (LFV τ decays), and the projected sensitivities (light-colored bars) are based on searches for $Z \to \tau\mu$ at the CEPC Z pole run with 100 ab^{-1} and $\tau \to \mu$ transitions at Belle II with 50 ab^{-1} [8], see Tables 7 and 8. The Wilson coefficients have been set equal to one uniformly. This plot is taken from Ref. [202]

.

remains constant for large values of the center-of-mass energy squared s, while the Higgs current interactions in Eq. (8.1) result in a cross section that decreases as $1/s$ for large s. In contrast, contributions to the $e^+e^- \to \tau\mu$ cross section from contact interactions – *i.e.*, 4-fermion operators such as $(\bar{e}\gamma_\mu P_X e)(\bar{\mu}\gamma^\mu P_Y \tau)$ $(X, Y = L, R)$ – increases linearly with s. Overall, the Tera-Z factories can test NP scales up to $\mathcal{O}(10$ TeV), rivaling the sensitivities of searching for the LFV tau decays at Belle II. The framework provided by this study enables a disentanglement of contributions from different operators, exploiting the complementarity of searches at various center-of-mass energies. Additional diagnostic measures could be provided also by measurements of forward-backward asymmetry or CP violation.

The LFU tests have been discussed in the FCCC and FCNC b-hadron decays in Section 3 and Section 4. These tests can be also performed in Z decays. Currently, the LFUV for the Z boson couplings have been constrained to per mil level [150]:

$$\frac{\mathrm{BR}(Z \to \mu^+\mu^-)}{\mathrm{BR}(Z \to e^+e^-)} = 1.0009 \pm 0.0028\,, \qquad \frac{\mathrm{BR}(Z \to \tau^+\tau^-)}{\mathrm{BR}(Z \to e^+e^-)} = 1.0019 \pm 0.0032\,. \tag{8.3}$$

While the used data sets are old (1.7×10^7 Z events at LEP, and 6×10^5 Z events with polarized beams at SLC), these constraints have strongly limited the space for NP models aiming to address the anomalies in FCCC and FCNC semileptonic B decays [169]. In addition, an enhanced rate of $Z \to \mu^+\mu^-$ is predicted within a wide class of NP models addressing the muon $g-2$ anomaly [208]. Improving on the above observables could then probe LFUV NP with high precision. In the future, reaching a precision of $\mathcal{O}(10^{-4})$ in the measurements of $\mathrm{BR}(Z \to \ell^+\ell^-)$ will allow to probe the scale Λ of the flavor-conserving counterpart of the operators in Eq. (8.1) involving τ leptons up to ≈ 20 TeV. Similarly, a Z LFU test with such a level of precision would reach $\Lambda \approx 10$ TeV for the scale of the semileptonic operator $(\bar{Q}_3\gamma_\mu Q_3)(\bar{L}_3\gamma_\mu L_3)$ only comprising third generation fermions, which can also provide relevant contributions to other LFU observables such as $R_{D^{(*)}}$ [169], cf. Eq. (3.6). Notably, in a Tera-Z factory these prospected measurements would be mainly limited by systematics, while statistical and systematic errors are of the same order of magnitude at the LEP. Hence, further scrutiny on these systematic uncertainties is necessary to assess the CEPC capability of performing the tests of LFU in Z decays. The theoretical uncertainties of the SM prediction also need to be estimated.

8.2 Factorization Theorem and Hadron Inner Structure

During the Z-factory phase of CEPC, a precise measurement can be achieved for various Z decays. Apart from the well-known decay channels of lepton pair and quark pair and the LFV ones induced by NP, one could explore exclusive hadronic Z decays, such as $Z \to J/\psi\gamma$ and $Z \to \pi^+\pi^-$, which have never been observed before. Different from heavy flavor physics at the bottom and charm mass scales, these decays occur at the EW scale and usually have a better convergence behavior. This may greatly benefit the examination of QCD factorization theorem and the investigation of hadron inner structure.

The factorization formalism for exclusive decays [209–212] are standard. Their application to B decays however is hindered by large power corrections of $\mathcal{O}(\Lambda^n_{\mathrm{QCD}}/m_b^n)$ where their convergence is weak due to the smallness of b quark mass. This theorem, however, can be circumvented for exclusive Z decays, as the large Z mass yields a more efficient suppression for these power corrections. The factorization of exclusive Z decays therefore can serve as a touchstone for examining the factorization formalism. The benchmark channel $Z \to J/\psi\,\gamma$, with a BR $\sim 10^{-7}$ [213], could be measured at the CEPC [159] with a precision much higher than that for the current limit of $< 1.4 \times 10^{-6}$ [214]. The Z decays into two mesons have an even smaller BR of $\lesssim 10^{-11}$ [215, 216]. While a discovery would be unattainable at both the LHC and the CEPC, the CEPC is expected to establish much more stringent upper limits for their event rates.

The radiative decay $Z \to M\gamma$ can serve as a tool to investigate the internal structure of light mesons, which are crucial theoretical inputs to factorization formulas, typically formulated by the light-cone distribution amplitudes (LCDAs). While the parton-distribution function (PDF) can be precisely determined by high-energy inclusive processes, a comparable comprehensive experimental determination of meson LCDAs is still lacking. However, the $Z \to M\gamma$ processes provide an ideal platform for extracting the leading-power LCDAs of mesons. This is due not only to the involvement of only one meson in the process,

Measurement	SM Prediction (Tao Liu: Which theory? SM?)	Current Limits [149]	CEPC prelim.
$\mathrm{BR}(Z \to \pi^+\pi^-)$	$(8.3 \pm 0.5) \times 10^{-13}$ [215]	-	$\mathcal{O}(10^{-10})$
$\mathrm{BR}(Z \to \pi^+\pi^-\pi^0)$	-	-	$\mathcal{O}(10^{-9})$
$\mathrm{BR}(Z \to J/\psi\gamma)$	$(8.02 \pm 0.45) \times 10^{-8}$ [213]	$< 1.4 \times 10^{-6}$	$10^{-9} - 10^{-10}$
$\mathrm{BR}(Z \to \rho\gamma)$	$(4.19 \pm 0.47) \times 10^{-9}$ [213]	$< 2.5 \times 10^{-5}$	

Table 9: Preliminary estimates on the Tera-Z sensitivities for measuring exclusive hadronic Z decays [159], with the CEPC full simulation samples. The exact results and systematic effects remain to be explored.

but also because the large Z mass once again significantly suppresses power corrections, resulting in a clean environment. As indicated in Table 9, the CEPC is expected to be able to determine the LCDAs of mesons such as J/ψ and ρ by accurately measuring their corresponding radiative decays.

Flavor-specific examples also encompass the Higgs exclusive hadronic decays, believed to be more sensitive to NP, especially to non-standard Yukawa couplings of the Higgs boson [217]. Such decays can be examined within the Higgs factory mode of the CEPC, and are thus primarily limited by statistics rather than systematic uncertainties. Despite the challenging nature of measuring these rare processes, exclusive decays $h \to V\gamma$ of the Higgs boson at the LHC, the high luminosity run of the LHC and the CEPC could provide the much-needed platform to investigate these processes. These measurements could be vital for testing the QCD factorization approach and extracting valuable information about the LCDAs of various mesons.

9 Flavor Physics beyond Z Pole

Similar to the case of Z boson decays, flavor physics can be explored in physical processes of other EW-scale particles such as W boson, Higgs boson and top quark. The productions of these particles are rich in the CEPC runs beyond Z pole including at WW threshold, Higgs factory and also $t\bar{t}$ threshold (see Table 1). Such a strategy well-complements the study of heavy flavor physics (b, c, τ), as the probed energy domain and hence the relevant physical effects (e.g., QCD effects) could be very different. This will necessarily provide new insights into fundamental rules in flavor physics. It is thus of high scientific value to extend the flavor-physics study from the heavy-flavor fermions to these EW-scale particles. In this section, instead of a comprehensive study we will demonstrate several benchmark cases involving W boson, Higgs boson and top quark, respectively.

9.1 Flavor Physics and W Boson Decays

CEPC is expected to produce $\gtrsim 10^9$ W bosons combing the WW threshold and Higgs factory operation. This large statistics and clean machine environment provides excellent opportunities for looking into the relevant flavor physics.

One important case in flavor physics CEPC can address is to measure the CKM matrix elements, particularly $|V_{cb}|$, in the on-shell W boson decays. Currently, there is a long-

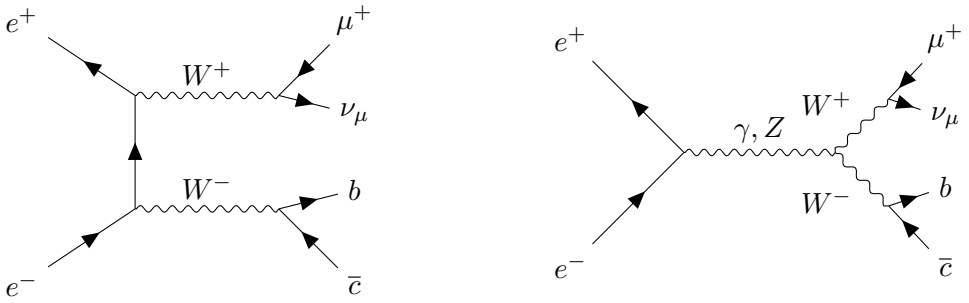

Figure 29: Illustrative Feynman diagrams for the process $e^+e^- \to W^+W^- \to cb\mu\nu$.

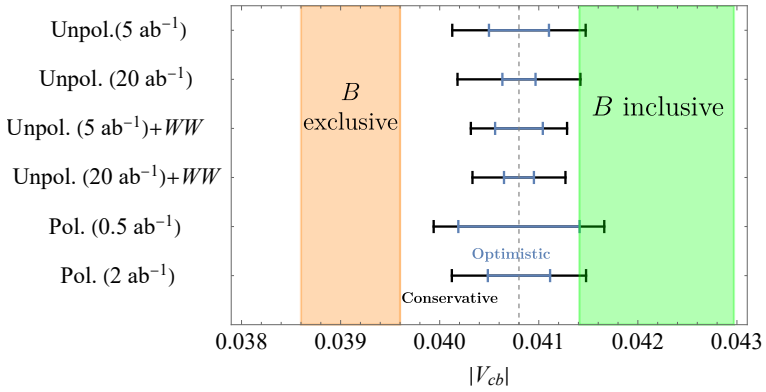

Figure 30: The projected sensitivities of $|V_{cb}|$ measurement from $W \to cb$ decays in different future lepton collider benchmarks. For CEPC, it corresponds to the fourth row, which means an unpolarized Higgs factory with an extended run and a WW threshold run. Two systematic uncertainty scenarios are illustrated as black and blue error bars. For comparison, the current values of $|V_{cb}|$ from inclusive and exclusive B decays are also included [11]. The PDG average of $|V_{cb}|$ [149] is taken as a nominal central value for all future measurements. See the main text and [221] for more details.

standing discrepancy ($\sim 3\sigma$ or 0.0031 in absolute value) on the determination of $|V_{cb}|$ between inclusive and exclusive B meson decays [11]. This discrepancy, however, is not very indicative for the NP, as both methods rely on semileptonic b-hadron decays and consequently are susceptible to theoretical uncertainties from non-perturbative QCD [11, 218]. These QCD effects could be significantly suppressed at a higher energy scale, thereby improving the theoretical predictability [219]. The studies in Ref. [78, 220] suggested that the W bosons produced from WW threshold runs of the e^+e^- colliders could yield a measurement of $|V_{cb}|$ with a relative uncertainty $\lesssim 0.5\%$ (for illustrative Feynman diagrams, see Figure 29). Such a relative $|V_{cb}|$ precision is better than the current ones, typically $\gtrsim 1\%$ [11]. A dedicated study [221] indicates that the Higgs factory mode ($\sqrt{s}$ =240 GeV) of CEPC may provide a comparable or even better sensitivity of $|V_{cb}|$ due to the large integrated luminosity (~ 20 ab^{-1}) of this operation mode.

A simulation of $e^+e^- \to W^+W^- \to \ell\nu cb$ signal with various backgrounds is performed, with the full simulation of the CEPC CDR baseline detector design [2]. Major

backgrounds include other semileptonic WW events and various e^+e^- to 4(2) fermion processes. Several kinematic cuts are first applied to separate semileptonic WW events from other backgrounds. The selected events go through a multivariate classifier to select $e^+e^- \to W^+W^- \to \ell\nu cb$ signals. By combining both lepton flavors of $WW \to \ell\nu cb$, the relative statistical uncertainty for $|V_{cb}|$ is determined to be $\lesssim 0.4\%$ [221], which has the potential to resolve the tension between inclusive and exclusive methods. The advanced jet origin identification [34] algorithm played a critical role in this analysis. Despite this encouraging outcome, the precision of measuring $|V_{cb}|$ can be further improved by improving the jet flavor tagging with, e.g., advanced algorithms and innovative designs for the vertex detector system and including the data at the WW threshold. On the other hand, the final performance of $|V_{cb}|$ determination relies on controlling systematic uncertainties, especially the flavor tagging efficiency and mistag rates. The projected overall sensitivities of CEPC and other Higgs factory benchmarks on both muon and electron signal channels are demonstrated in Figure 30, including both statistical and systematic uncertainties.

Measurements of leptonic W boson decays at the CEPC will benefit from its large statistics also. This raises new possibilities of testing the LFU in the charged-current processes, in addition to the ones discussed in Sections 3 and 7.2. Currently the world averages for the width ratios of leptonic W boson decays are [149]:

$$\begin{aligned} &\frac{\mathrm{BR}(W \to \mu\nu)}{\mathrm{BR}(W \to e\nu)} = 1.002 \pm 0.006\,, \quad \frac{\mathrm{BR}(W \to \tau\nu)}{\mathrm{BR}(W \to e\nu)} = 1.015 \pm 0.020\,, \\ &\frac{\mathrm{BR}(W \to \tau\nu)}{\mathrm{BR}(W \to \mu\nu)} = 1.002 \pm 0.020\,, \end{aligned} \tag{9.1}$$

which are consistent with the SM prediction about the LFU at percent and even subpercent levels. These results are mainly based on the measurements in the LHC experiments [222–224], and are more precise than those of the combined LEP analyses by a factor of approximately two [225]. With $\sim 10^4$ times larger statistics than the LEP one and improved control of systematic errors, the CEPC is expected to be in a position to substantially improve the LFU test in the W boson decays.

9.2 FCNC Higgs Boson Decays

With a yield of 4.3×10^6 Higgs bosons, the study on FCNC flavor physics can be reasonably extended from the CEPC Z pole to its Higgs factory, by investigating the Higgs hadronic decays $H \to sb, sd, db, uc$ [6]. These hadronic FCNC Higgs boson decays are forbidden in the SM at tree level, and have a BR up to $\mathcal{O}(10^{-7})$ due to loop-level contributions. New dynamics such as multiple Higgs doublets models, however, could enhance their BRs by orders of magnitude [229, 230]. As these FCNC Higgs boson decays produce two flavors of quarks in their final state, excellent flavor-tagging efficiency becomes crucial for their precision measurements. Using the method of machine learning, the study in Ref. [34] developed a tool to extract the information on jet origin and estimated the potential sensitivities of measuring the FCNC Higgs boson decays. As shown in Figure 31, the BRs for

[6] Here sb denotes $s\bar{b}$, and similarly for sd, db, and uc.

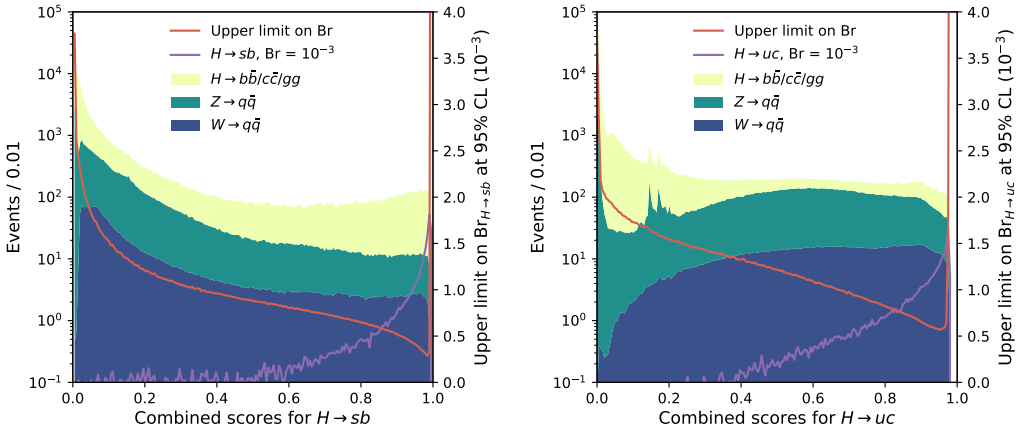

Figure 31: Projected sensitivities for measuring $H \to sb$ (left panel) and $H \to uc$ (right panel) in the $\nu\bar{\nu}H$ process at the CEPC [34]. (Tao Liu: The panels for diagonal modes have been removed which are off the mainline. What is the luminosity assumed for this analysis?)

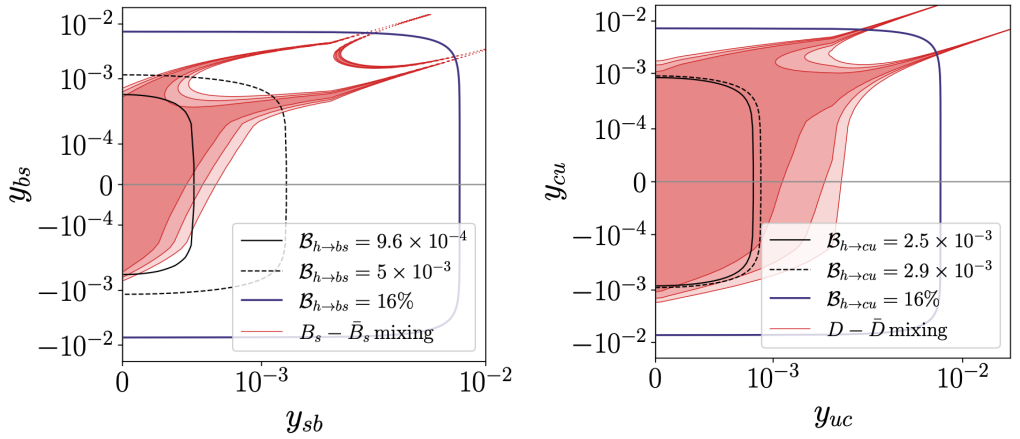

Figure 32: Current and projected direct limits on the FCNC Higgs boson decays $H \to bs$ (left) and $H \to cu$ (right). Here y_{ij} denote the FCNC coupling of Higgs boson to a left-chiral quark i and a right-chiral quark j. The 16% limit in the plot is based on the upper limit on the Higgs to undetermined decays from current LHC measurements [226, 227]. The black lines with $\sim \mathcal{O}(10^{-3})$ limits are expected direct limits at future Higgs factories based on FCC-*ee* flavor tagging performance. The red shaded regions, from dark to light, in both panels represent the indirect constraints at 1σ, 2σ, 3σ C.L.s, respectively, interpreted from current $\bar{B}_s^0 - B_s^0$ and $\bar{D}^0 - D^0$ mixings results. The plots are taken from Ref. [228].

the decays $H \to sb$ and uc can be measured with an upper limit $\sim 0.03\%$ and 0.08% at 95% C.L., respectively.

A study on the FCNC Higgs boson decays at the FCC-*ee* [228] obtained comparable sensitivities on BR($H \to bs$) and BR($H \to cu$), estimating upper limits at the $\mathcal{O}(10^{-3})$

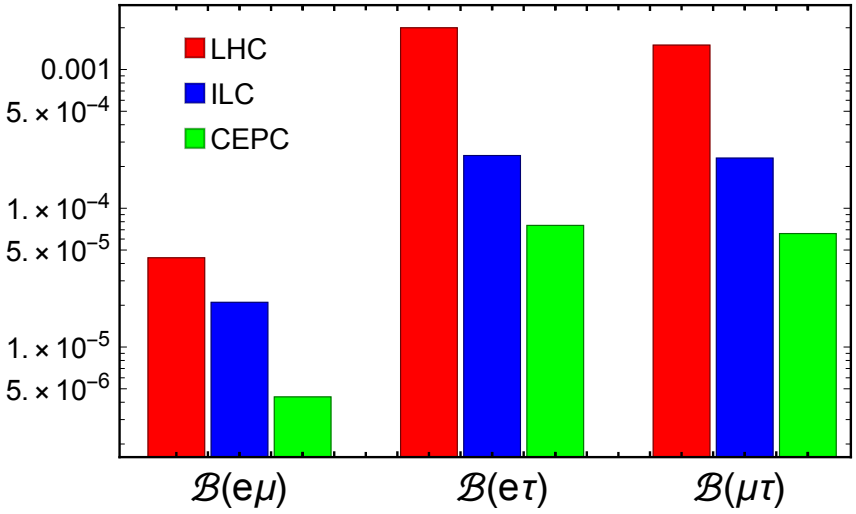

Figure 33: Anticipated upper limits on LFV Higgs decays at CEPC, ILC, and LHC. Figure updated from [231].

level. Since the FCNC Higgs couplings contribute also to low-energy-scale observables, such as the $\bar{B}_s^0 - B_s^0$ and $\bar{D}^0 - D^0$ mass splitting and the $B_s^0 \to \mu^+\mu^-$ and $B_s^0 \to \tau^+\tau^-$ decay rates, measuring these observables can yield indirect constraints on the FCNC Higgs interactions. A comparison between the direct and indirect limits on typical FCNC Higgs couplings is demonstrated in Figure 32. As illustrated by this figure, the direct limits that can be obtained by measuring the FCNC Higgs boson decays at the FCC-ee are expected to be comparable with the indirect ones set by the current measurements of $\bar{B}_s^0 - B_s^0$ and $\bar{D}^0 - D^0$ mixing.

The method in [34] can be also applied to the Z FCNC hadronic decay. Giving the nominal yields of 4 Tera Z boson, we anticipate the 95% C.L. upper limits to reach 10^{-7} for the $Z \to bs$ and $Z \to bd$ decays, 3×10^{-7} for $Z \to cu$, and 7×10^{-6} for $Z \to sd$. These results only rely on statistical uncertainties, while the calibration and systematic control will be the main challenge for these measurements, which is still an open question and will require dedicated efforts to understand and to tame. On the other hand, these limits are orders of magnitudes better than current limits, especially for the $Z \to bs$ FCNC decay modes, whose anticipated accuracy is only two times larger than the SM prediction – showing that those measurements will be a promising probe to New Physics models that can significantly enhance those hadronic FCNC decay modes.

CEPC can give even stronger limits on LFV Higgs decays, $h \to \ell_i^+\ell_j^-$ $(i \neq j)$, giving the fact that different species of leptons could be identified at a much high efficiency and purity compared to the jets. The study in [231] showed that the upper limits on the LFV branching ratios of the Higgs could reach the 10^{-5} level with 1 million Higgs bosons. Extrapolating to the CEPC TDR setup with 4.3 million Higgs bosons, the uper limit can be further reduced by by more than a factor of two, see Fig. 33, where the expectation for ILC and LHC is also shown. Note that for the $e\tau$ and $\mu\tau$ channels only the leptonic decay products of are utilized for τ reconstruction [231] at lepton colliders. If the hadronic

final states of the τ are also taken into account, it is anticipated that the upper limits for these two channels would become more stringent. In conclusion, the statistical uncertainty on $\mathrm{BR}(h \to \tau\ell)$ can reach the $10^{-5} - 10^{-4}$ level, while the sensitivity can increase to the $\mathcal{O}(10^{-6})$ level when considering the $h \to \mu e$ decay. However, the rate of this process is indirectly constrained to be $\mathrm{BR}(h \to \mu e) \lesssim 10^{-8}$ by the LFV muon decays [232].

9.3 FCNC Top Quark Physics

Top quark physics may play a crucial role in reaching a deeper understanding of the dynamics of EW symmetry breaking, see, *e.g.*, [233]. The CEPC program provides opportunities to probe top-quark-related FCNC processes via both anomalous single top production below the top pair production threshold and FCNC top decays with the $t\bar{t}$ dataset at $\sqrt{s} = 360$ GeV. A case study of the FCNC top production in the Higgs factory mode is shown in this section. Currently no dedicated study on top FCNC above the top pair threshold is available. It will be explored in the future work of the CEPC flavor program.

This study targets the anomalous single top production process $e^+e^- \to t(\bar{t})j$ at $\sqrt{s} = 240$ GeV. Here "j" denotes a light jet. While being suppressed by the GIM mechanism in the SM, this channel can be enhanced by NP two-fermion current operators and four-fermion contact operators, as shown in Figure 34.

The LHC TOP Working Group [234] provides a systematic SMEFT description on FCNC top quark physics. The operators relevant to the $e^+e^- \to t(\bar{t})j$ process are

$$O_{\varphi q}^{1(ij)} = i\left(\Phi^\dagger \overleftrightarrow{D}_\mu \Phi\right)\left(\bar{q}_i \gamma^\mu q_j\right), \tag{9.2}$$

$$O_{\varphi q}^{3(ij)} = i\left(\Phi^\dagger \tau^I \overleftrightarrow{D}_\mu \Phi\right)\left(\bar{q}_i \gamma^\mu \tau^I q_j\right), \tag{9.3}$$

$$O_{\varphi u}^{(ij)} = i\left(\Phi^\dagger \overleftrightarrow{D}_\mu \Phi\right)\left(\bar{u}_i \gamma^\mu u_j\right), \tag{9.4}$$

$$O_{uW}^{(ij)} = \left(\bar{q}_i \sigma^{\mu\nu} \tau^I u_j\right)\tilde{\Phi} W_{\mu\nu}^I, \tag{9.5}$$

$$O_{uB}^{(ij)} = \left(\bar{q}_i \sigma^{\mu\nu} u_j\right)\tilde{\Phi} B_{\mu\nu}, \tag{9.6}$$

for the two-fermion interactions, and

$$O_{lq}^{1(ijkl)} = \left(\bar{l}_i \gamma_\mu l_j\right)\left(\bar{q}_k \gamma^\mu q_l\right), \tag{9.7}$$

$$O_{lq}^{3(ijkl)} = \left(\bar{l}_i \gamma_\mu \tau^I l_j\right)\left(\bar{q}_k \gamma^\mu \tau^I q_l\right), \tag{9.8}$$

$$O_{lu}^{(ijkl)} = \left(\bar{l}_i \gamma_\mu l_j\right)\left(\bar{u}_k \gamma^\mu u_l\right), \tag{9.9}$$

$$O_{eq}^{(ijkl)} = \left(\bar{e}_i \gamma_\mu e_j\right)\left(\bar{q}_k \gamma^\mu q_l\right), \tag{9.10}$$

$$O_{eu}^{(ijkl)} = \left(\bar{e}_i \gamma_\mu e_j\right)\left(\bar{u}_k \gamma^\mu u_l\right), \tag{9.11}$$

$$O_{lequ}^{1(ijkl)} = \left(\bar{l}_i e_j\right)\varepsilon\left(\bar{q}_k u_l\right), \tag{9.12}$$

$$O_{lequ}^{3(ijkl)} = \left(\bar{l}_i \sigma_{\mu\nu} e_j\right)\varepsilon\left(\bar{q}_k \sigma^{\mu\nu} u_l\right), \tag{9.13}$$

for the four-fermion interactions, where i, j, k, l are flavour indices.

In total, 56 operators can contribute to $e^+e^- \to t(\bar{t})j$. For each light generation a ($a = 1, 2$), there are 28 Wilson coefficients. The 28 coefficients can be split into four groups

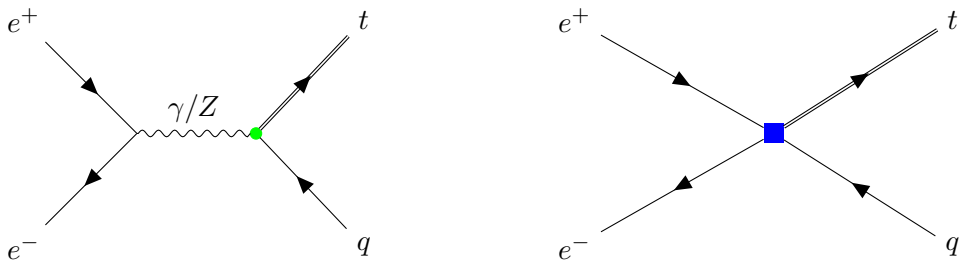

Figure 34: Illustrative Feynman diagrams for the FCNC single top production $e^+e^- \to t(\bar{t})j$. The green dot and blue square represent two-fermion current and four-fermion (two-lepton two-quark) contact operators, respectively.

with no interference between each group in the limit of massless quarks, so it is sufficient to focus on one group at a time in the analysis. For example, the CP-even coefficients involving a left-handed light quark can be written as follows [235]:

$$c_{\varphi q}^{-(3+a)} \equiv \Re\left\{C_{\varphi q}^{1(3a)} - C_{\varphi q}^{3(3a)}\right\}, \tag{9.14}$$

$$c_{uZ}^{(a3)} \equiv \Re\left\{-s_W C_{uB}^{(a3)} + c_W C_{uW}^{(a3)}\right\}, \tag{9.15}$$

$$c_{uA}^{(a3)} \equiv \Re\left\{c_W C_{uB}^{(a3)} + s_W C_{uW}^{(a3)}\right\}, \tag{9.16}$$

$$c_{lq}^{-(1,3+a)} \equiv \Re\left\{C_{lq}^{1(113a)} - C_{lq}^{3(113a)}\right\}, \tag{9.17}$$

$$c_{eq}^{(1,3+a)} \equiv \Re\left\{C_{eq}^{(113a)}\right\}, \tag{9.18}$$

$$c_{lequ}^{S(1,a3)} \equiv \Re\left\{C_{lequ}^{1(11a3)}\right\}, \tag{9.19}$$

$$c_{lequ}^{T(1,a3)} \equiv \Re\left\{C_{lequ}^{3(11a3)}\right\}. \tag{9.20}$$

Here $\Re$ represents the real part of the coefficients. The corresponding imaginary part of the coefficients produces CP-odd signals with identical experimental signature due to the lack of an SM amplitude to interfere with. The coefficients involving a right-handed light quark produce different experimental signatures due to the difference in top helicity state.

Currently, the best constraints on the FCNC two-fermion current operators and four-fermion contact operators are set by the LHC [236–240] and LEP2 data, respectively [241–244], see also [245, 246]. The measurements in the latter case are exactly based on the FCNC single top quark production $e^+e^- \to t(\bar{t})j$. The prospects for measuring these operators via the same channel at the CEPC have been studied in Ref. [235], assuming an integrated luminosity of 5.6 ab^{-1} at $\sqrt{s} = 240\,\text{GeV}$ and a CEPC detector profile as presented in [2]. For the semileptonic top quark decays, the signal signature contains one bottom jet, one up or charm quark jet, one charged lepton and missing energy, while the backgrounds receive contributions mainly from the WW production with one W boson decaying hadronically and the other one leptonically. Figure 35 shows some key kinematic features of reconstructed signal and background events. With basic cuts for these features, certain improvements to the currents limits on the FCNC top quark operators can be

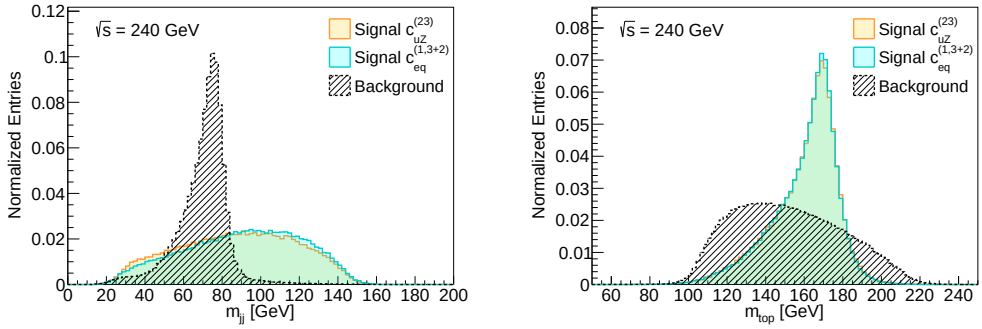

Figure 35: Kinematic distributions of reconstructed signal and background events for measuring $e^+e^- \to t(\bar{t})j$. This plot is taken from [235].

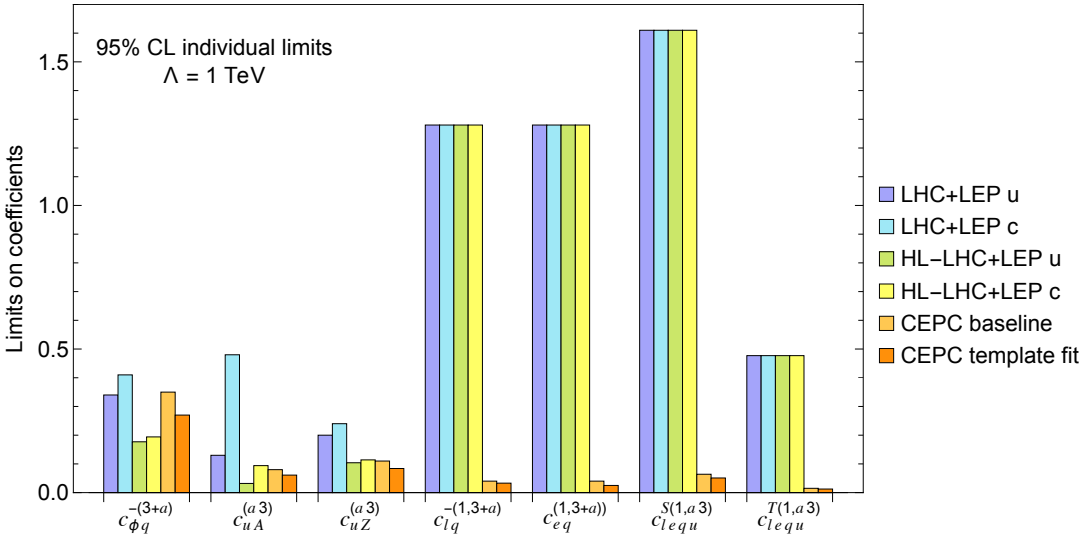

Figure 36: Projected constraints on the FCNC top quark operators at the CEPC, comparing with the existing LHC+LEP2 bounds and the projected limits from HL-LHC+LEP2 and FCC-ee. This plot is taken from [235]. The individual limits on the coefficients are obtained by switching on each operator at a time in the fit. The LHC bounds on the four-fermion operators are obtained by reinterpreting the $t \to q\ell\ell$ search results. The "CEPC baseline" column shows the expected limit from a basic cut and count analysis with baseline kinematic cuts tagging the single top quark signal in the leptonic decay signature. The "CEPC template fit" column shows the expected limit exploiting additional information of c-tagging (only applying to the $a = 2$ operators) and the top quark scattering angle on top of the baseline approach.

achieved. As shown in Figure 36, while the prospects of measuring the two-fermion current operators at the CEPC are not much better than HL-LHC (due to the excellent sensitivity of the latter to decays such as $t \to qZ$, $t \to qH$, $t \to qZ$ [246]), the current limits for the four-fermion contact operators can be improved at the CEPC by one to two orders of

magnitude. These constraints could be further improved by exploiting additional kinematic features of the FCNC single top quark production. For example, imposing a c-tagging requirement together with b-tagging can further suppress the background and improve the sensitivity to the FCNC top quark interactions with $j = c$. The capacity of tagging light-flavored jets at CEPC also presents the possibility to distinguish EFT operators related to u quarks from those related to c quarks. The Lorentz structure of the operators are reflected in the kinematic distributions of the top quark as well as its decay products. Observables like differential cross sections and forward-backward asymmetries may help lift the degeneracy between the coefficients and pinpoint the coefficient that gives rise to the excess if an FCNC signal is observed.

10 Spectroscopy and Exotics

Spectroscopy of hadrons is critical for understanding the mass generation in QCD, given the persisting mystery of color confinement. Although exotic hadrons, extending beyond conventional quark-antiquark mesons and three-quark baryons, have been postulated since the invention of the quark model, strong evidence for their existence only emerged recently as a result of significant experimental progress. In particular, the discovery of the $D^*_{s0}(2317)$ meson by BaBar [247] and the $X(3872)$ meson, also known as $\chi_{c1}(3872)$ [149], by Belle [248], has resulted in a surge of interest from both experimental and theoretical sides. During the past two decades dozens of exotic states, with a noteworthy characteristic of narrow states located near the threshold for production of a pair of open-flavor hadrons, have been identified. Nevertheless, intriguing resonant structures, that are explicitly exotic, were observed, such as the $Z_c(3900)^{\pm}$ by BESIII [249] and Belle [250], hidden-charm strange tetraquark Z_{cs} candidates by BESIII [251] and LHCb [252], hidden-charm P_c pentaquarks [253, 254], double-charm $T_{cc}(3875)^+$ tetraquark [255], and fully-charmed tetraquarks (*e.g.*, $X(6900)$) by LHCb [256], ATLAS [257] and CMS [258]. It is evident from Figure 37 that most of these newly observed states in the charmonium mass region go beyond the charmonium spectrum predicted by quark models (*e.g.*, the Godfrey-Isgur quark model [259]). These discoveries spur plenty of efforts in trying to reveal the nature of the new hadrons and to gain deeper understanding of nonperturbative strong interactions. For recent reviews, one may refer to Refs. [260–271]. A wide spectrum of potential new resonances and a multitude of observables make hadron spectroscopy a promising avenue for discoveries at CEPC. This is particularly relevant considering that the formation of multiquark exotics would favor the heavy-flavor systems, which can be well treated as non-relativistic systems [260, 264, 272–286], and the spectra of the fully-heavy exotics, such as $bb\bar{b}\bar{b}$, $cc\bar{c}\bar{c}$, $bb\bar{c}\bar{c}$, $bc\bar{b}\bar{c}$, etc., can be accessed at CEPC. Note that it is still unclear how many and what kinds of exotic multiquark states we should expect, and how these multiquark states can be stablized by the nonperturbative strong interactions. At CEPC, systematic measurements of these heavy-flavor multiquark states should be able to provide crucial insights into the underlying binding mechanism for these heavy-flavor exotic states.

Despite numerous works and tremendous efforts on the understanding of these novel structures observed in experiment, a comprehensive solution for describing and classifying

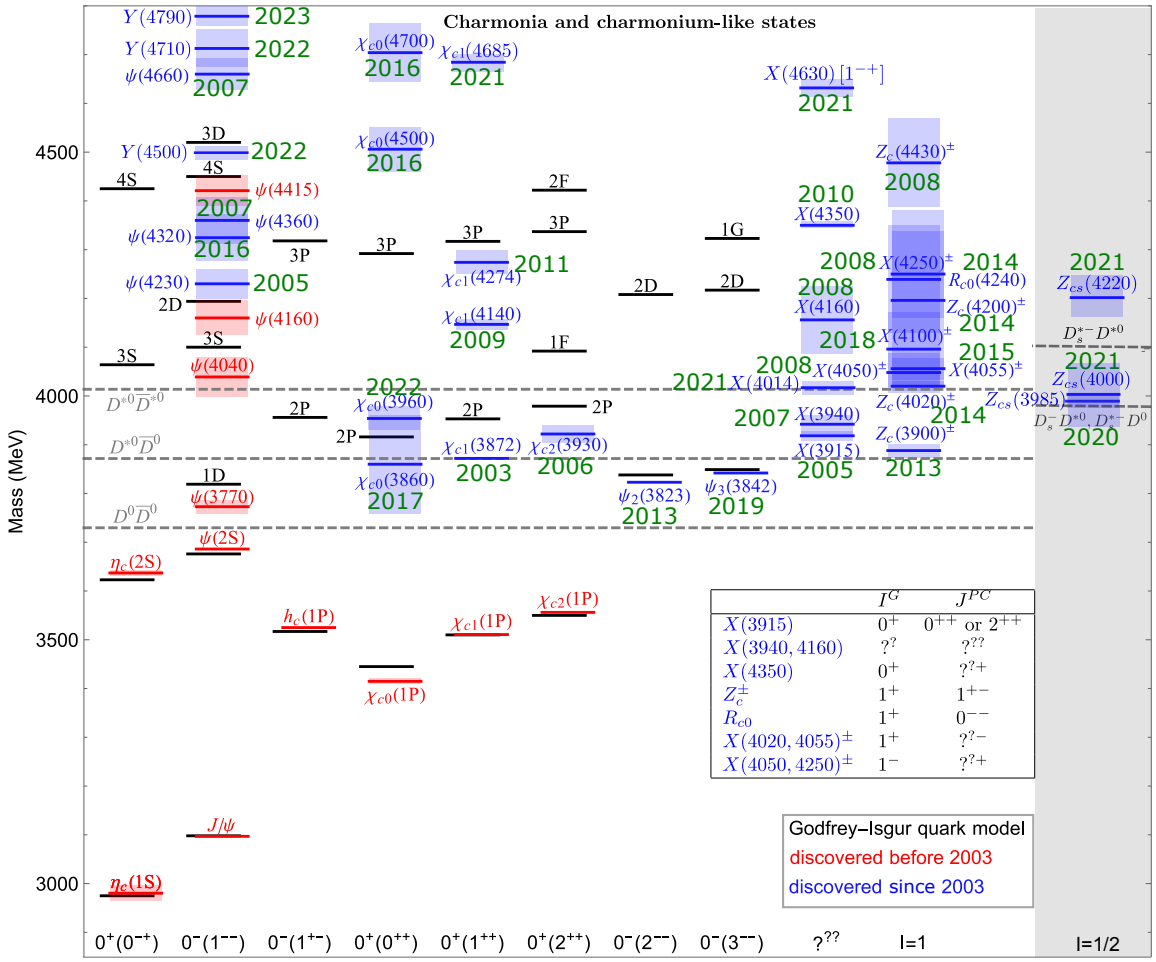

Figure 37: Spectrum of the charmonium and charmonium-like states. Black lines represent the masses in the Godfrey-Isgur quark model [259]. The red and blue lines represent the states observed experimentally before 2003 and since 2003, respectively. For the latter, the years when the states were observed are labeled in green. The height of each shadow indicates the width of the corresponding state. We also show a few two-body open-charm thresholds as dashed lines.

them remains elusive. Thereby, experimental data are paramount for further theoretical development. At CEPC, the production of exotic states from b-hadron decays, directly from the Z decays or from initial state radiation is expected.

For example, the hidden-charm exotic states such as $X(3872)$ and $P_c(4450)$ can be produced at CEPC via $b \to c\bar{c}s$ transitions after b-flavored hadrons are formed. Given the abundant production of heavy quark pairs (*e.g.*, the branching fraction of $Z \to b\bar{b}$ is $(15.12 \pm 0.05)\%$ [149]), a considerable amount of exotic hadrons, including known ones and new states, can be generated. It should be stressed that this also allows to access a broad spectrum of conventional heavy-flavor mesons and baryons, which can hardly be probed by the present facilities, including excited states and multi-heavy baryons such as Ξ_{bb}.

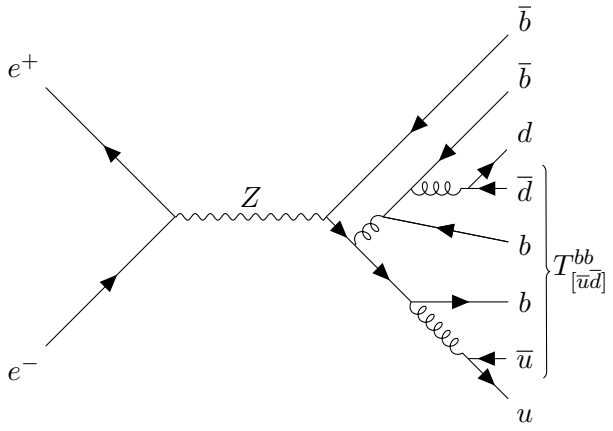

Figure 38: An illustrative Feynman diagram for the production of tetraquark state $T^{bb}_{[\bar{u}\bar{b}]}$ from the $Z \to bb\bar{b}\bar{b}$ decay.

At CEPC, another significant source of exotic or multi-flavored hadrons at the Z pole comes from $Z \to q\bar{q}q'\bar{q}'$. The multiple heavy quarks produced, either of the same or opposite signs, could hadronize into various (exotic) species if their relative velocity is low enough. The process is highly relevant to the B_c physics studies since B_c from the Z pole mainly comes from $Z \to b\bar{b}c\bar{c}$ decays [287–290]. In addition, the measurement of many inclusive rates of new resonances might occur for the first time, and the observation of numerous new decay modes is anticipated. With regards to doubly-heavy baryons (bbq, bcq and ccq) and doubly-heavy exotic states (for instance, the double-charm tetraquark $T_{cc}(3875)^+$ [255, 291], double-bottom tetraquarks [273, 292–294] and hidden-bottom pentaquarks [295]), the high mass threshold necessitates Z inclusive decays as their main production mechanism. An example of Feynman diagrams contributing to the production of a double-bottom tetraquark is shown in Figure 38.

Simplified assumptions and parton-level simulations were employed to deduce the inclusive decay rates: $\mathrm{BR}(Z \to X + T^{cc}_{[\bar{q}\bar{q}']}) \sim \mathcal{O}(10^{-6})$, $\mathrm{BR}(Z \to X + \Xi_{cc}) \sim 5 \times 10^{-5}$, and $\mathrm{BR}(Z \to X + \Omega_{cc}) \sim 1 \times 10^{-5}$ at the Z pole [296]. Additionally, $\mathrm{BR}(Z \to X + T^{bb}_{[\bar{q}\bar{q}']}) \sim \mathcal{O}(10^{-6})$ was also calculated [297]. It's worth noting that $T^{bb}_{[\bar{q}\bar{q}']}$ could have a mass lower than the sum of B and B^* meson mass, thus it could only decay via weak interaction - as predicted by various of theoretical and lattice works, resulting in a life time comparable to the B hadrons. Therefore, the typical decay chain ($T^{bb}_{[\bar{q}\bar{q}']} \to B \to D$) could result in very special event topology, which could be well reconstructed using state-of-art Vertex detector. Preliminary calculation shows that percentage level of accuracy in measuring $T^{bb}_{[\bar{q}\bar{q}']}$ signal strength could be achieved at CEPC.

One may also estimate the inclusive production cross section of double-charm tetraquarks of the hadronic molecular type (for systematic predictions, see, *e.g.*, [299]) by combining Monte Carlo event generators and nonrelativistic effective field theory (NREFT). Such method can successfully reproduce the inclusive cross section of the $X(3872)$ at hadron

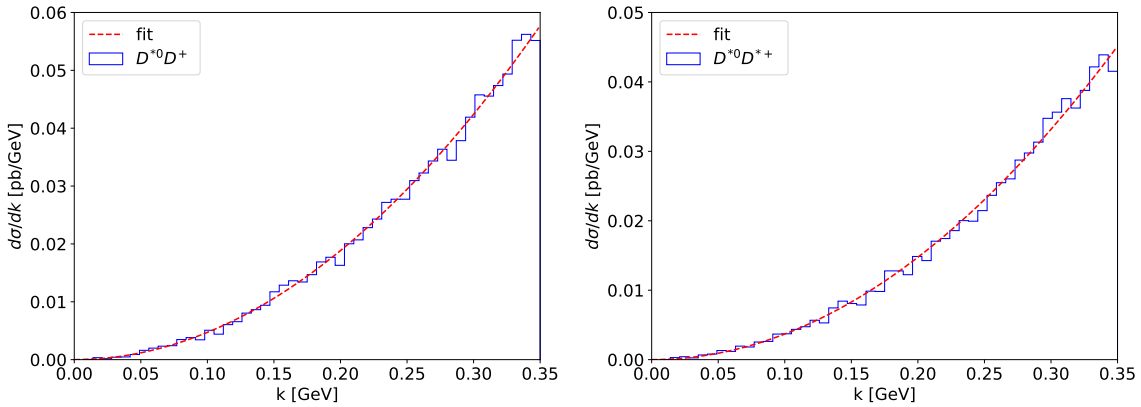

Figure 39: Differential cross sections of $e^+e^- \to Z^0 \to D^{*0}D^+$ and $D^{*0}D^{*+}$ generated using Pythia (histograms) and fit with $d\sigma/dk \propto k^2$, where k is the relative momentum between the D^{*0} and D^+ meson (dashed curves) [298].

colliders [300–302]. Using Pythia 8.3 [303] to generate differential distributions of the $D^{(*)}D^*$ pairs with low relative momenta (see Figure 39) and using NREFT to compute the effective couplings of the $T_{cc}(3875)$ to DD^* and its hypothesized spin partner T'_{cc} to D^*D^* [304], one finds that both the inclusive cross section for the $T_{cc}(3875)$ and T'_{cc} at the Z pole are of the order of a few to 10 fb [298]. Given the expected integrated luminosity of 100 ab^{-1} at the Z pole at CEPC (see Table 1), one expects $10^5 - 10^6$ T_{cc} and T'_{cc} to be produced, consistent with the estimate in Ref. [297]. Events involving these states can be reconstructed from the $DD\pi(\pi)$ final states or similar ones with the pions replaced by photons.

Due to the high uncertainties in their differential rates and decay final states, performing a MC simulation of such exotic hadron events and reconstructing their resonance is impractical without more advanced theoretical calculations or analysis algorithms. On the other hand, additional recent efforts have been predicted the production of doubly-flavored baryons, *i.e.*, Ξ_{cc}, Ξ_{bc}, and Ξ_{bb}, at the Z pole and provided the differential distributions [305, 306].

11 Light BSM States from Heavy Flavors

Light NP states are widely predicted in BSM scenarios involving dark sectors and feebly interacting particles [307], and may couple to lepton and quark sectors. Candidates for such particles include axions and axion-like-particles a [308–311], dark photons A' and light Z' bosons [312], heavy neutral leptons (HNL) [313–315], hidden valley hadrons such as the dark pion $\hat{\pi}$ [316], etc. As a paradigmatic example, let us consider an ALP a that couples with the SM fermions via the dimension-5 operators

$$\mathcal{L} \supset \frac{\partial_\mu a}{2f_a}\left(c^A_{ff'}\,\bar{f}\gamma^\mu\gamma^5 f' + c^V_{ff'}\,\bar{f}\gamma^\mu f'\right) , \tag{11.1}$$

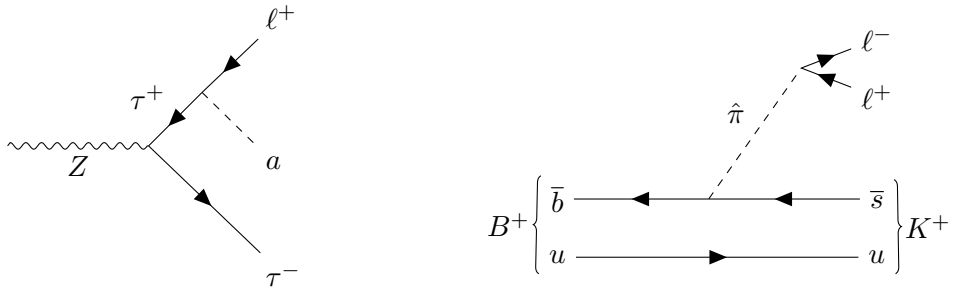

Figure 40: Illustrative Feynman diagrams of light BSM states produced via their couplings with the flavor sector, including the light dark pion $\hat{\pi}$ and the ALP a. **LEFT**: Illustrative Feynman diagrams for the ALP production in $Z \to \tau^+\tau^-$ events via lepton flavor violating couplings. **RIGHT**: $B^+ \to K^+\hat{\pi}(\to \mu^+\mu^-)$. The flavor-changing interaction between the SM quarks and $\hat{\pi}$ can arise either at the tree level or through an EW loop.

where f and f' are SM fermions, $c_{ff'}^{A,V}$ are dimensionless couplings, (with the vector ones c_{ff}^{V} being unphysical if $f = f'$), and f_a is the ALP decay constant that can be regarded as a measure of the NP energy scale. These light BSM states could thus be explored in flavor-physics experiments if they are produced via lepton and/or quark radiation or decay is turned on. Interestingly, the production in the former case does not conserve lepton flavor and the sensitivity to UV scales is parametrically enhanced by the narrow width of the SM fermions. Owing to their feebly-interacting nature, (so as for them to remain undetected so far), the produced BSM particles tend to be long-lived. They are often subject to displaced decays or they contribute to missing energy directly. Both kinematic features being used as collider signatures of light BSM particles have been widely studied. Note that the heavy-flavored particles in the SM are also long-lived; to enable their identification, detectors have often been designed for reconstructing the tracking/vertexing information with high quality. Even if the light BSM particle in question is invisible, the techniques for reconstructing the missing energy at the Z pole can facilitate the reconstruction of its invariant mass. Therefore, the exploration of light BSM states in this context is naturally expected. Below, let us consider the detection of light BSM states which are produced via the decays of heavy-flavored leptons and quarks, using the ALP and dark pion as respective examples.

11.1 Lepton Sector

As discussed in Sections 3, 4, and 7, the CEPC has a strong potential for carrying out τ-related searches, due to the excellent performance of its tracker. A prominent example is the LFV decay $\tau \to \ell a$ (see the left panel of Figure 40) with the ALP a being invisible [317]. The major backgrounds then arise from the $\tau \to \ell\nu\nu$ decays, which share the signal signature of one visible object and missing energy. Let us consider a full reconstruction of the $Z \to \tau\tau$ event. Indeed, the 3-prong decays of the second τ in the $Z \to \tau\tau$ event can yield an efficient determination for the τ momentum direction. Combining this result with some other kinematic constraints, such as the τ mass on-shell condition and energy-momentum

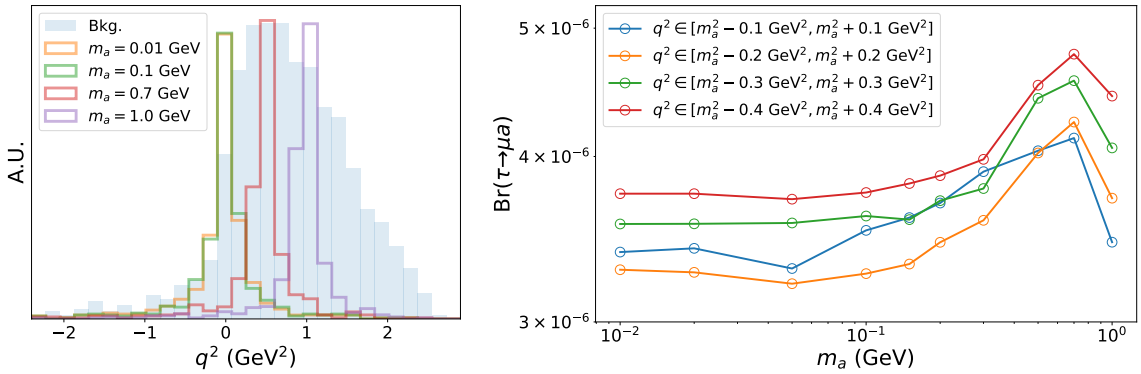

Figure 41: Preliminary sensitivity analysis for searching for an invisible ALP in the $Z \to \tau(\to \mu a)\tau(\to 3\pi\nu)$ events at the CEPC. **LEFT:** Reconstruction of $q^2 \equiv (p_\tau - p_\mu)^2$. **RIGHT:** Upper limits on BR($\tau \to \mu a$) with 95% C.L., where four q^2 windows have been considered.

conservation, we are able to reconstruct the invisible mass $q^2 \equiv (p_\tau - p_\ell)^2 = m_a^2$ accurately. The results from a preliminary sensitivity analysis are presented in Figure 41, where the events are simulated with non-zero spatial beam spread, initial state radiation, and finite tracking/calorimetry resolution. As shown in the left panel, the reconstructed q^2 for the signal events sharply peaks at m_a^2, in contrast to that of the backgrounds. The right panel shows the expected CEPC 95% C.L upper limits on BR($\tau \to \mu a$). Compared with the current Belle II bound, *i.e.*, BR($\tau \to \mu a$) $< 5.9 \times 10^{-4}$ (95% CL) for a practically massless ALP [318], the estimated CEPC limits are about two orders of magnitude stronger. In terms of the interactions in Eq. (11.1), this implies that a NP scale as high as $f_a/c_{\tau\mu}^{A,V} \sim \mathcal{O}(10^8)$ GeV could be probed at the CEPC.

The light ALPs can be also searched for by their lepton-flavor-conserving radiation, such as that in the $Z \to \tau\tau a$ process [310]. Currently, the ALP coupling with τ leptons is essentially yet unconstrained. For the case of $Z \to \mu\mu a$, where the dynamics is relatively simple, it has been shown [310] that the CEPC has the potential to reach BR($Z \to \mu\mu a$) $\lesssim 3 \times 10^{-11}$, yielding a limit to the ALP coupling with muons of $f_a/c_{\mu\mu}^{A} \gtrsim 1$ TeV.

Moreover, both Dirac and Majorana HNLs can be produced via LFV processes. The HNLs might be responsible for the origin of neutrino mass, the puzzle of dark matter and even the cosmic baryon asymmetry. Their mixing with neutrinos allows them to be produced via τ decays such as $\tau \to \ell\nu N$ and $\tau \to \pi N$, if they are lighter than the τ lepton. This provides an alternative to the $Z \to \nu N$ decays in searching for HNLs at the Z pole [319]. Nevertheless, the relevant sensitivity analysis is yet to be explored.

11.2 Quark Sector

Light BSM particles can be also produced in heavy-flavored quark decays [96, 316, 321–325]. As an example, let us consider a dark pion from the strong dynamics of a hidden sector, where this dark pion also couples with the SM leptons, yielding a signature of a displaced di-lepton vertex from its decay (see the right panel of Figure 40) [316]. The reconstruction

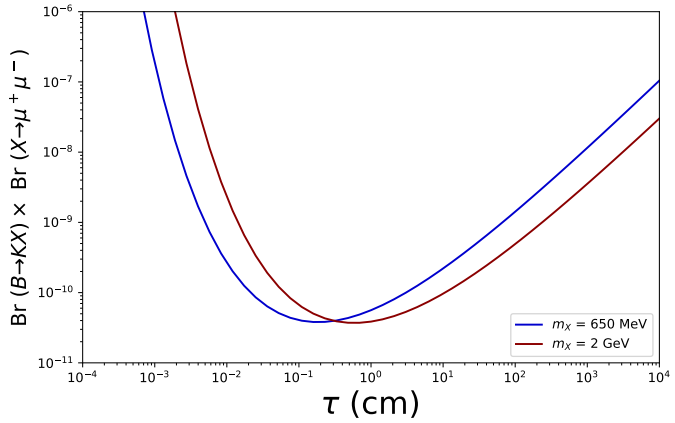

Figure 42: Preliminary expected limits for searching for a long-lived dark pion in $B \to K\hat{\pi}(\to \mu\mu)$ events at the CEPC as a function of the $\hat{\pi}$ decay length [320].

of a narrow di-lepton resonance away from the primary vertex with high quality then allows for the efficient distinction of the signal events from the backgrounds. Figure 42 demonstrates preliminary limits for searching for a long-lived particle in $B \to KX(\to \mu\mu)$ events at the CEPC [322], where X denotes the long-lived new particle. The strongest constraints, namely $\text{BR}(B \to KX(\to \mu\mu)) \lesssim 10^{-10}$, are achieved while the proper lifetime of X is $\sim 0.1 - 10$ cm. It will be convenient to describe such a new light degree of freedom by Eq. (11.1) if the new particle is a pseudoscalar since it behaves as an ALP at low energy scales. The BR limit above can then be interpreted as a probe of the decay constant f_a of an ALP through its coupling with SM quarks. Even when the FCNC couplings are absent at tree level, they will be generated at one loop by EW interactions. In the case where the couplings to all fermions are close to unity ($c^A_{ff} \sim \mathcal{O}(1)$), the constraint on f_a by the CEPC will be up to $\sim \mathcal{O}(10^7)$ GeV [316]. If a large FCNC coupling $c^V_{bs} \sim 1$ presents at tree level, the constraints on f_a will be even higher, though all such limits will also depend on other parameters that control the dark pion lifetime, such as $m_{\hat{\pi}}$.

Finally, we remark that this strategy can be applied to searching for other long-lived light BSM bosons, if they are produced and decay in a similar way. Also, it is interesting to extend this study to the case where these particles decay outside the detector and hence contribute to the missing energy directly. In the latter case, the CLEO analysis performed about twenty years ago [326] still provides the current strongest constraints on $\text{BR}(B^\pm \to \pi^\pm/K^\pm + X) < 4.9 \times 10^{-5}$. These constraints can be interpreted as $f_a \gtrsim 10^8$ GeV in the relevant QCD axion scenarios [325]. However, the sensitivity prospect for such a measurement at the CEPC is still missing.

12 Detector Performance Requirements

The CEPC's extensive flavor physics program consequently imposes stringent and multi-faceted requirements on detector performance, which becomes a key challenge in the design and optimization of the CEPC detector.

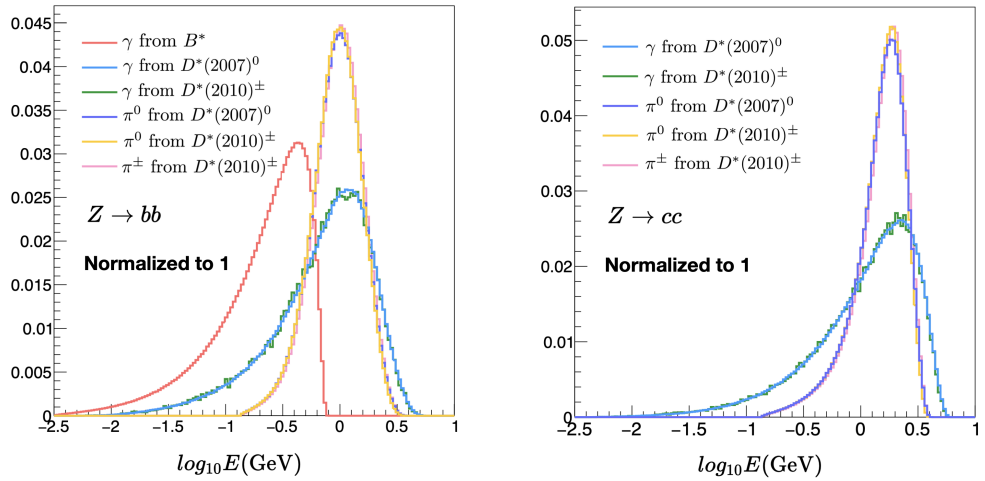

Figure 43: Energy distributions of γ, π^0, and $\pi^{\pm}$ generated from typical excited heavy hadrons decays in $Z \to b\bar{b}, c\bar{c}$ ($\sqrt{s} = 91.2$ GeV) processes.

Many physics benchmark analyses presented in this manuscript also serve as references for detector requirement and optimization studies, as these analyses quantify the correlations between anticipated accuracies and critical detector performances. These studies indicate that a suitable detector for the CEPC flavor physics measurements should:

- Provide large acceptance of nearly 4π solid angle coverage, low P_T threshold for tracks, and low energy thresholds for photons and neutral hadrons. In flavor physics, many measurements relate to the excited heavy hadron states generated inside the jet, those excited state could decay into the base state together with a photon or a pion with typical energy of $\mathcal{O}(100)$ MeV, as shown in Figure 43. The low energy/momentum threshold is especially critical to these processes.

- Clearly separate different final state particles, or say to provide excellent Particle Flow Reconstruction. The success of the CEPC flavor physics program hinges on the analysis of hadronic events at the Z pole, where accurately identifying the correct combination of final state particles is crucial. For example, distinguishing the decay products of a specific b-hadron within a b-jet is a challenging task. Additionally, precise identification of the decay products of a highly boosted tau lepton is vital for various physics measurements involving $Z \to \tau\tau$ events. Therefore, the accurate identification of all final state particles - including charged particles, photons, and neutral hadrons - is imperative for successful flavor physics measurements.

- To pursue excellent reconstruction of missing energy and momentum. The CEPC offers a comparative advantage over the LHCb experiment in conducting physics measurements involving missing energy and momentum in the final state. This includes measurements through semi-leptonic decays of b-hadrons and potentially dark matter searches. Given that many of these measurements rely on hadronic events at the Z pole, reconstructing the four-momentum of all visible final state particles

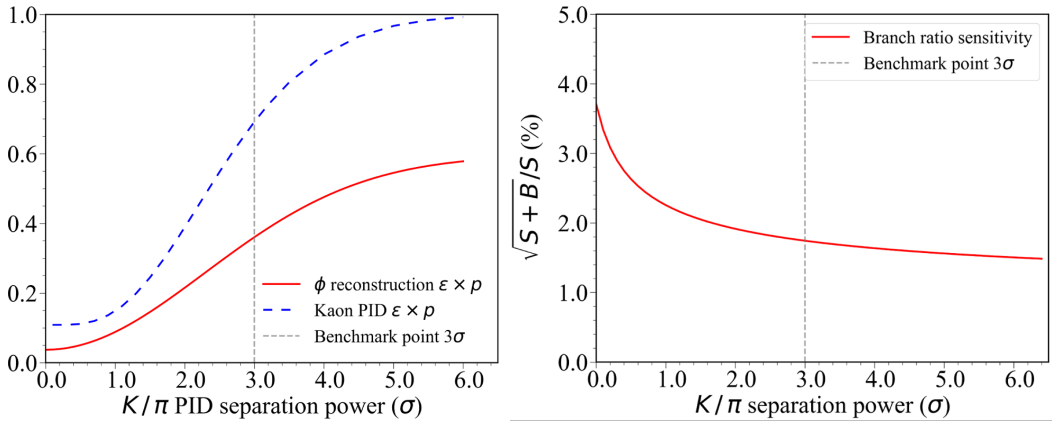

Figure 44: Dependence between the charged hadron identification performance and **LEFT:** the reconstruction efficiency and purity of ϕ; **RIGHT:**, the anticipated accuracy in the $B_s^0 \to \phi\nu\bar{\nu}$ analysis.

is critical for determining missing energy and momentum. This reconstruction quality is typically quantified by the BMR metric. Quantitative analysis indicates that achieving a BMR smaller than 4% is essential for CEPC Higgs physics measurements, enabling efficient separation of the qqH signal from the qqZ background using recoil mass in the di-jet system. The CEPC flavor physics program always benefits from improved reconstruction of missing energy and momentum, underscoring the ongoing need for enhanced BMR capabilities.

- Distinguish different species of charged final state particles, especially charged kaons. Quantitatively, the CEPC detector should provide π/K separation power better than $3\,\sigma$ [37, 56], see Figure 44, where the separation power is defined as $|Mean_1 - Mean_2|/\sqrt{\sigma_1^2 + \sigma_2^2}$. This PID requirement can be satisfied by different technologies. For example, the CEPC CDR baseline detector employs TPC as its main tracker, which could provide dE/dx or even dN/dx measurement. The dE/dx (or dN/dx) measurement is then required to reach a relative accuracy of 3%, at which, together with a TOF measurement of 50 ps at cluster level [42], the reconstruction efficiency and purity of inclusive charged kaons in the hadronic Z pole sample can reach higher than 95%.

- Pursue excellent intrinsic resolution of sub-detectors. Typically, we'd require an intrinsic momentum resolution for the tracks reaching 0.1% level and the intrinsic energy of ECAL energy resolution better than $3\%/\sqrt{E} \oplus 0.3\%$. For instance, an ECAL energy resolution better than $3\%/\sqrt{E} \oplus 0.3\%$ is required by the separation of B^0/B_s^0 once these mesons decay into photons [33] Similarly, the tracker momentum resolution should reach per mille level in the barrel region, and the vertex position resolution should be better than 5 μm and be placed closer enough to the interaction point.

- Be extremely stable. Many of the physics measurements, including a set of the flavor

physics measurements [34, 40, 221], would be limited by systematic uncertainties. To have a stable detector is a prerequisite for controlling the systematic uncertainties, yet, more quantitative studies are needed.

The detector requirements raised from CEPC flavor physics measurements actually pointing to the 1-1 correspondence reconstruction between the visible final state particle and the reconstructed ones, which means efficiently reconstruct all the final state particles, and to control the failure of pattern recognition which could leads to fake particles or in-efficiencies. 1-1 correspondence also emphasize on the identification of the species information for all the final state particles. Using the state-of-art detector design and reconstruction algorithm, dedicated studies are operated towards this goal.

A very fundamental, but yet highly non-trivial, requirement for the detector is to be suited for the collision environment. This requirement is twofold: first, the detector design must be able to sustain the beam induced background and limit its impact on physics measurements to a tolerable level. To meet this requirement, dedicated design and optimization studies are needed in areas such as the machine-detector interface, integration study, and machine protection design, all of which still need significant effort. Secondly, the CEPC detector should be capable of reconstructing physics events with extremely high efficiency, while keeping the noise contamination in the data to an acceptable level. Given the physics event rate of 10^5 Hz at the Z pole, the study and design of a dedicated Trigger-DAQ system are necessary to fulfill this requirement (known as the triggerless equivalent scenario). In addition, the online and offline time building is highly non-trivial, because the event rate at the CEPC Z pole is so high, and different subdetectors take time to respond (for instance TPC and calorimeters — the neutron induced hits may occur at milliseconds later after the collision), causing the overlap of physics events in time. It is impossible to separate the physics events using only time information. Therefore, new reconstruction technologies are required not only to reconstruct low-level physics objects (*e.g.*, tracks, clusters, etc.) with high efficiency and purity, but also to correctly associate them with different vertices. For example, particle flow algorithm using both spatial and time information is probably the technology that can address this requirement.

These requirements need to be addressed by intensive detector design and R&D studies. Meanwhile, these requirements should also be considered coherently, since many of these requirements are correlated and can even be contradictory. For example, while the incorporation of TOF systems can significantly enhance PID performance, it concurrently introduces additional upstream material, which can adversely affect the intrinsic ECAL energy resolution.

13 Summary and Outlook

The electron-positron Higgs factory is identified as the highest priority future collider, as it could significantly improve the discovery potential for NP compared to existing facilities, including LHC and Super-KEKB. Several electron-positron Higgs factories are therefore proposed, supported by intensive physics study as well as critical design and technology

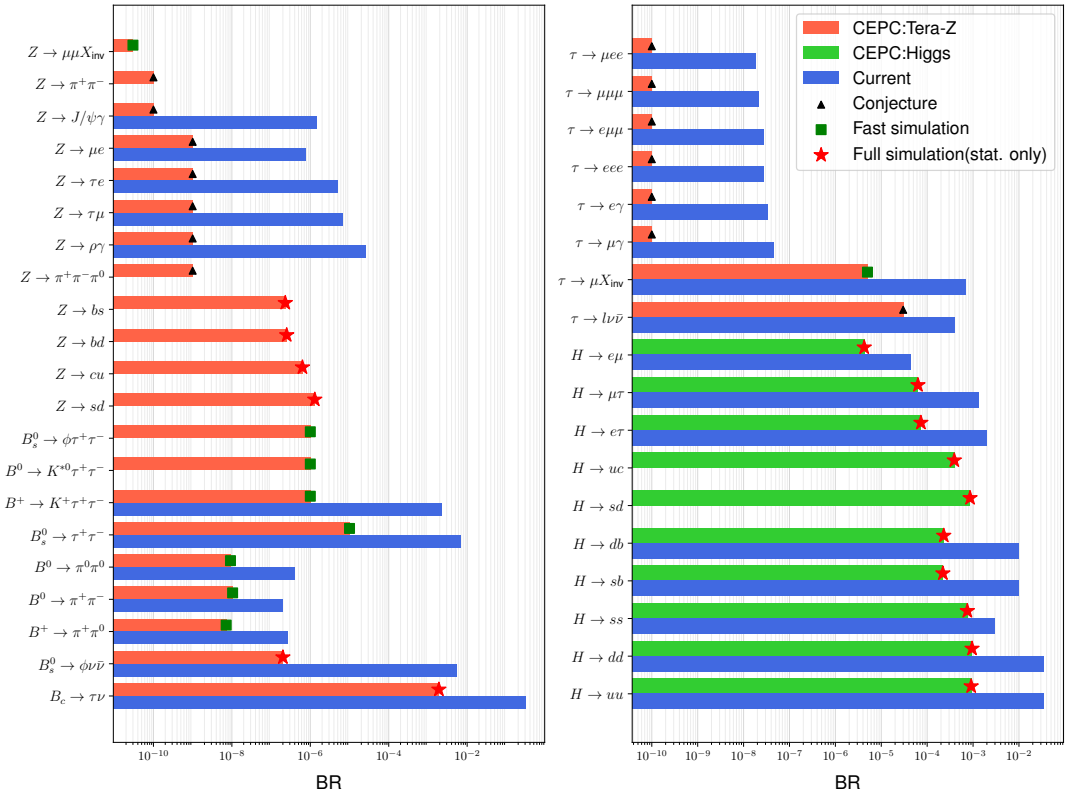

Figure 45: Anticipated values on up limits or precisions

R&D studies. These proposed facilities are expected to produce millions of Higgs bosons in an extremely clean environment. The electron-positron Higgs factory would not only improve the precision of Higgs boson property measurements by approximately an order of magnitude compared to the ultimate precision achievable by the high-luminosity LHC, but also generates huge numbers of Z, W, Higgs boson, and even top quarks. This facility opens novel avenues for exploring NP through multiple observational windows, making a significant leap forward in the field of high energy physics.

Among the proposed facilities, the CEPC and FCC are two circular colliders that could deliver Teras of Z bosons, surpassing the Z boson yields of the LEP-I operation by at least five orders of magnitude. In fact, the instantaneous luminosity of CEPC is so high that it could produce the entire statistics of LEP-I in roughly one minute. This enormous Z-boson sample, together with samples acquired at higher center-of-mass energies, provides an unprecedented opportunity for flavor physics measurements, EW precision measurements, and so on.

This manuscript delineated the flavor physics landscape at the CEPC. Our investigation encompasses approximately ten topics, including rare/exotic b-hadron decays, LFU/LFV, CP violation, exotic states, etc., as detailed in different sections. We have collected accuracy estimations from 40 different benchmark studies, as detailed in Table 10. These benchmark studies were performed adopting different methodologies, *i.e.*, full

No.	Process	$\sqrt{s}$ (GeV)	Observable/physics parameter of interest	Current precision	CEPC precision	Estimation method	Key performance	Relevant section
1	$B^0 \to K^{*0}\tau^+\tau^-$	91.2	BR	-	$\lesssim \mathcal{O}(10^{-6})$ [85]	Fast simulation	Tracker Vertex Jet origin ID	4
2	$B_s^0 \to \phi\tau^+\tau^-$	91.2	BR	-	$\lesssim \mathcal{O}(10^{-6})$ [85]	Fast simulation	Tracker Vertex Jet origin ID	4
3	$B^+ \to K^+\tau^+\tau^-$	91.2	BR	$< 2.25 \times 10^{-3}$ [149]	$\lesssim \mathcal{O}(10^{-6})$ [85]	Fast simulation	Tracker Vertex Jet origin ID	4
4	$B_s^0 \to \tau^+\tau^-$	91.2	BR	$< 6.8 \times 10^{-3}$ [149]	$\lesssim \mathcal{O}(10^{-5})$ [85]	Fast simulation	Tracker Vertex Jet origin ID	4
5	$B_c \to \tau\nu$	91.2	BR ($\lvert V_{cb}\rvert$)	$\lesssim 30\%$ [327]	relative (stat. only) $\mathcal{O}(0.5\%)^*$ [68]	Full simulation	Tracker Lepton ID Missing energy Jet origin ID	3
6	$B_s^0 \to \phi\nu\bar{\nu}$	91.2	BR	$< 5.4 \times 10^{-3}$ [149]	relative (stat. only) $\lesssim 1\%^*$ [37]	Full simulation	Tracker Vertex Missing energy PID	4
7	$B_c \to J/\psi\ell\nu$	91.2	$R_{J/\psi}$	$\pm 0.17 \pm 0.18$ [328] relative $\pm 24\% \pm 25\%$	relative (stat. only) $\lesssim 2.5\%^*$ [40]	Fast simulation	Tracker Vertex	3
8	$B_s^0 \to D_s^{(*)}\ell\nu$	91.2	$R_{D_s^{(*)}}$	-	relative (stat. only) $\lesssim 0.2\%^*$ [40]	Fast simulation	Tracker Vertex	3
9	$\Lambda_b \to \Lambda_c\ell\nu$	91.2	R_{Λ_c}	± 0.076 [329] relative 31%	relative (stat. only) $\sim 0.05\%^*$ [40]	Fast simulation	Tracker Vertex	3
10	$B_s^0 \to J/\psi\phi$	91.2	Γ_s, $\Delta\Gamma_s$, ϕ_s	$\sigma(\Gamma_s) = \pm\ 2.3\ \text{ns}^{-1}$ [149] $\sigma(\Delta\Gamma_s) = \pm 4.3 \pm 3.7\ \text{ns}^{-1}$ [330] $\sigma(\phi_s) = \pm 36 \pm 21$ mrad [330]	$\sigma(\Gamma_s) = 0.036\ \text{ns}^{-1*}$ $\sigma(\Delta\Gamma_s) = 0.12\ \text{ns}^{-1*}$ [56] $\sigma(\phi_s) = 2.2$ mrad*	Full simulation	Tracker Vertex Lifetime resolution Jet origin ID	5
11	$B^0 \to \pi^0\pi^0$	91.2	BR, A_{CP} (α)	$\sigma(\text{BR})/\text{BR}^{00} = 16\%$ $\sigma(C_{CP}^{00}) = \pm\ 0.22$ [149]	$\sigma(\text{BR})/\text{BR}^{00} = 0.25\%^*$ $\sigma(a_{CP}^{00}) = \pm 0.01^*$ [33]	Fast simulation	ECAL Jet origin ID	5
12	$B^0 \to \pi^+\pi^-$	91.2	BR (α)	$\sigma(\text{BR})/\text{BR}^{+0} = 7\%$ [149]	$\sigma(\text{BR})/\text{BR}^{+0} = 0.1\%^*$ [33]	Fast simulation	ECAL Tracker Jet origin ID	5
13	$B^+ \to \pi^+\pi^0$	91.2	BR, A_{CP} (α)	$\sigma(\text{BR})/\text{BR}^{+-} = 4\%$ $\sigma(C_{CP}^{+-}) = \pm\ 0.030$ $\sigma(S_{CP}^{+-}) = \pm\ 0.030$ [149]	$\sigma(\text{BR})/\text{BR}^{+-} = 0.1\%^*$ $\sigma(C_{CP}^{+-}) = \pm 0.003^*$ [33] $\sigma(S_{CP}^{+-}) = \pm 0.003^*$	Fast simulation	ECAL Tracker Vertex Jet origin ID	5
14	$\tau \to eee$	91.2	BR	$< 2.7 \times 10^{-8}$ [149]	$\lesssim \mathcal{O}(10^{-10})$ [155, 159]	Conjecture	Tracker Lepton ID	7
15	$\tau \to e\mu\mu$	91.2	BR	$< 2.7 \times 10^{-8}$ [149]	$\lesssim \mathcal{O}(10^{-10})$ [155, 159]	Conjecture	Tracker Lepton ID	7
16	$\tau \to \mu ee$	91.2	BR	$< 1.8 \times 10^{-8}$ [149]	$\lesssim \mathcal{O}(10^{-10})$ [155, 159]	Conjecture	Tracker Lepton ID	7
17	$\tau \to \mu\gamma$	91.2	BR	$< 4.4 \times 10^{-8}$ [149]	$\lesssim \mathcal{O}(10^{-10})$ [155, 159]	Conjecture	Tracker Lepton ID ECAL	7
18	$\tau \to e\gamma$	91.2	BR	$< 3.3 \times 10^{-8}$ [149]	$\lesssim \mathcal{O}(10^{-10})$ [155, 159]	Conjecture	Tracker Lepton ID ECAL	7
19	$\tau \to \mu\mu\mu$	91.2	BR	$< 2.1 \times 10^{-8}$ [149]	$\lesssim \mathcal{O}(10^{-10})$ [155, 159]	Conjecture	Tracker Lepton ID	7
20	$\tau \to$ incl.	91.2	τ_τ (s) lifetime	$\pm 5 \times 10^{-16}$ [149]	$\pm 1 \times 10^{-18}$ [155]	Conjecture	-	7
21	$\tau \to$ incl.	91.2	m_τ (MeV)	± 0.12 [149]	$\pm$ 0.004 (stat.) $\pm$ 0.1 (sys.) [155]	Conjecture	-	7
22	$\tau \to \ell\nu\bar{\nu}$	91.2	BR	$\pm 4 \times 10^{-4}$ [149]	$\pm 3 \times 10^{-5}$ [155]	Conjecture	Tracker Lepton ID Missing energy	7

No.	Process	$\sqrt{s}$ (GeV)	Observable/physics parameter of interest	Current precision	CEPC precision	Estimation method	Key performance	Relevant section
23	$Z \to \pi^+\pi^-$	91.2	BR	-	$\lesssim \mathcal{O}(10^{-10})$ [159]	Conjecture	Tracker PID	8.2
24	$Z \to \pi^+\pi^-\pi^0$	91.2	BR	-	$\lesssim \mathcal{O}(10^{-9})$ [159]	Conjecture	Tracker PID ECAL	8.2
25	$Z \to \rho\gamma$	91.2	BR	$< 2.5 \times 10^{-5}$ [149]	$\lesssim \mathcal{O}(10^{-9})$ [159]	Conjecture	Tracker PID ECAL	8.2
26	$Z \to J/\psi\gamma$	91.2	BR	$< 1.4 \times 10^{-6}$ [149]	$\lesssim 10^{-9}$–10^{-10} [159]	Conjecture	Tracker PID ECAL	8.2
27	$Z \to \tau\mu$	91.2	BR	$< 6.5 \times 10^{-6}$ [206, 331, 332]	$\lesssim \mathcal{O}(10^{-9})$ [155, 159]	Conjecture	E_{beam} Tracker PID	8.1
28	$Z \to \tau e$	91.2	BR	$< 5.0 \times 10^{-6}$ [206, 331, 332]	$\lesssim \mathcal{O}(10^{-9})$ [155, 159]	Conjecture	E_{beam} Tracker PID	8.1
29	$Z \to \mu e$	91.2	BR	$< 7.5 \times 10^{-7}$ [206, 331, 332]	$\lesssim 1 \times 10^{-9}$ [203]	Conjecture	E_{beam} Tracker PID	8.1
30	$Z \to \mu\mu X_{\text{inv}}$	91.2	BR	-	$\lesssim 3 \times 10^{-11}$ [310]	Fast simulation	Tracker Missing energy	11
31	$\tau \to \mu X_{\text{inv}}$	91.2	BR	$\lesssim 7 \times 10^{-4}$ [318]	$\lesssim$ 3–5 $\times 10^{-6}$	Fast simulation	Tracker Missing energy	11
32	$H \to sb$	240	BR	$\lesssim 10^{-2}$ [333]	$\lesssim$ 0.02%—0.1% [34]	Full simulation	Jet origin ID	9
33	$H \to sd$	240	BR	-	$\lesssim$ 0.02%—0.1% [34]	Full simulation	Jet origin ID	9
34	$H \to db$	240	BR	$\lesssim 10^{-2}$ [333]	$\lesssim$ 0.02%—0.1% [34]	Full simulation	Jet origin ID	9
35	$H \to uc$	240	BR	-	$\lesssim$ 0.02%—0.1% [34]	Full simulation	Jet origin ID	9
36	$H \to ss$	240	BR	$\lesssim 0.3\%$ [334, 335]	$\lesssim 0.1\%$ [34]	Full simulation	Jet origin ID	9
37	$H \to uu$	240	BR	$\lesssim 3.5\%$ $\kappa_u < 560$ [336]	$\lesssim 0.1\%$ [34] $\kappa_u < 101$	Full simulation	Jet origin ID	9
38	$H \to dd$	240	BR	$\lesssim 3.5\%$ $\kappa_d < 260$ [336]	$\lesssim 0.1\%$ [34] $\kappa_d < 37$	Full simulation	Jet origin ID	9
39	$e^+e^- \to tq$	240	cross section	two-fermion, LHC [236–240] four-fermion, LEP2 [241–244]	1–2 orders of magnitude improvement compared to LEP2 [235]	Fast simulation	Tracker Missing energy Jet origin ID	9
40	$WW \to \ell\nu qq$	240	$\lvert V_{cb}\rvert$	$\pm 0.5 \times 10^{-3}$ (inclusive) $\pm 0.6 \times 10^{-3}$ (exclusive) [149] $\pm 1.2 \times 10^{-3}$ (average)	$\lesssim 0.2 \times 10^{-3}$ [221] $L = 20$ ab^{-1}	Full simulation	Jet origin ID	9

Table 10: Summary of flavor physics benchmarks. The related physics parameters of interest for some benchmarks are listed in brackets, such as the CKM matrix element $|V_{cb}|$ and the CKM angle α. The symbol X in benchmarks No. 30–31 denotes the particle related to NP with subscripts "inv" representing the invisible particles. The CEPC precision of some benchmarks marked with stars (*) are extrapolated to the statistic of 4 Tera-Z, and the CEPC precision of Higgs rare and FCNC decays (benchmarks No. 32–38) is statistical only.

simulation using the Geant4 [337] toolkit, fast simulation based on detector performance modelling [338], and conjecture/extrapolation from existing relevant studies. Based on these benchmarks we can conclude that the CEPC or Tera-Z factory could improve the flavour measurement precision by 1 or more orders of magnitudes, and open new windows for NP searches. ... **could access NP at energies up to 10 TeV or even higher.**

As summarized in Table 10, a Tera-Z collider could reveal many previously unobserved physical processes of strong interest for flavor physics studies (see, e.g., items 5–6 of Table 10), and boost the precision of many critical measurements by orders of magnitudes. On top of the Tera-Z, the CEPC will also provide flavor physics measurements at higher center-of-mass energies, for instance the measurements of Higgs rare/FCNC hadronic decays and top quark FCNC decays at the Higgs factory mode ($\sqrt{s} = 240$ GeV), and the $|V_{cb}|$ measurement from direct W boson decay at $\sqrt{s}$ of 160 GeV (for W boson mass measurement) and 240 GeV. It should be mentioned that to perform the Z line shape measurements and the W mass scan, the CEPC operation will scan a few energy points near the Z boson mass and WW threshold, which could be beneficial for certain flavor physics measurements as well.

Compared to the existing flavor physics platforms, especially the LHCb and Belle II, the CEPC has significant advantages, providing unique opportunities for many measurements and **serving as a highly complementary platform for a flavor physics program.** In contrast to hadron colliders, the CEPC intrinsically possesses a much cleaner collision environment as well as a precise and controllable initial state. Beyond the collision environment, the PFA oriented design of CEPC detector and the potential implementation of high precision calorimeter system enable a precise reconstruction of neutral and missing final states. Thus, the CEPC could focus on the physics measurements with photon, neutral pion, lepton, and neutrino final states, which is highly complementary to the LHCb measurements. With a well-defined initial state and less pile-up of events, the CEPC can access radiative or leptonic decays, therefore be sensitive to FCNC processes, LFV and LFU tests in τ decays, and many other rare decay modes. Compared to B and tau-charm factories [8, 27], the heavy hadrons/taus generated at CEPC have much higher energies and thus larger boost, which is beneficial for precise measurements of lifetimes and secondary vertices, especially for time-dependent CP measurements. The wide beam energy range of the CEPC also opens up the study of hadron states that could not be produced directly at Belle II, such as B_c, Λ_b, and many exotic hadronic states, see Section 10. On the other hand, the CEPC uniquely enables precise measurements of FCNC processes and offers direct assessment of the CKM matrix elements through the decay of W bosons.

To fulfil the flavor physics potential of the CEPC, the detector design is key, as we have discussed in detail in Section 12. On the other hand, the progress of advanced reconstruction algorithms, especially those based on machine learning and large language models, injects significant thrust to the CEPC physics and detector studies. An existing example is the jet origin identification presented in Section 2, which shows that using the CEPC CDR baseline detector and ParticleNet algorithm, 11 different types of jets (induced by u, d, s, c, b, their corresponding anti-quarks, and gluons) can be efficiently separated. In other words, the jet origin identification combines the jet flavor tagging, jet charge measurement,

s-tagging, gluon-tagging, and even u/d-jet identification all together.

The jet origin identification gives a strong boost to the precision in measurements of Higgs rare/exotic hadronic decays — by roughly 3 times to 2 orders of magnitude — and in $|V_{cb}|$ measurement from W boson decays, see Section 9. It will also enhance the precisions of time-dependent CP measurements [56] and weak-mixing angle measurements [339]. These new technologies will certainly alter the detector design and optimization studies. For instance, a recent study [340] shows that new algorithms, even with a much worse detector, could still have performance surpassing the conventional algorithm with a much better detector. Of course, these new progresses also impose other challenges, for example, it would be essential to understand and to interpret the performance of these advanced algorithms, while the calibration and relevant systematic control certainly become critical, which are also highly non-trivial.

It should be remarked that the flavor physics program at the CEPC, is so rich that this manuscript is by no means inclusive. Many interesting topics remain to be explored and quantified in the future. For instance, it would be valuable to quantify the impact of Tera-Z, on top of existing facilities, in terms of the CKM global fit. The physics measurements using $e^+e^- \to \tau^+\tau^-$ events, as well as those related to charm/strange physics, are also of interest. It is essential to control theoretical uncertainties, especially the QCD related ones. Furthermore, the relevant detector design and optimization studies, along with the development and exploration of new tools and new algorithms, need to continue.

To conclude, the flavor physics program at CEPC holds immense scientific promise. It provides the access to physics beyond SM at an energy scale of 10 TeV or even higher, and is highly complementary to existing flavor facilities. It is also very challenging to fully realize its potential, which needs dedicated detector design and critical R&D, as well as theoretical studies. We hope that the flavor physics studies for the CEPC will not only serve as a reference for the evaluation of CEPC physics potential and its detector design, but will also inspire innovative ideas towards NP measurements, new technologies, new algorithms, and new tools.

Acknowledgments

This white paper is supported by the Chinese Academy of Sciences under Grants No. YSBR-101 and No. XDB34030000; by the National Natural Science Foundation of China (NSFC) under Grants No. 12125507, and No. 12047503; by the National Key R&D Program of China under Grant No. 2023YFA1606703; NSFC under Grant No. 12135006 and 12075097; NSFC under Grant No. 12375086 and 2022YFA1601903; NSFC under Grant No. 12061141007; NSFC under the Grants No. 12035008 and 12211530479; NSFC (No. 12105100) and Beijing Natural Science Foundation (No. Q22002); NSFC under grant No. 12035008 and 12375091; NSFC under grant No. 12342502; NSFC under grant No. 12235018; NSFC under grant No. 12335003. This white paper is also supported by the Area of Excellence (AoE) under the Grant No. AoE/P-404/18-3, and by the General Research Fund (GRF) under Grant No. 16304321. Both of the AoE and GRF grants are issued by the Research Grants Council of Hong Kong S.A.R.

References

[1] CEPC Study Group collaboration, *CEPC Technical Design Report – Accelerator*, 2312.14363.

[2] CEPC Study Group collaboration, *CEPC Conceptual Design Report: Volume 2 - Physics & Detector*, 1811.10545.

[3] CEPC Accelerator Study Group collaboration, *Snowmass2021 White Paper AF3-CEPC*, 2203.09451.

[4] CEPC Study Group collaboration, *CEPC Technical Design Report – Accelerator*, 2312.14363.

[5] N. Cabibbo, *Unitary Symmetry and Leptonic Decays*, *Phys. Rev. Lett.* **10** (1963) 531.

[6] M. Kobayashi and T. Maskawa, *CP Violation in the Renormalizable Theory of Weak Interaction*, *Prog. Theor. Phys.* **49** (1973) 652.

[7] F. An et al., *Precision Higgs physics at the CEPC*, *Chin. Phys. C* **43** (2019) 043002 [1810.09037].

[8] Belle-II collaboration, *The Belle II Physics Book*, *PTEP* **2019** (2019) 123C01 [1808.10567].

[9] LHCb collaboration, *Measurement of the b-quark production cross-section in 7 and 13 TeV pp collisions*, *Phys. Rev. Lett.* **118** (2017) 052002 [1612.05140].

[10] LHCb collaboration, *Measurement of b hadron fractions in 13 TeV pp collisions*, *Phys. Rev. D* **100** (2019) 031102 [1902.06794].

[11] Heavy Flavor Averaging Group, HFLAV collaboration, *Averages of b-hadron, c-hadron, and τ-lepton properties as of 2021*, *Phys. Rev. D* **107** (2023) 052008 [2206.07501].

[12] LHCb collaboration, *Measurement of the B_c^- meson production fraction and asymmetry in 7 and 13 TeV pp collisions*, *Phys. Rev. D* **100** (2019) 112006 [1910.13404].

[13] X.-C. Zheng, C.-H. Chang, T.-F. Feng and X.-G. Wu, *QCD NLO fragmentation functions for c or $\bar{b}$ quark to B_c or B_c^* meson and their application*, *Phys. Rev. D* **100** (2019) 034004 [1901.03477].

[14] L. Gladilin, *Fragmentation fractions of c and b quarks into charmed hadrons at LEP*, *Eur. Phys. J. C* **75** (2015) 19 [1404.3888].

[15] DELPHI collaboration, *A Measurement of D meson production in Z0 hadronic decays*, *Z. Phys. C* **59** (1993) 533.

[16] ALEPH collaboration, *Production of charmed mesons in Z decays*, *Z. Phys. C* **62** (1994) 1.

[17] OPAL collaboration, *A Measurement of the production of D*+- mesons on the Z0 resonance*, *Z. Phys. C* **67** (1995) 27.

[18] A. Boehrer, *Inclusive particle production in hadronic decays of the Z boson at LEP-1*, *Phys. Rept.* **291** (1997) 107.

[19] LHCb collaboration, *Physics case for an LHCb Upgrade II - Opportunities in flavour physics, and beyond, in the HL-LHC era*, 1808.08865.

[20] FCC collaboration, *FCC Physics Opportunities*, *Eur. Phys. J.* **C79** (2019) 474.

[21] G. Bernardi et al., *The Future Circular Collider: a Summary for the US 2021 Snowmass Process*, 2203.06520.

[22] LCC Physics Working Group collaboration, *Tests of the Standard Model at the International Linear Collider*, 1908.11299.

[23] N. Bacchetta et al., *CLD – A Detector Concept for the FCC-ee*, 1911.12230.

[24] IDEA collaboration, *A proposal of a drift chamber for the IDEA experiment for a future e^+e^- collider*, *PoS* **ICHEP2020** (2021) 877.

[25] BaBar collaboration, *The BaBar detector*, *Nucl. Instrum. Meth. A* **479** (2002) 1 [hep-ex/0105044].

[26] BESIII collaboration, *Design and Construction of the BESIII Detector*, *Nucl. Instrum. Meth. A* **614** (2010) 345 [0911.4960].

[27] M. Achasov et al., *STCF Conceptual Design Report: Volume I - Physics & Detector*, 2303.15790.

[28] LHCb collaboration, *The LHCb Detector at the LHC*, *JINST* **3** (2008) S08005.

[29] ALEPH, CDF, D0, DELPHI, L3, OPAL, SLD, LEP Electroweak Working Group, Tevatron Electroweak Working Group, SLD Electroweak Working Group, SLD Heavy Flavor Group collaboration, *Precision Electroweak Measurements and Constraints on the Standard Model*, 0911.2604.

[30] T. Sjöstrand, S. Ask, J. R. Christiansen, R. Corke, N. Desai, P. Ilten et al., *An introduction to PYTHIA 8.2*, *Comput. Phys. Commun.* **191** (2015) 159 [1410.3012].

[31] M. Ruan and H. Videau, *Arbor, a new approach of the Particle Flow Algorithm*, in *International Conference on Calorimetry for the High Energy Frontier*, pp. 316–324, 2013, 1403.4784.

[32] J. S. Marshall and M. A. Thomson, *Pandora Particle Flow Algorithm*, in *International Conference on Calorimetry for the High Energy Frontier*, pp. 305–315, 2013, 1308.4537.

[33] Y. Wang, S. Descotes-Genon, O. Deschamps, L. Li, S. Chen, Y. Zhu et al., *Prospects for $B^0_{(s)} \to \pi^0\pi^0$ and $B^0_{(s)} \to \eta\eta$ modes and corresponding CP asymmetries at Tera-Z*, *JHEP* **12** (2022) 135 [2208.08327].

[34] H. Liang, Y. Zhu, Y. Wang, Y. Che, C. Zhou, H. Qu et al., *Jet-Origin Identification and Its Application at an Electron-Positron Higgs Factory*, *Phys. Rev. Lett.* **132** (2024) 221802 [2310.03440].

[35] LHCb collaboration, *Measurement of b-hadron branching fractions for two-body decays into charmless charged hadrons*, *JHEP* **10** (2012) 037 [1206.2794].

[36] H. Cui, M. Zhao, Y. Wang, H. Liang and M. Ruan, *Jet charge identification in ee-Z-qq process at Z pole operation*, 2306.14089.

[37] L. Li, M. Ruan, Y. Wang and Y. Wang, *Analysis of $B_s \to \phi\nu\nu$ at CEPC*, *Phys. Rev. D* **105** (2022) 114036 [2201.07374].

[38] Y. Zhu, S. Chen, H. Cui and M. Ruan, *Requirement analysis for dE/dx measurement and PID performance at the CEPC baseline detector*, *Nucl. Instrum. Meth. A* **1047** (2023) 167835 [2209.14486].

[39] F. Cuna, N. De Filippis, F. Grancagnolo and G. F. Tassielli, *Simulation of particle identification with the cluster counting technique*, in *International Workshop on Future Linear Colliders*, 5, 2021, 2105.07064.

[40] T. S. M. Ho, X.-H. Jiang, T. H. Kwok, L. Li and T. Liu, *Testing lepton flavor universality at future Z factories*, *Phys. Rev. D* **109** (2024) 093004 [2212.02433].

[41] F. Bedeschi, M. Caccia, R. Ferrari, P. Giacomelli, F. Grancagnolo, P. Azzi et al., "IDEA detector Letter of Intent." https://www.snowmass21.org/docs/files/summaries/EF/SNOWMASS21-EF1_EF4-IF3_IF6-096.pdf, 2021.

[42] Y. Che, V. Boudry, H. Videau, M. He and M. Ruan, *Cluster time measurement with CEPC calorimeter*, *Eur. Phys. J. C* **83** (2023) 93 [2209.02932].

[43] R. Manqi, "The CEPC simulation and tools: software and performance." http://ias.ust.hk/program/shared_doc/2019/201901hep/conf/20190121_4042_pm_Manqi%20Ruan.pdf, 2019.

[44] Y. Shen, H. Xiao, H. Li, S. Qin, Z. Wang, C. Wang et al., *Photon Reconstruction Performance at the CEPC baseline detector*, 1908.09062.

[45] P.-Z. Lai, M. Ruan and C.-M. Kuo, *Jet performance at the circular electron-positron collider*, *JINST* **16** (2021) P07037 [2104.05029].

[46] D. Yu, T. Zheng and M. Ruan, *Lepton identification performance in Jets at a future electron positron Higgs Z factory*, 2105.01246.

[47] T. Zheng, J. Wang, Y. Shen, Y.-K. E. Cheung and M. Ruan, *Reconstructing K_S^0 and Λ in the CEPC baseline detector*, *Eur. Phys. J. Plus* **135** (2020) 274.

[48] D. Yu, M. Ruan, V. Boudry, H. Videau, J.-C. Brient, Z. Wu et al., *The measurement of the $H \to \tau\tau$ signal strength in the future e^+e^- Higgs factories*, *Eur. Phys. J. C* **80** (2020) 7.

[49] CEPC CALORIMETRY WORKING GROUP collaboration, *High-granularity crystal calorimetry: conceptual designs and first studies*, *JINST* **15** (2020) C04056.

[50] M. T. Lucchini, L. Pezzotti, G. Polesello and C. G. Tully, *Particle flow with a hybrid segmented crystal and fiber dual-readout calorimeter*, *JINST* **17** (2022) P06008 [2202.01474].

[51] Z. Xiao and Z. Huaqiao, "Performance study of cross-crystal Fan Ecal for CEPC.." https://indico.ihep.ac.cn/event/16906/contributions/50989/attachments/24588/27822/cross-crystal_fan_Ecal.pptx, 2022.

[52] B. Qi and Y. Liu, *R&D of a Novel High Granularity Crystal Electromagnetic Calorimeter*, *Instruments* **6** (2022) 40.

[53] A. Ronzhin, S. Los, E. Ramberg, A. Apresyan, S. Xie, M. Spiropulu et al., *Study of the timing performance of micro-channel plate photomultiplier for use as an active layer in a shower maximum detector*, *Nucl. Instrum. Meth. A* **795** (2015) 288.

[54] J. Va'vra, *PID Techniques: Alternatives to RICH Methods*, *Nucl. Instrum. Meth. A* **876** (2017) 185 [1611.01713].

[55] X. She et al., *Development of Time Projection Chamber prototype integrated with UV laser tracks for the future circular e^+e^- collider*, *JINST* **18** (2023) C07015.

[56] X. Li, M. Ruan and M. Zhao, *Prospect for measurement of CP-violation phase ϕ_s study in the $B_s \to J/\Psi\phi$ channel at future Z factory*, 2205.10565.

[57] H. Qu and L. Gouskos, *ParticleNet: Jet Tagging via Particle Clouds*, *Phys. Rev. D* **101** (2020) 056019 [1902.08570].

[58] CEPC Study Group collaboration, "CEPC Software Homepage." http://cepcsoft.ihep.ac.cn/.

[59] F. U. Bernlochner, Z. Ligeti, M. Papucci and D. J. Robinson, *Combined analysis of semileptonic B decays to D and D^*: $R(D^{(*)})$, $|V_{cb}|$, and new physics*, *Phys. Rev. D* **95** (2017) 115008 [1703.05330].

[60] D. Bryman, V. Cirigliano, A. Crivellin and G. Inguglia, *Testing Lepton Flavor Universality with Pion, Kaon, Tau, and Beta Decays*, *Ann. Rev. Nucl. Part. Sci.* **72** (2022) 69 [2111.05338].

[61] S. Bifani, S. Descotes-Genon, A. Romero Vidal and M.-H. Schune, *Review of Lepton Universality tests in B decays*, *J. Phys.* **G46** (2019) 023001 [1809.06229].

[62] F. U. Bernlochner, M. F. Sevilla, D. J. Robinson and G. Wormser, *Semitauonic b-hadron decays: A lepton flavor universality laboratory*, *Rev. Mod. Phys.* **94** (2022) 015003 [2101.08326].

[63] W. Altmannshofer, S. Gori, M. Pospelov and I. Yavin, *Quark flavor transitions in $L_\mu - L_\tau$ models*, *Phys. Rev. D* **89** (2014) 095033 [1403.1269].

[64] P. Langacker, *The Physics of Heavy Z' Gauge Bosons*, *Rev. Mod. Phys.* **81** (2009) 1199 [0801.1345].

[65] A. Greljo, G. Isidori and D. Marzocca, *On the breaking of Lepton Flavor Universality in B decays*, *JHEP* **07** (2015) 142 [1506.01705].

[66] I. Doršner, S. Fajfer, A. Greljo, J. F. Kamenik and N. Košnik, *Physics of leptoquarks in precision experiments and at particle colliders*, *Phys. Rept.* **641** (2016) 1 [1603.04993].

[67] E. E. Jenkins, A. V. Manohar and P. Stoffer, *Low-Energy Effective Field Theory below the Electroweak Scale: Operators and Matching*, *JHEP* **03** (2018) 016 [1709.04486].

[68] T. Zheng, J. Xu, L. Cao, D. Yu, W. Wang, S. Prell et al., *Analysis of $B_c \to \tau\nu_\tau$ at CEPC*, *Chin. Phys. C* **45** (2021) 023001 [2007.08234].

[69] X. Zuo, M. Fedele, C. Helsens, D. Hill, S. Iguro and M. Klute, *Prospects for B_c^+ and $B^+ \to \tau^+\nu_\tau$ at FCC-ee*, *Eur. Phys. J. C* **84** (2024) [2305.02998].

[70] Y. Amhis, M. Hartmann, C. Helsens, D. Hill and O. Sumensari, *Prospects for $B_c^+ \to \tau^+\nu_\tau$ at FCC-ee*, *JHEP* **12** (2021) 133 [2105.13330].

[71] P. Gambino, P. Giordano, G. Ossola and N. Uraltsev, *Inclusive semileptonic B decays and the determination of —V(ub)—*, *JHEP* **10** (2007) 058 [0707.2493].

[72] UTfit collaboration, *New UTfit Analysis of the Unitarity Triangle in the Cabibbo-Kobayashi-Maskawa scheme*, *Rend. Lincei Sci. Fis. Nat.* **34** (2023) 37 [2212.03894].

[73] CKMfitter collaboration, "Recent ckmfitter updates on global fits of the ckm matrix." https://indico.cern.ch/event/891123/contributions/4601722/attachments/2351890/4013122/CKMfitter2021.pdf.

[74] Flavour Lattice Averaging Group (FLAG) collaboration, *FLAG Review 2021*, *Eur. Phys. J. C* **82** (2022) 869 [2111.09849].

[75] S. Narison, *$\overline{m}_c$ and $\overline{m}_b$ from M_{Bc} and improved estimates of f_{Bc} and $f_{Bc(2S)}$*, *Phys. Lett. B* **802** (2020) 135221 [1906.03614].

[76] HFLAV collaboration, *Averages of b-hadron, c-hadron, and τ-lepton properties as of 2018*, *Eur. Phys. J. C* **81** (2021) 226 [1909.12524].

[77] F. U. Bernlochner, Z. Ligeti and D. J. Robinson, *Model independent analysis of semileptonic B decays to D^{**} for arbitrary new physics*, *Phys. Rev. D* **97** (2018) 075011 [1711.03110].

[78] J. Charles, S. Descotes-Genon, Z. Ligeti, S. Monteil, M. Papucci, K. Trabelsi et al., *New physics in B meson mixing: future sensitivity and limitations*, *Phys. Rev. D* **102** (2020) 056023 [2006.04824].

[79] Y. Grossman and Z. Ligeti, *Theoretical challenges for flavor physics*, *Eur. Phys. J. Plus* **136** (2021) 912 [2106.12168].

[80] M. Artuso, G. Borissov and A. Lenz, *CP violation in the B_s^0 system*, *Rev. Mod. Phys.* **88** (2016) 045002 [1511.09466].

[81] P. Chang, K.-F. Chen and W.-S. Hou, *Flavor Physics and CP Violation*, *Prog. Part. Nucl. Phys.* **97** (2017) 261 [1708.03793].

[82] W. Altmannshofer and F. Archilli, *Rare decays of b and c hadrons*, in *Snowmass 2021*, 6, 2022, 2206.11331.

[83] L. Calibbi, A. Crivellin and T. Ota, *Effective Field Theory Approach to $b \to s\ell\ell^{(')}$, $B \to K^{(*)}\nu\overline{\nu}$ and $B \to D^{(*)}\tau\nu$ with Third Generation Couplings*, *Phys. Rev. Lett.* **115** (2015) 181801 [1506.02661].

[84] L. Allwicher, C. Cornella, G. Isidori and B. A. Stefanek, *New physics in the third generation. A comprehensive SMEFT analysis and future prospects*, *JHEP* **03** (2024) 049 [2311.00020].

[85] L. Li and T. Liu, *$b \to s\tau^+\tau^-$ physics at future Z factories*, *JHEP* **06** (2021) 064 [2012.00665].

[86] Y. Amhis, M. Kenzie, M. Reboud and A. R. Wiederhold, *Prospects for searches of $b \to s\nu\overline{\nu}$ decays at FCC-ee*, *JHEP* **01** (2024) 144 [2309.11353].

[87] Belle-II collaboration, *Snowmass White Paper: Belle II physics reach and plans for the next decade and beyond*, 2207.06307.

[88] J. F. Kamenik, S. Monteil, A. Semkiv and L. V. Silva, *Lepton polarization asymmetries in rare semi-tauonic $b \to s$ exclusive decays at FCC-ee*, *Eur. Phys. J. C* **77** (2017) 701 [1705.11106].

[89] B. Capdevila, A. Crivellin and J. Matias, *Review of semileptonic B anomalies*, *Eur. Phys. J. ST* **1** (2023) 20 [2309.01311].

[90] HFLAV collaboration. "Preliminary average of $R(D)$ and $R(D^*)$ for Moriond 2024" at https://hflav-eos.web.cern.ch/hflav-eos/semi/moriond24/html/RDsDsstar/RDRDs.html.

[91] LHCb collaboration, *Test of lepton universality with $\Lambda_b^0 \to pK^-\ell^+\ell^-$ decays*, *JHEP* **05** (2020) 040 [1912.08139].

[92] LHCb collaboration, *Branching fraction measurements of the rare $B_s^0 \to \phi\mu^+\mu^-$ and $B_s^0 \to f_2'(1525)\mu^+\mu^-$ decays*, 2105.14007.

[93] LHCb collaboration, *Measurement of the $B_s^0 \to \mu^+\mu^-$ branching fraction and effective lifetime and search for $B^0 \to \mu^+\mu^-$ decays*, *Phys. Rev. Lett.* **118** (2017) 191801 [1703.05747].

[94] S. Descotes-Genon, M. Novoa-Brunet and K. K. Vos, *The time-dependent angular analysis of $B_d \to K_S\ell\ell$, a new benchmark for new physics*, *JHEP* **02** (2021) 129 [2008.08000].

[95] R. Fleischer, E. Malami, A. Rehult and K. K. Vos, *Fingerprinting cp-violating new physics with $b \to k\mu^+\mu^-$.*, *JHEP* **03** (2023) 113 [2212.09575].

[96] B. Batell, M. Pospelov and A. Ritz, *Multi-lepton Signatures of a Hidden Sector in Rare B Decays*, *Phys. Rev. D* **83** (2011) 054005 [0911.4938].

[97] J. A. Dror, R. Lasenby and M. Pospelov, *Dark forces coupled to nonconserved currents*, *Phys. Rev. D* **96** (2017) 075036 [1707.01503].

[98] B. Bhattacharya, A. Datta, D. London and S. Shivashankara, *Simultaneous Explanation of the R_K and $R(D^{(*)})$ Puzzles*, *Phys. Lett. B* **742** (2015) 370 [1412.7164].

[99] Belle-II collaboration, *Evidence for $B+\to K+\nu\nu^-$ decays*, *Phys. Rev. D* **109** (2024) 112006 [2311.14647].

[100] A. J. Buras, J. Girrbach-Noe, C. Niehoff and D. M. Straub, *$B \to K^{(*)}\nu\overline{\nu}$ decays in the Standard Model and beyond*, *JHEP* **02** (2015) 184 [1409.4557].

[101] D. Bečirević, G. Piazza and O. Sumensari, *Revisiting $B \to K^{(*)}\nu\bar{\nu}$ decays in the Standard Model and beyond*, *Eur. Phys. J. C* **83** (2023) 252 [2301.06990].

[102] R. Aleksan, L. Oliver and E. Perez, *Study of CP violation in $B^\pm$ decays to $\overline{D^0}(D^0)K^\pm$ at FCCee*, 2107.05311.

[103] D. Hill, "*First steps with flavour physics studies at FCC-ee.*" *Talk at the 4th FCC Physics and Experiments Workshop*, 2020.

[104] LHCb collaboration, *Measurement of CP-violating and mixing-induced observables in $B_s^0 \to \phi\gamma$ decays*, *Phys. Rev. Lett.* **123** (2019) 081802 [1905.06284].

[105] LHCb collaboration, *First Observation of the Radiative Decay $\Lambda_b^0 \to \Lambda\gamma$*, *Phys. Rev. Lett.* **123** (2019) 031801 [1904.06697].

[106] C. Bobeth and U. Haisch, *New Physics in Γ_{12}^s: $(\bar{s}b)(\bar{\tau}\tau)$ Operators*, *Acta Phys. Polon. B* **44** (2013) 127 [1109.1826].

[107] Q. Qin, Y.-L. Shen, C. Wang and Y.-M. Wang, *Deciphering the Long-Distance Penguin Contribution to $B^-d,s\to\gamma\gamma$ Decays*, *Phys. Rev. Lett.* **131** (2023) 091902 [2207.02691].

[108] Y.-L. Shen, Y.-M. Wang and Y.-B. Wei, *Precision calculations of the double radiative bottom-meson decays in soft-collinear effective theory*, *JHEP* **12** (2020) 169 [2009.02723].

[109] S. W. Bosch and G. Buchalla, *The Double radiative decays $B \to \gamma\gamma$ in the heavy quark limit*, *JHEP* **08** (2002) 054 [hep-ph/0208202].

[110] Belle, Belle-II collaboration, *Search for the decay $B0\to\gamma\gamma$ using Belle and Belle II data*, *Phys. Rev. D* **110** (2024) L031106 [2405.19734].

[111] M. Chrzaszcz, R. G. Suarez and S. Monteil, *Hunt for rare processes and long-lived particles at FCC-ee*, *Eur. Phys. J. Plus* **136** (2021) 1056 [2106.15459].

[112] BaBar collaboration, *A search for the decay modes $B^{+-} \to h^{+-}\tau^{+-}l$*, *Phys. Rev. D* **86** (2012) 012004 [1204.2852].

[113] Belle collaboration, *Search for the Lepton Flavor Violating Decays $B+\to K+\tau\pm\ell\mp$ (ℓ=e, μ) at Belle*, *Phys. Rev. Lett.* **130** (2023) 261802 [2212.04128].

[114] LHCb collaboration, *Search for the lepton number violating decays $B^+ \to \pi^-\mu^+\mu^+$ and $B^+ \to K^-\mu^+\mu^+$*, *Phys. Rev. Lett.* **108** (2012) 101601 [1110.0730].

[115] LHCb collaboration, *Search for Majorana neutrinos in $B^- \to \pi^+\mu^-\mu^-$ decays*, *Phys. Rev. Lett.* **112** (2014) 131802 [1401.5361].

[116] LHCb collaboration, *Search for Baryon-Number Violating Ξ_b^0 Oscillations*, *Phys. Rev. Lett.* **119** (2017) 181807 [1708.05808].

[117] G. Elor, M. Escudero and A. Nelson, *Baryogenesis and Dark Matter from B Mesons*, *Phys. Rev. D* **99** (2019) 035031 [1810.00880].

[118] F. Elahi, G. Elor and R. McGehee, *Charged B mesogenesis*, *Phys. Rev. D* **105** (2022) 055024 [2109.09751].

[119] G. Alonso-Álvarez, G. Elor, M. Escudero, B. Fornal, B. Grinstein and J. Martin Camalich, *Strange physics of dark baryons*, *Phys. Rev. D* **105** (2022) 115005 [2111.12712].

[120] G. Alonso-Álvarez, G. Elor and M. Escudero, *Collider signals of baryogenesis and dark matter from B mesons: A roadmap to discovery*, *Phys. Rev. D* **104** (2021) 035028 [2101.02706].

[121] Y. Zheng, J.-N. Ding, D.-H. Li, L.-Y. Li, C.-D. Lü and F.-S. Yu, *Invisible and semi-invisible decays of bottom baryons**, *Chin. Phys. C* **48** (2024) 083109 [2404.04337].

[122] T. Liu, M. J. Ramsey-Musolf and J. Shu, *Electroweak Beautygenesis: From b \to s CP-violation to the Cosmic Baryon Asymmetry*, *Phys. Rev. Lett.* **108** (2012) 221301 [1109.4145].

[123] Y.-F. Shen, W.-J. Song and Q. Qin, *CP violation induced by neutral meson mixing interference*, *Phys. Rev. D* **110** (2024) L031301 [2301.05848].

[124] H. G. Moser and A. Roussarie, *Mathematical methods for B0 anti-B0 oscillation analyses*, *Nucl. Instrum. Meth. A* **384** (1997) 491.

[125] LHCb collaboration, *Flavour Tagging in the LHCb experiment*, *PoS* **LHCP2018** (2018) 230.

[126] R. Aleksan, L. Oliver and E. Perez, *CP violation and determination of the bs flat unitarity triangle at an FCC-ee*, *Phys. Rev. D* **105** (2022) 053008 [2107.02002].

[127] A. S. Dighe, I. Dunietz and R. Fleischer, *Extracting CKM phases and $B_s - \bar{B}_s$ mixing parameters from angular distributions of nonleptonic B decays*, *Eur. Phys. J. C* **6** (1999) 647 [hep-ph/9804253].

[128] S. Faller, R. Fleischer and T. Mannel, *Precision Physics with $B_s^0 \to J/\psi\phi$ at the LHC: The Quest for New Physics*, *Phys. Rev. D* **79** (2009) 014005 [0810.4248].

[129] M. T. Lucchini, W. Chung, S. C. Eno, Y. Lai, L. Lucchini, M.-T. Nguyen et al., *New perspectives on segmented crystal calorimeters for future colliders*, *JINST* **15** (2020) P11005 [2008.00338].

[130] J. Charles, O. Deschamps, S. Descotes-Genon and V. Niess, *Isospin analysis of charmless B-meson decays*, *Eur. Phys. J. C* **77** (2017) 574 [1705.02981].

[131] LHCb collaboration, *Evidence for CP violation in time-integrated $D^0 \to h^-h^+$ decay rates*, *Phys. Rev. Lett.* **108** (2012) 111602 [1112.0938].

[132] CDF collaboration, *Measurement of the difference of CP–violating asymmetries in $D^0 \to K^+K^-$ and $D^0 \to \pi^+\pi^-$ decays at CDF*, *Phys. Rev. Lett.* **109** (2012) 111801 [1207.2158].

[133] LHCb collaboration, *Observation of CP Violation in Charm Decays*, *Phys. Rev. Lett.* **122** (2019) 211803 [1903.08726].

[134] R. Bause, H. Gisbert, M. Golz and G. Hiller, *Rare charm $c \to u\,\nu\bar{\nu}$ dineutrino null tests for e^+e^- machines*, *Phys. Rev. D* **103** (2021) 015033 [2010.02225].

[135] NA62 collaboration, *The Beam and detector of the NA62 experiment at CERN*, *JINST* **12** (2017) P05025 [1703.08501].

[136] KOTO collaboration, *Search for the $K_L \to \pi^0\nu\bar{\nu}$ and $K_L \to \pi^0 X^0$ decays at the J-PARC KOTO experiment*, *Phys. Rev. Lett.* **122** (2019) 021802 [1810.09655].

[137] E. Goudzovski et al., *New physics searches at kaon and hyperon factories*, *Rept. Prog. Phys.* **86** (2023) 016201 [2201.07805].

[138] A. A. Alves Junior et al., *Prospects for Measurements with Strange Hadrons at LHCb*, *JHEP* **05** (2019) 048 [1808.03477].

[139] A. Dery, M. Ghosh, Y. Grossman and S. Schacht, *$K \to \mu^+\mu^-$ as a clean probe of short-distance physics*, *JHEP* **07** (2021) 103 [2104.06427].

[140] A. Dery, M. Ghosh, Y. Grossman, T. Kitahara and S. Schacht, *A precision relation between $\Gamma(K \to \mu^+\mu^-)(t)$ and $\mathcal{B}(K_L \to \mu^+\mu^-)/\mathcal{B}(K_L \to \gamma\gamma)$*, *JHEP* **03** (2023) 014 [2211.03804].

[141] G. Burdman, E. Golowich, J. L. Hewett and S. Pakvasa, *Rare charm decays in the standard model and beyond*, *Phys. Rev. D* **66** (2002) 014009 [hep-ph/0112235].

[142] S. de Boer and G. Hiller, *Flavor and new physics opportunities with rare charm decays into leptons*, *Phys. Rev. D* **93** (2016) 074001 [1510.00311].

[143] S. Fajfer and N. Košnik, *Prospects of discovering new physics in rare charm decays*, *Eur. Phys. J. C* **75** (2015) 567 [1510.00965].

[144] R. Bause, M. Golz, G. Hiller and A. Tayduganov, *The new physics reach of null tests with $D \to \pi\ell\ell$ and $D_s \to K\ell\ell$ decays*, *Eur. Phys. J. C* **80** (2020) 65 [1909.11108].

[145] D. Guadagnoli and P. Koppenburg, *Lepton-flavor violation and lepton-flavor-universality violation in b and c decays*, in *Snowmass 2021*, 7, 2022, 2207.01851.

[146] S. De Boer and G. Hiller, *Null tests from angular distributions in $D \to P_1P_2l^+l^-$, $l = e, \mu$ decays on and off peak*, *Phys. Rev. D* **98** (2018) 035041 [1805.08516].

[147] M. Golz, G. Hiller and T. Magorsch, *Pinning down $|\Delta c| = |\Delta u| = 1$ couplings with rare charm baryon decays*, *Eur. Phys. J. C* **82** (2022) 357 [2202.02331].

[148] BESIII collaboration, *Search for the decay $D^0 \to \pi^0\nu\bar{\nu}$*, *Phys. Rev. D* **105** (2022) L071102 [2112.14236].

[149] Particle Data Group collaboration, *Review of Particle Physics*, *PTEP* **2022** (2022) 083C01.

[150] ALEPH, DELPHI, L3, OPAL, SLD, LEP Electroweak Working Group, SLD Electroweak Group, SLD Heavy Flavour Group collaboration, *Precision electroweak measurements on the Z resonance*, *Phys. Rept.* **427** (2006) 257 [hep-ex/0509008].

[151] S. Banerjee et al., *Snowmass 2021 White Paper: Charged lepton flavor violation in the tau sector*, 2203.14919.

[152] X.-D. Shi, X.-R. Zhou, X.-S. Qin and H.-P. Peng, *A fast simulation package for STCF detector*, *JINST* **16** (2021) P03029 [2011.01654].

[153] R. Ferrari, "*PID with Dual-readout Calorimeters.*" *Talk at the 2021 IAS Program on Particle Physics*, 2021.

[154] S. Giagu, L. Torresi and M. Di Filippo, *Tau Lepton Identification With Graph Neural Networks at Future Electron–Positron Colliders*, *Front. in Phys.* **10** (2022) 909205.

[155] M. Dam, *Tau-lepton Physics at the FCC-ee circular e^+e^- Collider*, *SciPost Phys. Proc.* **1** (2019) 041 [1811.09408].

[156] A. Lusiani, "*LFV and LFU in tau decays.*" *Talk at the Workshop on CEPC New Physics and Flavor Physics Studies, Fudan University*, 2023.

[157] A. Lusiani, "*Tau Physics Prospects at FCC-ee.*" *FCC note doi:10.17181/9bkm6-h8906*, 2023.

[158] S. Banerjee, *Searches for Lepton Flavor Violation in Tau Decays at Belle II*, *Universe* **8** (2022) 480 [2209.11639].

[159] D. Yu, "*Lepton identification and backgrounds for flavor studies at the CEPC.*" *Talk at the 2021 International CEPC Workshop*, 2021.

[160] A. Celis, V. Cirigliano and E. Passemar, *Model-discriminating power of lepton flavor violating τ decays*, *Phys. Rev. D* **89** (2014) 095014 [1403.5781].

[161] L. Calibbi and G. Signorelli, *Charged Lepton Flavour Violation: An Experimental and Theoretical Introduction*, *Riv. Nuovo Cim.* **41** (2018) 71 [1709.00294].

[162] C. Cornella, D. A. Faroughy, J. Fuentes-Martin, G. Isidori and M. Neubert, *Reading the footprints of the B-meson flavor anomalies*, *JHEP* **08** (2021) 050 [2103.16558].

[163] A. Pich, *Precision Tau Physics*, *Prog. Part. Nucl. Phys.* **75** (2014) 41 [1310.7922].

[164] A. Lusiani, "*Lepton Flavour Universality tests and determination of Vus using the tau branching fractions fit.*" *Poster presented at ICHEP 2024*, 2024.

[165] BESIII collaboration, *Future Physics Programme of BESIII*, *Chin. Phys. C* **44** (2020) 040001 [1912.05983].

[166] Belle-II collaboration, *Measurement of the τ-lepton mass with the Belle II experiment*, *Phys. Rev. D* **108** (2023) 032006 [2305.19116].

[167] Belle-II collaboration, *Test of light-lepton universality in τ decays with the Belle II experiment*, *JHEP* **08** (2024) 205 [2405.14625].

[168] Belle collaboration, *Measurement of the τ-lepton lifetime at Belle*, *Phys. Rev. Lett.* **112** (2014) 031801 [1310.8503].

[169] F. Feruglio, P. Paradisi and A. Pattori, *On the Importance of Electroweak Corrections for B Anomalies*, *JHEP* **09** (2017) 061 [1705.00929].

[170] L. Allwicher, G. Isidori and N. Selimovic, *LFU violations in leptonic τ decays and B-physics anomalies*, *Phys. Lett. B* **826** (2022) 136903 [2109.03833].

[171] OPAL collaboration, *Measurement of the strong coupling constant alpha(s) and the vector and axial vector spectral functions in hadronic tau decays*, *Eur. Phys. J. C* **7** (1999) 571 [hep-ex/9808019].

[172] ALEPH collaboration, *Branching ratios and spectral functions of tau decays: Final ALEPH measurements and physics implications*, *Phys. Rept.* **421** (2005) 191 [hep-ex/0506072].

[173] ALEPH collaboration, *K0(S) production in tau decays*, *Eur. Phys. J. C* **4** (1998) 29.

[174] L3 collaboration, *Measurement of exclusive branching fractions of hadronic one space prong tau decays*, *Phys. Lett. B* **345** (1995) 93.

[175] ALEPH collaboration, *Branching ratios and spectral functions of tau decays: Final ALEPH measurements and physics implications*, *Phys. Rept.* **421** (2005) 191 [hep-ex/0506072].

[176] A. Pich, *Challenges for tau physics at the TeraZ*, *Eur. Phys. J. Plus* **136** (2021) 1117 [2012.07099].

[177] DELPHI collaboration, *Cross-sections and leptonic forward backward asymmetries from the Z0 running of LEP*, *Eur. Phys. J. C* **16** (2000) 371.

[178] L3 collaboration, *Measurements of cross-sections and forward backward asymmetries at the Z resonance and determination of electroweak parameters*, *Eur. Phys. J. C* **16** (2000) 1 [hep-ex/0002046].

[179] R. Tenchini, *Asymmetries at the Z pole: The Quark and Lepton Quantum Numbers*, *Adv. Ser. Direct. High Energy Phys.* **26** (2016) 161.

[180] X. Chen and Y. Wu, *Search for the Electric Dipole Moment and anomalous magnetic moment of the tau lepton at tau factories*, *JHEP* **10** (2019) 089 [1803.00501].

[181] A. Crivellin, M. Hoferichter and J. M. Roney, *Toward testing the magnetic moment of the tau at one part per million*, *Phys. Rev. D* **106** (2022) 093007 [2111.10378].

[182] CMS collaboration, *Observation of $\gamma\gamma \to \tau\tau$ in proton-proton collisions and limits on the anomalous electromagnetic moments of the τ lepton*, 2406.03975.

[183] DELPHI collaboration, *Study of tau-pair production in photon-photon collisions at LEP and limits on the anomalous electromagnetic moments of the tau lepton*, *Eur. Phys. J. C* **35** (2004) 159 [hep-ex/0406010].

[184] S. Eidelman and M. Passera, *Theory of the tau lepton anomalous magnetic moment*, *Mod. Phys. Lett. A* **22** (2007) 159 [hep-ph/0701260].

[185] Y. S. Tsai, *Search for new mechanism of CP violation through tau decay and semileptonic decay of hadrons*, *Nucl. Phys. B Proc. Suppl.* **55** (1997) 293 [hep-ph/9612281].

[186] J. H. Kuhn and E. Mirkes, *CP violation in semileptonic tau decays with unpolarized beams*, *Phys. Lett.* **B398** (1997) 407 [hep-ph/9609502].

[187] D. Kimura, K. Y. Lee, T. Morozumi and K. Nakagawa, *CP violation in tau decays*, in *Heavy Quarks and Leptons 2008 (HQ&L08)*, 5, 2009, 0905.1802.

[188] I. I. Bigi, *CP Violation in τ Decays at SuperB & Super-Belle II Experiments - like Finding Signs of Dark Matter*, *Nucl. Phys. Proc. Suppl.* **253-255** (2014) 91 [1210.2968].

[189] K. Kiers, *CP violation in hadronic τ decays*, *Nucl. Phys. Proc. Suppl.* **253-255** (2014) 95 [1212.6921].

[190] I. I. Bigi and A. I. Sanda, *A 'Known' CP asymmetry in tau decays*, *Phys. Lett.* **B625** (2005) 47 [hep-ph/0506037].

[191] Y. Grossman and Y. Nir, *CP Violation in $\tau \to \nu\pi K_S$ and $D \to \pi K_S$: The Importance of $K_S - K_L$ Interference*, *JHEP* **04** (2012) 002 [1110.3790].

[192] CLEO collaboration, *First search for CP violation in tau lepton decay*, *Phys. Rev. Lett.* **81** (1998) 3823 [hep-ex/9805027].

[193] CLEO collaboration, *Search for CP violation in tau —> K pi tau-neutrino decays*, *Phys. Rev. Lett.* **88** (2002) 111803 [hep-ex/0111095].

[194] Belle collaboration, *Search for CP violation in $\tau \to K^0_S \pi \nu_\tau$ decays at Belle*, *Phys. Rev. Lett.* **107** (2011) 131801 [1101.0349].

[195] BaBar collaboration, *Search for CP Violation in the Decay $\tau^- - > \pi^- K^0_S (>= 0\pi^0) \nu_t au$*, *Phys. Rev. D* **85** (2012) 031102 [1109.1527].

[196] F.-Z. Chen, X.-Q. Li, Y.-D. Yang and X. Zhang, *CP asymmetry in $\tau \to K_S \pi \nu_\tau$ decays within the Standard Model and beyond*, *Phys. Rev. D* **100** (2019) 113006 [1909.05543].

[197] V. Cirigliano, A. Crivellin and M. Hoferichter, *A no-go theorem for non-standard explanations of the $\tau \to K_S \pi \nu_\tau$ CP asymmetry*, *Phys. Rev. Lett.* **120** (2018) 141803 [1712.06595].

[198] J. Rendón, P. Roig and G. Toledo Sánchez, *Effective-field theory analysis of the $\tau^- \to (K\pi)^- \nu_\tau$ decays*, *Phys. Rev.* **D99** (2019) 093005 [1902.08143].

[199] F.-Z. Chen, X.-Q. Li and Y.-D. Yang, *CP asymmetry in the angular distribution of $\tau \to K_S \pi \nu_\tau$ decays*, *JHEP* **05** (2020) 151 [2003.05735].

[200] F.-Z. Chen, X.-Q. Li, S.-C. Peng, Y.-D. Yang and H.-H. Zhang, *CP asymmetry in the angular distributions of $\tau \to K_S \pi \nu_\tau$ decays. Part II. General effective field theory analysis*, *JHEP* **01** (2022) 108 [2107.12310].

[201] H. Sang, X. Shi, X. Zhou, X. Kang and J. Liu, *Feasibility study of CP violation in $\tau \to K_S \pi \nu_\tau$ decays at the Super Tau Charm Facility*, *Chin. Phys. C* **45** (2021) 053003 [2012.06241].

[202] L. Calibbi, X. Marcano and J. Roy, *Z lepton flavour violation as a probe for new physics at future e^+e^- colliders*, *Eur. Phys. J. C* **81** (2021) 1054 [2107.10273].

[203] W. Altmannshofer, P. Munbodh and T. Oh, *Probing Lepton Flavor Violation at Circular Electron-Positron Colliders*, 2305.03869.

[204] W. Buchmuller and D. Wyler, *Effective Lagrangian Analysis of New Interactions and Flavor Conservation*, *Nucl. Phys. B* **268** (1986) 621.

[205] B. Grzadkowski and J. F. Gunion, *Using decay angle correlations to detect CP violation in the neutral Higgs sector*, *Phys. Lett.* **B350** (1995) 218 [hep-ph/9501339].

[206] ATLAS collaboration, *Search for lepton-flavor-violation in Z-boson decays with τ-leptons with the ATLAS detector*, *Phys. Rev. Lett.* **127** (2022) 271801 [2105.12491].

[207] ATLAS collaboration, *Search for the charged-lepton-flavor-violating decay $Z \to e\mu$ in pp collisions at $\sqrt{s} = 13$ TeV with the ATLAS detector*, *Phys. Rev. D* **108** (2023) 032015 [2204.10783].

[208] A. Crivellin and M. Hoferichter, *Consequences of chirally enhanced explanations of $(g-2)_\mu$ for $h \to \mu\mu$ and $Z \to \mu\mu$*, *JHEP* **07** (2021) 135 [2104.03202].

[209] M. Beneke, G. Buchalla, M. Neubert and C. T. Sachrajda, *QCD factorization for $B \to \pi\pi$ decays: Strong phases and CP violation in the heavy quark limit*, *Phys. Rev. Lett.* **83** (1999) 1914 [hep-ph/9905312].

[210] M. Beneke, G. Buchalla, M. Neubert and C. T. Sachrajda, *QCD factorization for exclusive, nonleptonic B meson decays: General arguments and the case of heavy light final states*, *Nucl. Phys. B* **591** (2000) 313 [hep-ph/0006124].

[211] Y. Y. Keum, H.-N. Li and A. I. Sanda, *Penguin enhancement and $B \to K\pi$ decays in perturbative QCD*, *Phys. Rev. D* **63** (2001) 054008 [hep-ph/0004173].

[212] C.-D. Lu, K. Ukai and M.-Z. Yang, *Branching ratio and CP violation of $B \to \pi\pi$ decays in perturbative QCD approach*, *Phys. Rev. D* **63** (2001) 074009 [hep-ph/0004213].

[213] Y. Grossman, M. König and M. Neubert, *Exclusive Radiative Decays of W and Z Bosons in QCD Factorization*, *JHEP* **04** (2015) 101 [1501.06569].

[214] CMS collaboration, *Search for rare decays of Z and Higgs bosons to J/ψ and a photon in proton-proton collisions at $\sqrt{s} = 13$ TeV*, *Eur. Phys. J. C* **79** (2019) 94 [1810.10056].

[215] S. Cheng and Q. Qin, *$Z \to \pi^+\pi^-, K^+K^-$: A touchstone of the perturbative QCD approach*, *Phys. Rev. D* **99** (2019) 016019 [1810.10524].

[216] L. Bergstrom and R. W. Robinett, *ON the rare decays $Z \to VV$ and $Z \to VP$*, *Phys. Rev. D* **41** (1990) 3513.

[217] M. König and M. Neubert, *Exclusive Radiative Higgs Decays as Probes of Light-Quark Yukawa Couplings*, *JHEP* **08** (2015) 012 [1505.03870].

[218] A. Crivellin and S. Pokorski, *Can the differences in the determinations of V_{ub} and V_{cb} be explained by New Physics?*, *Phys. Rev. Lett.* **114** (2015) 011802 [1407.1320].

[219] S. Descotes-Genon, A. Falkowski, M. Fedele, M. González-Alonso and J. Virto, *The CKM parameters in the SMEFT*, *JHEP* **05** (2019) 172 [1812.08163].

[220] D. Marzocca, M. Szewc and M. Tammaro, *Direct CKM determination from W decays at future lepton colliders*, 2405.08880.

[221] H. Liang, L. Li, Y. Zhu, X. Shen and M. Ruan, *Measurement of CKM element $|V_{cb}|$ from W boson decays at the future Higgs factories*, 2406.01675.

[222] ATLAS collaboration, *Precision measurement and interpretation of inclusive W^+ , W^- and Z/γ^* production cross sections with the ATLAS detector*, *Eur. Phys. J. C* **77** (2017) 367 [1612.03016].

[223] ATLAS collaboration, *Test of the universality of τ and μ lepton couplings in W-boson decays with the ATLAS detector*, *Nature Phys.* **17** (2021) 813 [2007.14040].

[224] CMS collaboration, *Precision measurement of the W boson decay branching fractions in proton-proton collisions at $\sqrt{s} = 13$ TeV*, *Phys. Rev. D* **105** (2022) 072008 [2201.07861].

[225] ALEPH, DELPHI, L3, OPAL, LEP Electroweak collaboration, *Electroweak Measurements in Electron-Positron Collisions at W-Boson-Pair Energies at LEP*, *Phys. Rept.* **532** (2013) 119 [1302.3415].

[226] CMS collaboration, *A portrait of the higgs boson by the cms experiment ten years after the discovery*, *Nature* **607** (2022) 60–68.

[227] ATLAS collaboration, *A detailed map of higgs boson interactions by the atlas experiment ten years after the discovery*, *Nature* **607** (2022) 52–59.

[228] J. F. Kamenik, A. Korajac, M. Szewc, M. Tammaro and J. Zupan, *Flavor-violating Higgs and Z boson decays at a future circular lepton collider*, *Physical Review D* **109** (2024) [2306.17520].

[229] N. Escudero, C. Muñoz and A. M. Teixeira, *Flavor changing neutral currents in supersymmetric multi-higgs doublet models*, *Phys. Rev. D* **73** (2006) 055015.

[230] A. Crivellin, J. Heeck and D. Müller, *Large $h \to bs$ in generic two-Higgs-doublet models*, *Phys. Rev. D* **97** (2018) 035008 [1710.04663].

[231] Q. Qin, Q. Li, C.-D. Lü, F.-S. Yu and S.-H. Zhou, *Charged lepton flavor violating Higgs decays at future e^+e^- colliders*, *Eur. Phys. J. C* **78** (2018) 835 [1711.07243].

[232] R. Harnik, J. Kopp and J. Zupan, *Flavor Violating Higgs Decays*, *JHEP* **03** (2013) 026 [1209.1397].

[233] C. T. Hill and E. H. Simmons, *Strong Dynamics and Electroweak Symmetry Breaking*, *Phys. Rept.* **381** (2003) 235 [hep-ph/0203079].

[234] D. Barducci et al., *Interpreting top-quark LHC measurements in the standard-model effective field theory*, 1802.07237.

[235] L. Shi and C. Zhang, *Probing the top quark flavor-changing couplings at CEPC*, *Chin. Phys. C* **43** (2019) 113104 [1906.04573].

[236] ATLAS collaboration, *Search for single top-quark production via flavour-changing neutral currents at 8 TeV with the ATLAS detector*, *Eur. Phys. J. C* **76** (2016) 55 [1509.00294].

[237] ATLAS collaboration, *Search for flavor-changing neutral currents in top quark decays $t \to Hc$ and $t \to Hu$ in multilepton final states in proton-proton collisions at $\sqrt{s} = 13$ TeV with the ATLAS detector*, *Phys. Rev. D* **98** (2018) 032002 [1805.03483].

[238] ATLAS collaboration, *Search for flavour-changing neutral current top-quark decays $t \to qZ$ in proton-proton collisions at $\sqrt{s} = 13$ TeV with the ATLAS detector*, *JHEP* **07** (2018) 176 [1803.09923].

[239] CMS collaboration, *Search for Anomalous Single Top Quark Production in Association with a Photon in pp Collisions at $\sqrt{s} = 8$ TeV*, *JHEP* **04** (2016) 035 [1511.03951].

[240] CMS collaboration, *Search for anomalous Wtb couplings and flavour-changing neutral currents in t-channel single top quark production in pp collisions at $\sqrt{s} = 7$ and 8 TeV*, *JHEP* **02** (2017) 028 [1610.03545].

[241] OPAL collaboration, *Search for single top quark production at LEP-2*, *Phys. Lett. B* **521** (2001) 181 [hep-ex/0110009].

[242] ALEPH collaboration, *Search for single top production in e^+e^- collisions at $\sqrt{s}$ up to 209-GeV*, *Phys. Lett. B* **543** (2002) 173 [hep-ex/0206070].

[243] L3 collaboration, *Search for single top production at LEP*, *Phys. Lett. B* **549** (2002) 290 [hep-ex/0210041].

[244] DELPHI collaboration, *Search for single top quark production via contact interactions at LEP2*, *Eur. Phys. J. C* **71** (2011) 1555 [1102.4455].

[245] G. Durieux, F. Maltoni and C. Zhang, *Global approach to top-quark flavor-changing interactions*, *Phys. Rev. D* **91** (2015) 074017 [1412.7166].

[246] A. Cerri et al., *Report from Working Group 4: Opportunities in Flavour Physics at the HL-LHC and HE-LHC*, *CERN Yellow Rep. Monogr.* **7** (2019) 867 [1812.07638].

[247] BaBar collaboration, *Observation of a narrow meson decaying to $D_s^+\pi^0$ at a mass of 2.32-GeV/c^2*, *Phys. Rev. Lett.* **90** (2003) 242001 [hep-ex/0304021].

[248] Belle collaboration, *Observation of a resonance-like structure in the $pi^{\pm}\psi'$ mass distribution in exclusive $B \to K\pi^{\pm}\psi'$ decays*, *Phys. Rev. Lett.* **100** (2008) 142001 [0708.1790].

[249] BESIII collaboration, *Observation of a Charged Charmoniumlike Structure in $e^+e^- \to \pi^+\pi^- J/\psi$ at $\sqrt{s}$ =4.26 GeV*, *Phys. Rev. Lett.* **110** (2013) 252001 [1303.5949].

[250] Belle collaboration, *Study of $e^+e^- \to \pi^+\pi^- J/\psi$ and Observation of a Charged Charmoniumlike State at Belle*, *Phys. Rev. Lett.* **110** (2013) 252002 [1304.0121].

[251] BESIII collaboration, *Observation of a Near-Threshold Structure in the K^+ Recoil-Mass Spectra in $e^+e^- \to K^+(D_s^- D^{*0} + D_s^{*-} D^0)$*, *Phys. Rev. Lett.* **126** (2021) 102001 [2011.07855].

[252] LHCb collaboration, *Observation of New Resonances Decaying to $J/\psi K^+$ + and $J/\psi\phi$*, *Phys. Rev. Lett.* **127** (2021) 082001 [2103.01803].

[253] LHCb collaboration, *Observation of $J/\psi p$ Resonances Consistent with Pentaquark States in $\Lambda_b^0 \to J/\psi K^- p$ Decays*, *Phys. Rev. Lett.* **115** (2015) 072001 [1507.03414].

[254] LHCb collaboration, *Observation of a narrow pentaquark state, $P_c(4312)^+$, and of two-peak structure of the $P_c(4450)^+$*, *Phys. Rev. Lett.* **122** (2019) 222001 [1904.03947].

[255] LHCb collaboration, *Observation of an exotic narrow doubly charmed tetraquark*, *Nature Phys.* **18** (2022) 751 [2109.01038].

[256] LHCb collaboration, *Observation of structure in the J/ψ -pair mass spectrum*, *Sci. Bull.* **65** (2020) 1983 [2006.16957].

[257] ATLAS collaboration, *Observation of an Excess of Dicharmonium Events in the Four-Muon Final State with the ATLAS Detector*, *Phys. Rev. Lett.* **131** (2023) 151902 [2304.08962].

[258] CMS collaboration, *Observation of new structure in the $J/\psi J/\psi$ mass spectrum in proton-proton collisions at $\sqrt{s}$ = 13 TeV*, 2306.07164.

[259] S. Godfrey and N. Isgur, *Mesons in a Relativized Quark Model with Chromodynamics*, *Phys. Rev. D* **32** (1985) 189.

[260] H.-X. Chen, W. Chen, X. Liu and S.-L. Zhu, *The hidden-charm pentaquark and tetraquark states*, *Phys. Rept.* **639** (2016) 1 [1601.02092].

[261] A. Hosaka, T. Iijima, K. Miyabayashi, Y. Sakai and S. Yasui, *Exotic hadrons with heavy flavors: X, Y, Z, and related states*, *PTEP* **2016** (2016) 062C01 [1603.09229].

[262] H.-X. Chen, W. Chen, X. Liu, Y.-R. Liu and S.-L. Zhu, *A review of the open charm and open bottom systems*, *Rept. Prog. Phys.* **80** (2017) 076201 [1609.08928].

[263] A. Esposito, A. Pilloni and A. D. Polosa, *Multiquark Resonances*, *Phys. Rept.* **668** (2017) 1 [1611.07920].

[264] R. F. Lebed, R. E. Mitchell and E. S. Swanson, *Heavy-Quark QCD Exotica*, *Prog. Part. Nucl. Phys.* **93** (2017) 143 [1610.04528].

[265] F.-K. Guo, C. Hanhart, U.-G. Meißner, Q. Wang, Q. Zhao and B.-S. Zou, *Hadronic molecules*, *Rev. Mod. Phys.* **90** (2018) 015004 [1705.00141].

[266] A. Ali, J. S. Lange and S. Stone, *Exotics: Heavy Pentaquarks and Tetraquarks*, *Prog. Part. Nucl. Phys.* **97** (2017) 123 [1706.00610].

[267] S. L. Olsen, T. Skwarnicki and D. Zieminska, *Nonstandard heavy mesons and baryons: Experimental evidence*, *Rev. Mod. Phys.* **90** (2018) 015003 [1708.04012].

[268] Y.-R. Liu, H.-X. Chen, W. Chen, X. Liu and S.-L. Zhu, *Pentaquark and Tetraquark states*, *Prog. Part. Nucl. Phys.* **107** (2019) 237 [1903.11976].

[269] N. Brambilla, S. Eidelman, C. Hanhart, A. Nefediev, C.-P. Shen, C. E. Thomas et al., *The XYZ states: Experimental and theoretical status and perspectives*, *Phys. Rep.* **873** (2020) 1 [1907.07583].

[270] F.-K. Guo, X.-H. Liu and S. Sakai, *Threshold cusps and triangle singularities in hadronic reactions*, *Prog. Part. Nucl. Phys.* **112** (2020) 103757 [1912.07030].

[271] H.-X. Chen, W. Chen, X. Liu, Y.-R. Liu and S.-L. Zhu, *An updated review of the new hadron states*, *Rept. Prog. Phys.* **86** (2023) 026201 [2204.02649].

[272] Y. Iwasaki, *A Possible Model for New Resonances-Exotics and Hidden Charm*, *Prog. Theor. Phys.* **54** (1975) 492.

[273] J. P. Ader, J. M. Richard and P. Taxil, *DO NARROW HEAVY MULTI - QUARK STATES EXIST?*, *Phys. Rev. D* **25** (1982) 2370.

[274] S. Zouzou, B. Silvestre-Brac, C. Gignoux and J. M. Richard, *FOUR QUARK BOUND STATES*, *Z. Phys. C* **30** (1986) 457.

[275] L. Heller and J. A. Tjon, *On Bound States of Heavy $Q^2\bar{Q}^2$ Systems*, *Phys. Rev. D* **32** (1985) 755.

[276] R. J. Lloyd and J. P. Vary, *All charm tetraquarks*, *Phys. Rev. D* **70** (2004) 014009 [hep-ph/0311179].

[277] J.-M. Richard, A. Valcarce and J. Vijande, *String dynamics and metastability of all-heavy tetraquarks*, *Phys. Rev. D* **95** (2017) 054019 [1703.00783].

[278] M. N. Anwar, J. Ferretti, F.-K. Guo, E. Santopinto and B.-S. Zou, *Spectroscopy and decays of the fully-heavy tetraquarks*, *Eur. Phys. J. C* **78** (2018) 647 [1710.02540].

[279] M. Karliner, S. Nussinov and J. L. Rosner, *$QQ\bar{Q}\bar{Q}$ states: masses, production, and decays*, *Phys. Rev. D* **95** (2017) 034011 [1611.00348].

[280] Y. Bai, S. Lu and J. Osborne, *Beauty-full Tetraquarks*, *Phys. Lett. B* **798** (2019) 134930 [1612.00012].

[281] A. V. Berezhnoy, A. V. Luchinsky and A. A. Novoselov, *Tetraquarks Composed of 4 Heavy Quarks*, *Phys. Rev. D* **86** (2012) 034004 [1111.1867].

[282] V. R. Debastiani and F. S. Navarra, *A non-relativistic model for the $[cc][\bar{c}\bar{c}]$ tetraquark*, *Chin. Phys. C* **43** (2019) 013105 [1706.07553].

[283] A. Esposito and A. D. Polosa, *A $bb\bar{b}\bar{b}$ di-bottomonium at the LHC?*, *Eur. Phys. J. C* **78** (2018) 782 [1807.06040].

[284] C. Hughes, E. Eichten and C. T. H. Davies, *Searching for beauty-fully bound tetraquarks using lattice nonrelativistic QCD*, *Phys. Rev. D* **97** (2018) 054505 [1710.03236].

[285] J. Wu, Y.-R. Liu, K. Chen, X. Liu and S.-L. Zhu, *Heavy-flavored tetraquark states with the $QQ\bar{Q}\bar{Q}$ configuration*, *Phys. Rev. D* **97** (2018) 094015 [1605.01134].

[286] M.-S. Liu, Q.-F. Lü, X.-H. Zhong and Q. Zhao, *All-heavy tetraquarks*, *Phys. Rev. D* **100** (2019) 016006 [1901.02564].

[287] C.-H. Chang and Y.-Q. Chen, *The Production of $B_{(c)}$ or $\bar{B}_{(c)}$ meson associated with two heavy quark jets in Z^0 boson decay*, *Phys. Rev.* **D46** (1992) 3845.

[288] OPAL collaboration, *Search for the B_c meson in hadronic Z^0 decays*, *Phys. Lett. B* **420** (1998) 157 [hep-ex/9801026].

[289] DELPHI collaboration, *Search for the B(c) Meson*, *Phys. Lett. B* **398** (1997) 207.

[290] ALEPH collaboration, *Search for the B_c meson in hadronic Z decays*, *Phys. Lett. B* **402** (1997) 213.

[291] LHCb collaboration, *Study of the doubly charmed tetraquark T_{cc}^+*, *Nature Commun.* **13** (2022) 3351 [2109.01056].

[292] A. V. Manohar and M. B. Wise, *Exotic Q Q anti-q anti-q states in QCD*, *Nucl. Phys. B* **399** (1993) 17 [hep-ph/9212236].

[293] M. Karliner and J. L. Rosner, *Discovery of doubly-charmed Ξ_{cc} baryon implies a stable $(bb\bar{u}\bar{d})$ tetraquark*, *Phys. Rev. Lett.* **119** (2017) 202001 [1707.07666].

[294] E. J. Eichten and C. Quigg, *Heavy-quark symmetry implies stable heavy tetraquark mesons $Q_iQ_j\bar{q}_k\bar{q}_l$*, *Phys. Rev. Lett.* **119** (2017) 202002 [1707.09575].

[295] J.-J. Wu, L. Zhao and B. S. Zou, *Prediction of super-heavy N^* and Λ^* resonances with hidden beauty*, *Phys. Lett. B* **709** (2012) 70 [1011.5743].

[296] Q. Qin, Y.-F. Shen and F.-S. Yu, *Discovery potentials of double-charm tetraquarks*, *Chin. Phys. C* **45** (2021) 103106 [2008.08026].

[297] A. Ali, A. Y. Parkhomenko, Q. Qin and W. Wang, *Prospects of discovering stable double-heavy tetraquarks at a Tera-Z factory*, *Phys. Lett. B* **782** (2018) 412 [1805.02535].

[298] Z.-S. Jia, P.-P. Shi, Z.-H. Zhang, G. Li and F.-K. Guo, *Production of hadronic molecules at the Z pole (in preparation)*, 2023.

[299] X.-K. Dong, F.-K. Guo and B.-S. Zou, *A survey of heavy-heavy hadronic molecules*, *Commun. Theor. Phys.* **73** (2021) 125201 [2108.02673].

[300] P. Artoisenet and E. Braaten, *Estimating the Production Rate of Loosely-bound Hadronic Molecules using Event Generators*, *Phys. Rev. D* **83** (2011) 014019 [1007.2868].

[301] F.-K. Guo, U.-G. Meißner, W. Wang and Z. Yang, *Production of the bottom analogs and the spin partner of the X(3872) at hadron colliders*, *Eur. Phys. J. C* **74** (2014) 3063 [1402.6236].

[302] M. Albaladejo, F.-K. Guo, C. Hanhart, U.-G. Meißner, J. Nieves, A. Nogga et al., *Note on X(3872) production at hadron colliders and its molecular structure*, *Chin. Phys. C* **41** (2017) 121001 [1709.09101].

[303] C. Bierlich et al., *A comprehensive guide to the physics and usage of PYTHIA 8.3*, 2203.11601.

[304] M.-L. Du, V. Baru, X.-K. Dong, A. Filin, F.-K. Guo, C. Hanhart et al., *Coupled-channel approach to T_{cc}^+ including three-body effects*, *Phys. Rev. D* **105** (2022) 014024 [2110.13765].

[305] X. Luo, Y.-Z. Jiang, G.-Y. Zhang and Z. Sun, *Doubly-charmed baryon production in Z boson decay*, 2206.05965.

[306] J.-J. Niu, J.-B. Li, H.-Y. Bi and H.-H. Ma, *Production of Excited Doubly Heavy Baryons at the Super-Z Factory*, 2305.15362.

[307] C. Antel et al., *Feebly Interacting Particles: FIPs 2022 workshop report*, in *Workshop on Feebly-Interacting Particles*, 5, 2023, 2305.01715.

[308] M. Bauer, M. Neubert and A. Thamm, *Collider Probes of Axion-Like Particles*, *JHEP* **12** (2017) 044 [1708.00443].

[309] J. Liu, X. Ma, L.-T. Wang and X.-P. Wang, *ALP explanation to the muon (g-2) and its test at future Tera-Z and Higgs factories*, *Phys. Rev. D* **107** (2023) 095016 [2210.09335].

[310] L. Calibbi, Z. Huang, S. Qin, Y. Yang and X. Yin, *Testing axion couplings to leptons in Z decays at future e+e- colliders*, *Phys. Rev. D* **108** (2023) 015002 [2212.02818].

[311] K. Cheung and C. J. Ouseph, *Axion Like Particle Search at Higgs Factories*, 2303.16514.

[312] M. He, X.-G. He, C.-K. Huang and G. Li, *Search for a heavy dark photon at future e^+e^- colliders*, *JHEP* **03** (2018) 139 [1712.09095].

[313] FCC-ee study Team collaboration, *Search for Heavy Right Handed Neutrinos at the FCC-ee*, *Nucl. Part. Phys. Proc.* **273-275** (2016) 1883 [1411.5230].

[314] J.-N. Ding, Q. Qin and F.-S. Yu, *Heavy neutrino searches at future Z-factories*, *Eur. Phys. J. C* **79** (2019) 766 [1903.02570].

[315] Y.-F. Shen, J.-N. Ding and Q. Qin, *Monojet search for heavy neutrinos at future Z-factories*, *Eur. Phys. J. C* **82** (2022) 398 [2201.05831].

[316] H.-C. Cheng, L. Li and E. Salvioni, *A theory of dark pions*, *JHEP* **01** (2022) 122 [2110.10691].

[317] L. Calibbi, D. Redigolo, R. Ziegler and J. Zupan, *Looking forward to lepton-flavor-violating ALPs*, *JHEP* **09** (2021) 173 [2006.04795].

[318] Belle-II collaboration, *Search for Lepton-Flavor-Violating τ Decays to a Lepton and an Invisible Boson at Belle II*, *Phys. Rev. Lett.* **130** (2023) 181803 [2212.03634].

[319] A. Blondel et al., *Searches for long-lived particles at the future FCC-ee*, *Front. in Phys.* **10** (2022) 967881 [2203.05502].

[320] H.-C. Cheng, X.-H. Jiang and L. Li, *Phenomenology of Electroweak Portal Dark Showers: High Energy Direct Probes and Low Energy Complementarity*, 2408.13304.

[321] J. F. Kamenik and C. Smith, *FCNC portals to the dark sector*, *JHEP* **03** (2012) 090 [1111.6402].

[322] H.-C. Cheng, X.-H. Jiang, L. Li and E. Salvioni, *Dark showers from Z-dark Z' mixing*, *JHEP* **04** (2024) 081 [2401.08785].

[323] L. Calibbi, F. Goertz, D. Redigolo, R. Ziegler and J. Zupan, *Minimal axion model from flavor*, *Phys. Rev. D* **95** (2017) 095009 [1612.08040].

[324] D. Aloni, C. Fanelli, Y. Soreq and M. Williams, *Photoproduction of Axionlike Particles*, *Phys. Rev. Lett.* **123** (2019) 071801 [1903.03586].

[325] J. Martin Camalich, M. Pospelov, P. N. H. Vuong, R. Ziegler and J. Zupan, *Quark Flavor Phenomenology of the QCD Axion*, *Phys. Rev. D* **102** (2020) 015023 [2002.04623].

[326] CLEO collaboration, *Search for the familon via B+- —> pi+- X0, B+- —> K+- X0, and B0 —> K0(S)X0 decays*, *Phys. Rev. Lett.* **87** (2001) 271801 [hep-ex/0106038].

[327] A. Akeroyd and C.-H. Chen, *Constraint on the branching ratio of $B_c \to \tau\bar{\nu}$ from LEP1 and consequences for $R(D^{(*)})$ anomaly*, *Phys. Rev. D* **96** (2017) 075011 [1708.04072].

[328] LHCb collaboration, *Measurement of the ratio of branching fractions* $\mathcal{B}(B_c^+ \to J/\psi\tau^+\nu_\tau)/\mathcal{B}(B_c^+ \to J/\psi\mu^+\nu_\mu)$, *Phys. Rev. Lett.* **120** (2018) 121801 [1711.05623].

[329] LHCb collaboration, *Observation of the decay* $\Lambda_b^0 \to \Lambda_c^+\tau^-\overline{\nu}_\tau$, *Phys. Rev. Lett.* **128** (2022) 191803 [2201.03497].

[330] ATLAS collaboration, *Measurement of the CP-violating phase* ϕ_s *in* $B_s^0 \to J/\psi\phi$ *decays in ATLAS at 13 TeV*, *Eur. Phys. J. C* **81** (2021) 342 [2001.07115].

[331] ATLAS collaboration, *Search for the lepton flavor violating decay* $Z\to e\mu$ *in pp collisions at* $\sqrt{s}$ *TeV with the ATLAS detector*, *Phys. Rev. D* **90** (2014) 072010 [1408.5774].

[332] ATLAS collaboration, *Search for charged-lepton-flavour violation in Z-boson decays with the ATLAS detector*, *Nature Phys.* **17** (2021) 819 [2010.02566].

[333] M. Ilyushin, P. Mandrik and S. Slabospitskii, *Constraints on the Higgs boson anomalous FCNC interactions with light quarks*, *Nuclear Physics B* **952** (2020) 114921.

[334] J. Duarte-Campderros, G. Perez, M. Schlaffer and A. Soffer, *Probing the Higgs–strange-quark coupling at* e^+e^- *colliders using light-jet flavor tagging*, *Phys. Rev. D* **101** (2020) 115005 [1811.09636].

[335] A. Albert et al., *Strange quark as a probe for new physics in the Higgs sector*, in *Snowmass 2021*, 3, 2022, 2203.07535.

[336] J. de Blas et al., *Higgs Boson Studies at Future Particle Colliders*, *JHEP* **01** (2020) 139 [1905.03764].

[337] GEANT4 collaboration, *GEANT4–a simulation toolkit*, *Nucl. Instrum. Meth. A* **506** (2003) 250.

[338] DELPHES 3 collaboration, *DELPHES 3, A modular framework for fast simulation of a generic collider experiment*, *JHEP* **02** (2014) 057 [1307.6346].

[339] Z. Zhao, S. Yang, M. Ruan, M. Liu and L. Han, *Measurement of the effective weak mixing angle at the CEPC**, *Chin. Phys. C* **47** (2023) 123002 [2204.09921].

[340] Y. Zhu, H. Liang, Y. Wang, H. Qu, C. Zhou and M. Ruan, *ParticleNet and its application on CEPC jet flavor tagging*, *Eur. Phys. J. C* **84** (2024) 152 [2309.13231].